Faculties of Engineering, Science, and Medicine
Aalborg University

Department of Biotechnology, Chemistry, and Environmental Engineering

TITLE:

Comparison of Shear and Compressive Yield Stress Ratio for Sewage Sludge and Inorganic Particulate Suspensions

PROJECT PERIOD:

September 1st 2007 - June 6th 2008

PROJECT GROUP:

K9-10K

AUTHOR:

Maria Kristjansson

SUPERVISORS:

Kristian Keiding
Peter J. Scales

NUMBER OF COPIES: 4

REPORT PAGES: 78

TOTAL PAGES: 95

ENCLOSED: CD-rom

SYNOPSIS:

The shear (τ_y) and compressive (P_y) yield stress behaviour of a coagulated alumina suspension, a sewage sludge, and a dual-polymer flocculated alumina suspension were characterised with focus on determining the variation in the P_y/τ_y ratio with solids volume fraction. Shear yield stress was determined using the vane technique developed by Nguyen and Boger (1983) by employing different vane dimensions. Shear yield stress values ranging from 0.9-15,000 Pa were measured. Compressive yield stress was determined through equilibrium pressure filtration, centrifugation, and batch settling tests. Compressive yield stresses could be determined in the range from 0.007-300 kPa.
Sewage sludge is difficult to characterise due to its slow dewatering properties. A flocculated alumina suspension, expected to exhibit sludge behaviour, was produced as a potential substitute.
The three suspensions were more easily deformed by shear than by compression. The P_y/τ_y ratios increased with volume fraction for all three suspensions. An increase from 2-14 was observed for the coagulated alumina suspension in the volume fraction range from 0.075-0.50 v/v. The ratio of sewage sludge increased from 5-8 in the volume fraction range from 0.035-0.09 v/v and the ratio of the flocculated alumina suspension increased from 8-11 in the volume fraction range from 0.09-0.43 v/v.
The filtration behaviour of the coagulated alumina suspension was traditional and the solids diffusivity constant at $1{\cdot}10^{-7}$ m^2/s with volume fraction above the gel point. The flocculated alumina suspension exhibited non-traditional filtration behaviour (a behaviour often exhibited by sludges) at low pressures, 5-20 kPa, and a non classified filtration behaviour at higher pressures, 40-300 kPa. The solids diffusivity ranged from $1{\cdot}10^{-7}$-$2{\cdot}10^{-6}$ m^2/s and showed a maximum near the gel point and the decrease with volume fraction was followed by an increase. The sewage sludge showed a similar solids diffusivity with volume fraction which varied from $6{\cdot}10^{-11}$-$5{\cdot}10^{-9}$ m^2/s.

De Ingeniør-, Natur- og Sundhedsvidenskabelige Fakulteter
Aalborg Universitet

Institut for Kemi, Miljøteknik og Bioteknologi

TITEL:

Sammenligning af kompressiblet and shear yield stress for kloak slam og uorganiske partikulære suspensioner

PROJEKTPERIODE:

1. september 2007 -
6. juni 2008

PROJEKTGRUPPE:

K9-10K

FORFATTER:

Maria Kristjansson

VEJLEDERE:

Kristian Keiding
Peter J. Scales

ANTAL KOPIER: 4

RAPPORT SIDEANTAL:78

TOTAL SIDEANTAL: 95

VEDLAGT: CD-rom

SYNOPSIS:

Variationen i kompressibel (P_y) og shear (τ_y) yield stress af en koaguleret aluminiumoxidsuspension, kloakslam og en dobbelt-polymer flokkuleret aluminiumoxidsuspension er blevet undersøgt, med henblik på at bestemme variationen i P_y/τ_y forholdet, som funktion af tørstofvolumenfraktionen. τ_y blev bestemt med vane teknik metoden udviklet af Nguyen and Boger (1983) ved at benytte forskellige vane størrelser. τ_y værdier fra 0,9-15.000 Pa blev målt. P_y blev bestemt ved hjælp af ligevægt trykfiltrering, centrifugering, og settling. P_y værdier fra 0,007-300 kPa blev målt.
Kloakslam er svært at karakterisere, fordi det er langsomt til at afvande. En flokkuleret suspension, som forventedes at opføre sig som slam, blev fremstillet som en mulig erstatning til karakterisering af slam.
De tre suspensioner blev lettere deformeret ved hjælp en shear kraft end en kompressibel kraft. P_y/τ_y forholdet steg som en funktion af volumenfraktionen for alle tre suspensioner. En stigning fra 2-14 blev bestemt for den koagulerede aluminiumoxidsuspension i volumenfraktionsområdet fra 0,075-0,50 v/v. Forholdet for kloakslam steg fra 5-8 i volumenfraktionsområdet fra 0,035-0,09 v/v og forholdet for den flokkuleret aluminiumoxidsuspension steg fra 8-11 i volumenfraktionsområdet fra 0,09-0,43 v/v.
Filtrering, af den koagulerede aluminiumoxidsuspension, var traditionel, og tørstofsdiffusiviteten var konstant på $1{\cdot}10^{-7}$ m^2/s, som en funktion af volumenfraktionen over gelpunktet. Den flokkulerede aluminiumoxidsuspension udviste en non-traditional filtrering (en filtrering ofte observeret i forbindelse med filtrering af slam) ved lave tryk, 5-20 kPa, og en uklassificeret filtrering ved højere tryk, 40-300 kPa. Tørstofsdiffusiviteten varierede fra $1{\cdot}10^{-7}$-$2{\cdot}10^{-6}$ m^2/s, og havde et maksimum tæt på gelpunktet, hvilket blev efterfulgt af et fald for derefter at stige igen. Tørstofdiffusiviteten for kloakslam havde et lignende forløb, som funktion af volumenfraktionen, og varierende fra $6{\cdot}10^{-11}$-$5{\cdot}10^{-9}$ m^2/s.

Preface

The references are stated in accordance with the Harvard Method [author, year]. If no author is stated the publisher is given. The report is divided into chapters, sections, and subsections. The chapters are numbered with one number and its sections are numbered with an additional number. Figures, tables, and equations are consecutive numbered according to the chapters. In Appendices the theoretical background of the employed methods are enclosed. Furthermore calculation methods are found in Enclosures. Additionally experimental data can be found on the enclosed CD-rom.

The author would like to thank Shane P. Usher and Ross G. De Kretser, The solid-liquid separation group University of Melbourne, for supervision and the remaining people in the solid-liquid separation group for help with practically matters.

.....

Maria Kristjansson

Contents

Chapter 1

Introduction

The field of solid-liquid separation is of importance for a large number of industrial processes. These include wastewater treatment, chemical purification, and mineral extraction. Particulate fluids form a three dimensional network structure above a critical concentration, defined the gel point (ϕ_g). A critical stress is required to break down this network structure. Solid-liquid separation of particulate fluids is often achieved by applying a compressive force. The compressive force is in many processes combined with a shear force e.g. compression of a flowing suspension. A one-dimensional applied compressive force has widely been investigated by means of pressure filtration or centrifugation. There is limited knowledge about how suspensions behave under two-dimensional compressive loads or combined shear and compressive loads. In order to optimise and improve current employed techniques, an understanding of this superposition of shear and arbitrary compression is crucial. Stickland and Buscall (2008) bring up this question in their article "Whither Compressional Rheology?" where it is stated that shear applied to a material often reduces the required compressive load, which has been observed in e.g. cross-flow filters and racked thickeners. To understand these observations, the focus in the article is pointed toward soil mechanics theory, which combines shear (τ_y) and compressive (P_y) yield stress.

Investigations in the P_y/τ_y ratio with volume fraction has been performed by a number of authors. Generally, only a defined area of the ratio between compressive and shear yield stress is investigated. The conclusions are often that a linear correlation between the shear and compressive yield stress exists. This is however not believed to be the case at low volume fractions, near the gel point, and at high volume fractions, near the maximum packing fraction.

Buscall *et al.* (1987) investigated the rheology of strongly flocculated polystyrene lattices and compared shear and compression for a particle size of 0.49 μm in the volume fraction range from 0.05-0.25 v/v. There appears to be a slight increases in the ratio with volume fraction. A rough estimation of the difference has been done, which suggests that the ratio increases from approximately 20-55, from the lowest to the highest volume fraction measured. Meeten (1994) worked with bentonite suspensions and estimated the ratio to be 11.1. Green (1997) estimated the ratio to be 15 for zirconia and non constant for titania. Channel and Zukoski (1997) investigated the suspension behaviour of an alumina suspension (AKP-15) and determined the ratio between compressive and shear yield stress to be independent of volume fraction with a value of 55. Zhou

(2000) investigated different alumina suspensions and a titania suspension. The ratio between compressive and shear yield stress below ϕ= 0.40 was determined to be about 14 for the alumina suspensions and about 29 for the titania suspension. At volume fractions above ϕ=0.40 the ratio of both suspensions increased with volume fraction. The higher ratio estimated by Channel and Zukoski (1997) can be ascribed to the fact that the estimated ratio mainly is based on data from higher volume fractions than ϕ=0.40 where Zhou (2000) also observe an increase in the ratio.

A prediction of P_y from τ_y is especially of interest for systems where compressive yield stresses are difficult to obtain. Sludges are known to be difficult and slow to dewater [Scales *et al.*, 2004]. Characterisation of sludges is furthermore complicated by factors such as bioactivity, health issues, and the fact that they often exhibit non-traditional filtrations behaviour (Figure 1.1). Traditional filtration theory is base on a linear correlation between time vs. specific filtrate volume^2. This linear region, which correspond to the cake formation region, is very small in the non-traditional filtration behaviour. This complicates modelling and prediction of filtration behaviour of sludges.

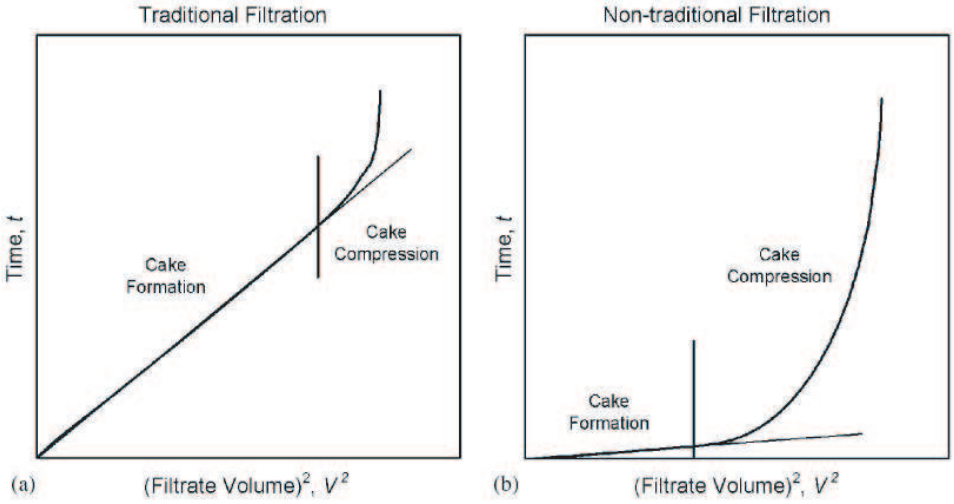

Figure 1.1: Non-traditional filtration [Stickland *et al.*, 2007].

Non-traditional filtration has also been observed in a dual flocculated alumina suspension [Glover, 2003]. The compound in sludge, that is believed to have the major impact on the dewater ability of sludge, is extra cellular polymers (ECP) [Dignac *et al.*, 2007]. It is believed that the polymers employed to flocculate the alumina suspension have a similar effect.

1.1 Problem Statement

In order to obtain a wide range of compressive and shear yield stresses for a suspension, as a function of volume fraction, a large sample volume is required. An easily produced sample with a known surface chemistry and high reproducibility is therefore desirable. Mineral suspensions such as alumina have previous been investigated with regard to compressive and shear yield stress with good reproducibility [Zhou, 2000]. The almost incompressible spherical particles with a narrow size distribution make up an almost ideal system for characterisation. Utilisation

of such a system enables characterisation of the compressive and shear yield stress for a wide volume fraction range. At the isoelectric point of the suspension (ζ=0) only attractive van der Waals forces are present.

Sludge is known to be difficult to dewater. This makes it difficult to obtain the desired yield stresses for the material as e.g. sewage sludge from a treatment plant often has a low volume fraction. This needs to be concentrated in order to obtain the different volume fractions desired for characterisation.

For general characterisation and understanding of sludge behaviour in compression and shear, it would be desirable to create a model system, that exhibits the characteristics of sludge. In work done by Glover (2003) non-traditional filtration behaviour, which is a sludge behaviour characteristics, has been observed. This work characterised a dual-polymer flocculated alumina suspension.

In this work, an alumina suspension, a flocculated suspension, and a sewage sludge will be characterised. It will not be of interest to optimise or characterise the flocculation process for the flocculated system. The focus will be on producing a reproducible system for characterisation. Comparison of the three systems will be done with focus on variation in the ratio between compressive and shear. This leads to the following problem statement.

How do shear yield stress and compressive yield stress vary with the volume fraction of an alumina suspension, a flocculated alumina suspension, and sewage sludge? Is there a relationship between the determined shear yield stress and compressive yield stress? What is the correlation between the ratio determined for the alumina suspension, the flocculated alumina suspension, and sewage sludge?

Chapter 2

Microstructure of Suspensions

In this chapter, an introduction to the microstructure of a suspension will be given. The compressive and shear yield stress of a suspension are determined by and vary with changes in the microstructure.

2.1 Forces Acting on Particles in a Suspension

Particles small enough to be unaffected by gravity are often defined as colloids. The quantitative definition of colloids is often particles $<1\mu$m. As the densities of the particles vary so will the gravitational effect on these particles and the definition is thus only a generalisation. A colloid in a suspension will constantly undergo thermal randomising motion. It will be influenced by the surrounding liquid and interact with the remaining colloids in the suspension. These three forces acting in a colloidal suspension, called; Brownian forces, hydrodynamic forces, and colloidal forces, respectively, will be explained further.

2.1.1 Brownian Motion

Thermal randomising motion is ever present. This diffusive force will try to restore and maintain a random equilibrium distribution of particles in a solution. The equilibrium state of the particle distribution is disturbed when shear is induced in the suspension. This alteration, of the particle distribution caused by introduced shear, is known as the convective effect. The magnitude of the hydrodynamic force determines whether the Brownian motion is able to restore the equilibrium distribution in the suspension or not. The relative importance of the convection compared to diffusion can be expressed by the Peclet number [Hiemenz and Rajagopalan, 1997]:

$$Pe = 6\pi\eta_0 r^3/k_B T \tag{2.1}$$

where η_0 is the viscosity of the continuous phase, r is the radius of the particle, k_B is Boltzmann constant, and T is the temperature. At Pe«1 diffusion in the suspension will dominate and restore perturbation caused by shear. In the case of Pe»1 convection will dominate over diffusion and usually cause shear thinning of the liquid which will be discussed in Chapter 3 [Hiemenz and Rajagopalan, 1997].

2.1.2 Hydrodynamic Forces

Hydrodynamic forces are present in flowing suspensions and arise from interactions between particles and the flowing medium. The viscosity of a suspension is determined by these interactions. The perturbation of the particles in flow field is responsible for increasing viscosity. In most cases, deviations from Newtonian behaviour such as shear thinning and shear thickening, are observed [Mascosko, 1994]. The particle shape, size, concentration, and their ability to deform determine the interactions amongst them and thus the resulting viscosity [Barnes, 2000].

2.1.3 Colloidal Interaction

The colloid forces are constituted by the positive van der Waals forces and the negative repulsive electrostatic forces.

Van der Waals Interactions

Van der Waals forces are weak long-range (>3nm) interactions that exist between all types of atoms and molecules. This makes it one of the most important forces when considering surface chemistry. These attractive forces arise from either permanent or induced dipoles in molecules. In general, three different kinds of van der Waals interactions exist. The Keesom interactions (between two permanent dipoles), the Debye interactions (between a permanent dipole and an induced dipole), and the ever present dispersion (London) forces which exist between two induced dipoles [Hiemenz and Rajagopalan, 1997].

The interaction potential between two spherical particles of different sizes can be expressed by [Israelachvili, 1992]:

$$V_A = -\frac{A}{6D}\frac{r_1 \cdot r_2}{(r_1 + r_2)} \tag{2.2}$$

where A is the Hamaker constant, D is the distance between the two particles surfaces, and r_1 and r_2 are the radius of the two particles. In an ideal system where two similar spherical particles are considered this equation can be reduced to:

$$V_A = -\frac{A \cdot r}{12D} \tag{2.3}$$

in the case where the inter-particle distance between the particles is significantly smaller than the radius of the particle (r»D).

Repulsive Electrostatic Forces

Colloids dispersed in an electrolyte solution are often charged. The charges can arise from dissociated surface groups or from adsorption of ions from the electrolyte solutions to the colloids. The charge of the colloid will attract counter ions. The repulsive force between the co-ions and constant Brownian motion ensures that the counter ions do not accumulate but instead form an ionic cloud around the colloid surface. As the concentration of the counter ions in the ionic cloud is high, it will together with the surface charge of the colloid form an electrical double layer [Ohshima, 2006].

2.2 The Electrical Double Layer

The electrical double layer can be divided into an inner and an outer layer. The inner layer is known as the Stern Layer. In this compact layer, the ions are assumed to be adsorbed to the surface of the particle. Beyond the Stern layer a more diffuse layer is found. It arises as a result of decreasing ion concentration with increasing distance from the particle surface (Figure 2.1). This layer is often referred to as the electrical double layer with the magnitude expressed by κ^{-1} [Hiemenz and Rajagopalan, 1997]:

$$\kappa^{-1} = \left(\frac{\epsilon_0 \epsilon k_B T}{e^2 2I}\right)^{1/2} \tag{2.4}$$

where ϵ_0 and ϵ are the dielectric constant for vacuum and the medium, respectively, k_B is the Boltzmann constant, T is the temperature, e is the electronic charge, and I is the ionic strength defined as:

$$I = (1/2)\sum n_i z_i^2 \tag{2.5}$$

where n_i is the number concentration of ions, i, in the medium, and z_i is the valence of the ions, i.

However an approximation of the electrical double layer is given by Equation (2.6) [Barnes, 2000].

$$\kappa^{-1} = 0.3c^{1/2}[z]^{-1} \tag{2.6}$$

Where the Debye length is given in nanometres, the electrolyte concentration, c, is given in mol/L, and z is the valence of the electrolyte. As an example, the length of the electrical double layer in a suspension with an electrolyte concentration of 10^{-3} mol/L and with z=1 would be approximately 10 nm [Barnes, 2000].

The plane at which shear occurs, when a particle or surface is set in motion, is called the shear plane. The potential at the shear plane is called the zeta potential.

The electrical double layer repulsion potential, that occurs when two identical spheres with a low surface potential ($\psi_0 <$ 25mV) are approaching each other, can be expressed as follows [Israelachvili, 1992] :

$$V_R = 2\pi r \epsilon_0 \epsilon \psi_0^2 e^{\kappa D} \tag{2.7}$$

where r is the radius, ϵ_0 and ϵ are the dielectric constant of vacuum and the medium, respectively, ψ_0 is the electrostatic surface potential, κ is the inverse Debye length, and D is the distance between the two surfaces of the spheres.

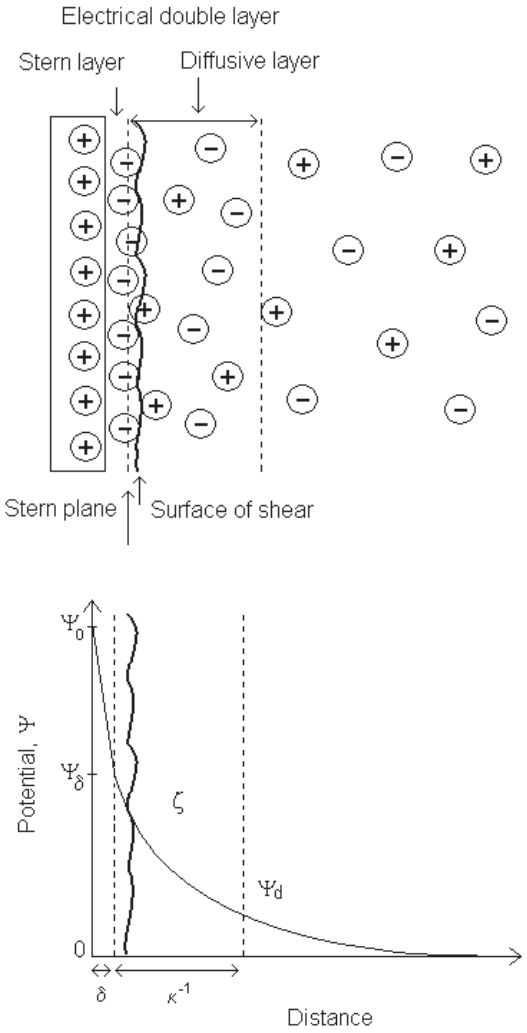

Figure 2.1: A positively charged surface surrounded mainly by counter ions and the potential as a function of the distance away from the surface is depicted. The Stern and Diffusive layer have a higher potential than that found in the bulk suspension. The potential at the surface is denoted ψ_0 and at the surface of shear it is denoted the zeta potential (ζ). Furthermore, the potential at the Stern plane (ψ_δ) and at the diffuse layer boundary (ψ_d) is defined.

2.3 DLVO theory

The stability of a colloid suspension is determined by its microstructure i.e. by the mutual interactions of the colloids. An approach to understand the stability of a suspension, by considering how two charged colloid particles interact with each other, has been made by Derjaguin & Landau and Verwey & Overbeek. This theory is called the DLVO theory. The two main forces acting on two colloidal particles, approaching each other, are the electrostatic double-layer forces and van der Waals forces. The total interaction force (V_T) can thus be expressed [Ohshima, 2006]:

$$V_T = V_A + V_R \tag{2.8}$$

with V_A expressing the van der Waals forces and V_R the electrostatic double-layer forces. The sum of these forces can either be attractive or repulsive depending on the magnitude (Figure 2.2).

The DLVO theory uses the resulting potential energy to explain the stability of the suspension. It is assumed that the motion of the colloid is negligible compared to the motion of the electrolyte ions. The two colloids can thus be considered to be at a fixed distance from each other, with the electrolyte ions moving around them [Ohshima, 2006].

For two identical particles the total interaction energy can be expressed by:

$$V_T = -\frac{A \cdot r}{12D} + 2\pi a \epsilon_0 \epsilon \psi_0^2 e^{\kappa D} \tag{2.9}$$

where A is the Hamaker constant, D is the distance between the two surfaces of the particles, r is the radius, ϵ_0 and ϵ are the dielectric constant of vacuum and the medium, respectively, ψ_0 is the electrostatic surface potential, and κ is the inverse Debye length. From Equation (2.9), it can be deduced that the attractive van der Waals forces decay with the inverse power of the distance (x) from the particle surface, and that the repulsive double layer forces decay exponentially. As a consequence, the attractive van der Waals forces will often either dominate the total interaction energy at all distances (x) or both at short and long distances. In the case of the latter, the repulsive electrical double layer forces will constitute an energy barrier, to be overcome, before particle coagulation can occur. If Equation (2.7) is considered (and the liquid medium is unchanged) the magnitude of this energy barrier is determined by two parameters. The potential at the Stern plane ($\psi_D \approx \zeta$) and the Debye length (κ^{-1}) which can be related to the surface chemistry of the suspension including the pH and the ionic strength. At the isoelectic point (IEP) of a suspension (the pH where ζ=0) the repulsive electrical double layer forces are non-existing (Figure 2.2e). In the case where the zeta potential is high and/or the ionic strength is low, a high energy barrier exists. If the energy barrier is insurmountable by thermal energy, the suspension will be dispersed and colloid stability occur. At low zeta potential and/or high ionic strength the energy barrier is low and if the thermal energy of the particles is high enough to overcome the barrier and reach the primary minimum, coagulation will occur.

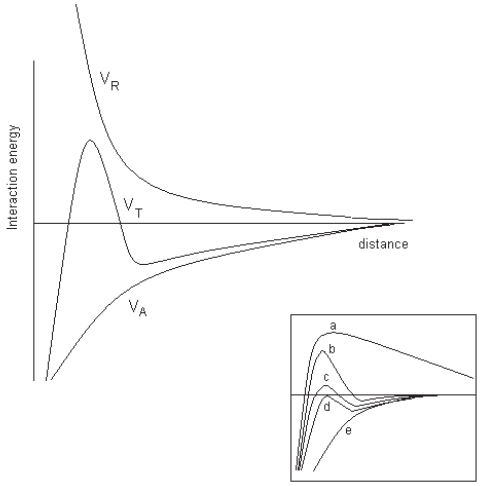

Figure 2.2: The DLVO theory picturing the attractive van der Waals forces (V_A), the repulsive double-layer interactions (V_R), and the sum of these (V_T). The numbers from a-e show the effect of increasing salt which result in a decreasing surface potential.

2.4 Non-DLVO Forces

At short separation distances (<3nm), other forces than van der Waals and DLVO forces becomes more significant. In other words the DLVO theory fails to describe short range interactions. Attractive non-DLVO forces, including bridging and depletion forces, often arise in flocculated suspensions. As the terms coagulation and flocculation often are used indiscriminately, a distinction between them will be made in this work to minimise confusion. Coagulation describes the phenomenon where particles are driven together by means of chemical additives resulting in a diminished repulsion and a dominant attraction between the particles. An example, is adding acid or base to change pH and reach the IEP point. At the IEP the particles have no charge and thus no electric double layer repulsive force exists. Flocculation, on the other hand, is in this work used to describe aggregation of particles caused by addition of high molecular weight polymers.

2.4.1 Bridging Forces

The phenomenon of bridging occurs when a polymer is adsorbed to more than one particle surface. A technique often used to flocculate particles in order to improve solid-liquid separation processes. A low degree of surface coverage by the adsorbing polymers in the suspension enhances the possibility of bridging [Israelachvili, 1992; Johnson *et al.*, 2000].

2.4.2 Depletion Forces

Attraction between two particles can arise due to depletion forces. A particulate suspension, with a non absorbing low molecular weight polymer, is considered. When the particles are separated, with a larger distance than the radius of the polymer, there is no net force between the particles. The dispersed polymer molecules will exert an osmotic pressure on all sides of the particles. In the case where the two particles are in closer proximity, such that the distance between them is smaller than the radius of the polymer molecules, the polymer molecules are excluded from the close contact area. An osmotic pressure is exerted on the remaining part of the particles leading to a net attractive force between the particles [Hiemenz and Rajagopalan, 1997].

Chapter 3

Rheology of Suspensions

Rheology of particulate fluids is more complicated than rheology of pure fluids. As concentration in a particulate fluid is increased the particles will interact with each other and form a three dimensional network structure. This structure will be able to store some energy elastically and the suspension will have a yield stress. The yield stress is the minimum stress required to break down this three dimensional network structure.

3.1 Definition of Viscoelastic Behaviour

Particulate fluids are viscoelastic materials as they exhibit both elastic and viscous properties. If a stress below the yield stress is applied to the suspension, the suspension will act elastic and store all the energy applied to the suspension. After removal of the stress complete spontaneous recovery of the deformation will result. On the other hand, if a suspension is deformed such that the three dimensional network is broken down, the suspension will start to flow at a critical stress (shear yield stress, τ_y). The time scale at which experiments are observed is thus the determining factor of how the suspension will behave.

This can be explained by the dimensionless Deborah number (De) which is defined as [Goodwin and Hughes, 2000]:

$$De = \frac{t_r \quad \text{(stress relaxation time)}}{t \quad \text{(observation time)}} \tag{3.1}$$

the stress relaxation time (t_r) can be defined as the time it takes for the molecules in a deformed suspension to diffuse from the higher energy state, which they have been shifted to during the deformation, to a lower energy equilibrium state. If the observation time is significant longer than the stress relaxation time, diffusion will have occurred and the suspension will then have lost its initial shape and started to flow and behave liquid-like ($De \ll 1$). In the other case, where the stress relaxation time is significantly longer than the observation time, the suspension will appear solid-like as no diffusion has occurred and all the energy is stored in the suspension ($De \gg 1$). In most cases both behaviours will be observed [Goodwin and Hughes, 2000].

3.2 Viscosity of Suspensions

The viscosity of very diluted suspensions is not of interest for this work. The concentration a which the particles in a suspensions start forming a network is defined as the gel point ($\phi_(g)$). Concentrations from the gel point to the maximum packing fraction (ϕ_{cp}) are those of interest.

The simplest flow behaviour, for yield stress materials is the ideal plastic flow (Bingham plastic behaviour) which is described with the Bingham model:

$$\tau = \tau_B + \eta_{pl}\,\dot{\gamma}, \quad \tau \geq \tau_B \tag{3.2}$$

that suggests a linear relationship between shear rate ($\dot{\gamma}$) and shear stress (τ) above the Bingham yield stress (τ_B) with the slope of the line being the viscosity (η_{pl}) describing the viscoplastic flow. Equation (3.2) assumes that the structure, which can resist irreversible deformation, breaks down completely the moment the yield stress is applied or exceeded. However, this behaviour is in most cases only observed at high shear rates, which can indicate that in most suspensions a gradual degradation of the network during shear is the case, rather than an instant degradation. An empirical model to describe a nonlinear dependence has been proposed by Herschel and Bulkley (1926):

$$\tau = \tau_{HB} + k\,\dot{\gamma}^{m}, \quad \tau \geq \tau_{HB} \tag{3.3}$$

with τ being the shear stress, τ_{HB} the yield stress, $\dot{\gamma}$ the shear rate and, m and k constants and power law parameters often used to describe flow behaviour. If the viscosity declines with shear rate, $m<1$, the suspension is classified as yield-pseudo plastic. At $m=1$ the equation reduces to the Bingham model (Equation (3.2)). If the viscosity is increasing, $m>1$, the suspension is classified as yield-dilatant plastic. Another model to describe a nonlinear dependence has been proposed by Casson (1959):

$$\tau^{1/2} = \tau_C^{1/2} + (\eta_\infty\,\dot{\gamma})^{1/2}, \quad \tau \geq \tau_C \tag{3.4}$$

This model includes only two parameters beside the shear stress (τ) and the shear rate ($\dot{\gamma}$): the Casson yield stress (τ_C) and the constant viscosity obtained at an infinite shear rate (η_∞) [Nguyen and Boger, 1992].

The three kinds of different viscosities can be viewed in Figure 3.1.

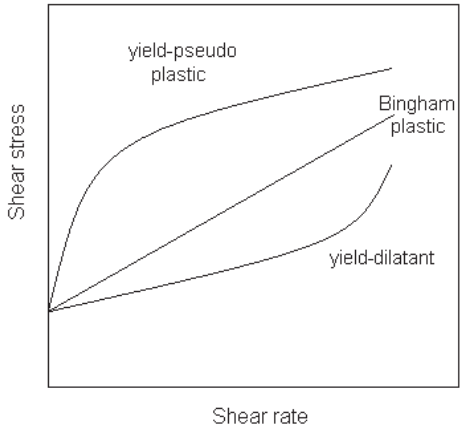

Figure 3.1: Flow behaviour of plastic material. Ideal plastic flow exhibit a yield stress followed by a linear dependence of shear stress on shear rate. Shear thinning behaviour beyond the yield stress is noted yield-pseudo plastic and shear thickening beyond the yield stress yield-dilatant.

3.2.1 Shear Thinning or yield Psudoplastic Behaviour

Shear thinning properties are often observed in colloidal suspensions. In aggregated suspensions dominated by attractive forces, the decrease in viscosity with shear rate is believed to be due to aggregates either breaking up or densifying. The microstructure can be used to explain this, as Brownian motion dominates at low shear rates and maintain the equilibrium structure whereas hydrodynamic forces dominate at high shear rates, rearranging or altering the aggregate structure resulting in altered flow [Ackerson, 1990].

At low shear rates, Brownian motion maintains random distributed particles but as the shear rates is increased convection becomes dominant (Pe»1) and particles arrange in string like structures as illustrated in Figure 3.2 [Barnes, 2000].

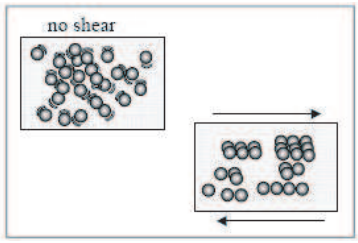

Figure 3.2: Spatial arrangement of particles which when non sheared is dominated by Brownian motion and during shear form string like structures, that make flow occur easier and promote shear thinning [Barnes, 2000]

The string like arrangement of the particles at high shear rate decreases the distance between the particles in the flow direction, and increases the distance between the particle layers which promotes flow and yield shear thinning. In some cases the decrease in viscosity can be followed by an increase in viscosity i.e. shear thickening behaviour at high shear rates. The further increase in shear rate/stress can result in a break down of the previous formed string like structures to lumps or the strings can be aligned crosswise to the flow direction, which in both cases lead to an increase in viscosity.

The shear thinning effect is greater for larger particles, as these are less influenced by Brownian motion and will be arranged more easily. This is illustrated in Figure 3.3.

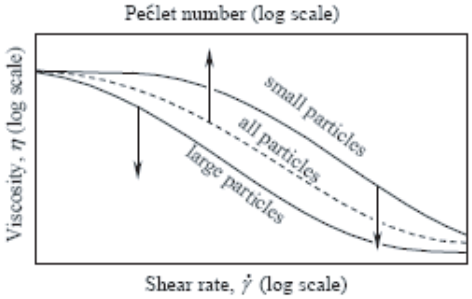

Figure 3.3: The effect of particle size on the viscosity. Small particles are more influenced by Brownian motion which maintain random distributed particles and maintain a higher viscosity compared to the viscosity of larger particles [Barnes, 2000]

The Peclet number accounts for the relative influence of Brownian motion versus convection. The viscosity as a function of the Peclet number is thus the same for different sizes particles.

3.2.2 Shear Thickening or yield Dilatant Behaviour

An increase in viscosity as a function of shear rate is called shear thickening behaviour. This type of behaviour is often encountered in highly concentrated fluids and an explanation is given forthwith. In concentrated fluids, high density packing of the particles allows only a small quantity of liquid between the particles. When the suspension is sheared at low shear rates this liquid is enough to lubricate the motion of particle past each other. At higher shear rates, the dense packing breaks down and the suspension expands resulting in a solid-solid friction. Due to lack of liquid between the particles, which causes the stress to increase more rapidly and thus the viscosity increases more rapidly. As is the case with shear thinning behaviour, shear thickening behaviour can often be modelled by a straight line on a log-log scale of shear rate vs. shear stress and Equation (3.3), where $m>1$ can thus be employed to model this behaviour [Barnes, 2000].

3.3 Time-Dependent Behaviour

Changes in the microstructure of a suspension as a result of shear do not take place instantaneously in any suspension, but in most cases the utilized viscometers are too slow to measure the short delay. For some suspensions, the response takes longer and the suspension is said to have a time dependent behaviour. Shear history of the suspension will then affect the measurement of rheological properties. The flow properties can be affected by both shear rate and time of shearing. Two types of time-dependent behaviour can be experienced; Thixotropy or anti-thixotropy (rheopexy) [Barnes, 1997].

3.3.1 Thixotropy

A material is classified to be thixotropic if the viscosity decreases with time of shearing at constant shear rate or shear stress. During shear, the structure of the liquid gradually breaks down and hence the viscosity decreases with shear. By cessation of flow the Brownian motion present in the suspension will slowly build up the microstructure again to reach a more energetically favourable state, which can take from hours to days. A method for testing whether a material exhibits thixotropic behaviour or not is to apply a constant high shear rate to a material until equilibrium is reached followed by a sudden drop to a lower constant shear rate. If there is structure breakdown at high shear rates and structure build up at low shear rates as shown in Figure 3.4 the suspension is thixotropic [Barnes, 2000; Chhabra, 2007].

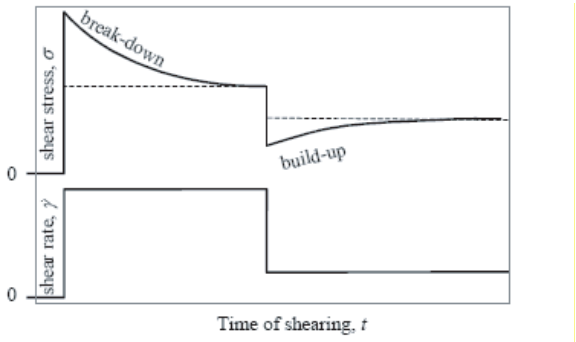

Figure 3.4: The response exhibited by a thixotropic suspension, when a constant high shear rate followed by a low constant shear rate is applied to the suspension initially in rest [Barnes, 2000].

3.3.2 Anti-Thixotropy or Rheopexy

Very few suspensions exhibit the opposite behaviour i.e. increasing viscosity with constant shear or stress. In this case, a structural build up during shear occurs which breaks down again when the suspension is at rest [Chhabra, 2007].

3.4 Shear Yield Stress

The existence of a shear yield stress has been well debated over the years. The doubt about its existence is based on the perspective that any material will flow if given enough time. Barnes and Walters (1985) published an article "The Yield Stress Myth?" and initiated the debate by claiming that 'if a material flows at high stresses it will also flow, however slowly, at low stresses'. About 70 years after the yield stress concept was introduced for fluids by Bingham and Green (1920) its existence was verified by Hartnett and Hu (1989). Through a simple experiment using a falling ball, they showed that a nylon ball, placed in an aqueous Carbopol solution with a lower density, did not move a measurable distance over several months. Today, the yield stress is an accepted meaningful rheological parameter.

The yield stress is the minimum applied stress for a suspension to flow and designates a transition from solid-like behaviour to liquid like behaviour. In most systems, this transition does not take

place instantaneously but occurs over a range of stresses in which the material exhibits viscoelastic behaviour (also referred to as viscoplastic flow). This observation leads to the definition of two different yield stresses; the transition from a solid-like behaviour to a viscoelastic behaviour and the transition from a viscoelastic behaviour to a liquid-like behaviour often denoted the static and the dynamic yield, respectively. The three dimensional structure formed, above the gel point, in a suspension is believed to be responsible for the ability of a suspension to elastically resist low stresses. As the stress is increased this three dimensional structure will gradually break down and in the end finally allow viscous flow to occur. Therefore, the yield stress can be viewed as the force per unit area it takes to break down the three dimensional network [Liddell and Boger, 1995].

The shear yield stress can be measured with a number of different techniques that are either classified as direct or indirect. Indirect techniques often extrapolate shear stress-shear rate data to a zero shear rate by means of models which means that the techniques employed are techniques normally used to measure viscosity (Section 3.2). To obtain accurate estimation of the yield stress by extrapolating data, the data in the low shear rate region should be known. However, when using conventional rheometers such as a capillary rheometer or a Weissenberg rheogoniometer it is often difficult to measure low shear rate data due to problems such as wall slip. In a suspension consisting of smooth spherical particles, for example, the distribution of the particles in the bulk suspension will be random. However, at the wall, the particle concentration will be zero and a rapid increase in concentration will be observed when moving away from the wall. This results in wall slip (wall depletion) [Barnes *et al.*, 1989]. The problem is mostly observed at low shear rates.

The direct methods measure a defined yield stress. This can be the transition between elastic behaviour and plastic behaviour or the transition between plastic deformation and start of viscous flow behaviour. The three most common techniques for measuring yield stress directly are creep/recovery, stress relaxation, or stress growth experiments. In creep/recovery experiments, different constant stresses are applied to the suspension for a defined period of time and then removed. An applied stress below the yield stress leads to a constant strain value with time and complete recovery after removal of the stress. The yield stress is defined as the stress where the strain increases indefinitely i.e. the point where the suspension starts to flow and incomplete strain recovery is obtained after removal of the stress.

In the stress growth experiments the suspension is sheared at a low constant shear rate and the yield stress (transition from viscoelastic to viscous behaviour) is defined as the maximum stress obtained in a stress-time profile, i.e. the point at which the three dimensional structure breaks down and the suspension starts to flow (Figure 3.5).

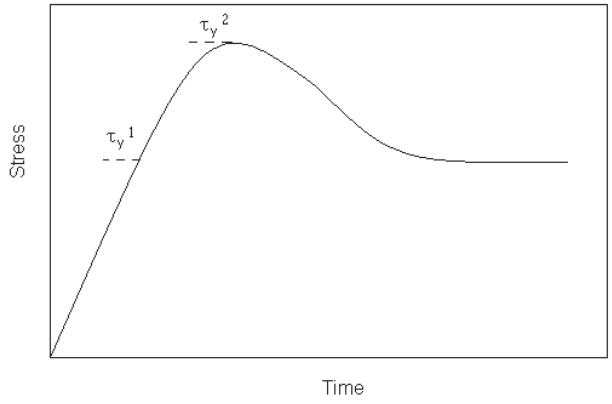

Figure 3.5: Stress growth experiment to determination of the static (τ_y^1) and dynamic (τ_y^2) yield stress

3.5 Compressive Yield Stress

The compressive yield stress $P_y(\phi)$ is defined as the minimum pressure required to compact and irreversible deform a suspension to obtain a given volume fraction, ϕ. $P_y(\phi)$ is considered a material property depending of the particles and the surface chemistry and can thus be obtained by employing different techniques [Miller *et al.*, 1996]. These include either mechanical and chemical driving force techniques. The former including: pressure filtration, centrifugation, and sedimentation techniques and the latter: slip casting and osmotic consolidation which make use of a chemical potential gradient to obtain consolidation.

By observing dewatering from a rheological perspective $P_y(\phi)$ was introduced by Buscall and White (1987) together with another material constant the hindered settling function ($R(\phi)$). $R(\phi)$ describes the permeability of a suspension during dewatering which is determined by the magnitude of the hydrodynamic force, resulting from either moving solids through liquid, as is the case in centrifugation and settling or moving liquid through solids as is the case in filtrations. [Scales *et al.*, 2004]. The hindered settling function and the compressive yield stress describe the permeability and the compressive behaviour which in the classical filtration theory established by Darcy [Ruth *et al.*, 1933] is described by k and the specific cake resistance α, respectively. Landman *et al.* (1995) defined a diffusivity function $D(\phi)$ which take both $P_y(\phi)$ and $R(\phi)$ into account.

3.5.1 Hindered settling function R(ϕ)

The hindered settling function $R(\phi)$ can be calculated from settling experiments or from filtration employing the initial fall rate in the bed height in sedimentation or the inverse linear rate of cake formation (β^2) in filtration [Landman and White, 1994]:

$$\beta^2 = \frac{1}{\frac{dt}{dV^2}} \tag{3.5}$$

where t is the time and V is the filtrate volume pr unit membrane. The hindered settling function

can then be calculated 3.6 [Landman *et al.*, 1999]:

$$R(\phi_f) = \frac{\lambda}{V_P} r(\phi) = \frac{2}{\frac{d\beta^2}{d\Delta P}} \left(\frac{1}{\phi_0} - \frac{1}{\phi_f} \right) (1 - \phi_f)^2 \tag{3.6}$$

where λ is Stoke's drag coefficient for a single particle, V_P denotes the volume of a single particle, *r(ϕ)* is the hindered settling factor, ϕ_0 is the initial volume fraction, ϕ_f is the final volume fraction, and $\frac{d\beta^2}{d\Delta P}$ is the slope of a plot of β^2 vs. Δ P.

3.5.2 Solids diffusivity D(ϕ)

The solids diffusivity D(ϕ) can be either calculated from knowledge of R(ϕ), the slope of $P_y(\phi)$ vs. ϕ, and the final volume fraction (ϕ_f) or from the slope of β^2 vs. ϕ_f, ϕ_0 and ϕ_f [Landman *et al.*, 1999]:

$$D(\phi_f) = \frac{dP_y(\phi)}{d\phi} \frac{(1 - \phi_f)^2}{R(\phi_f)} = \frac{1}{2} \frac{d\beta^2}{d\phi_f} \left(\frac{1}{\phi_0} - \frac{1}{\phi_f} \right)^{-1} \tag{3.7}$$

The function form of $P_y(\phi)$, R(ϕ), and D(ϕ) can be viewed as a function of the volume fraction in Figure 3.6 [Landman and White, 1997]

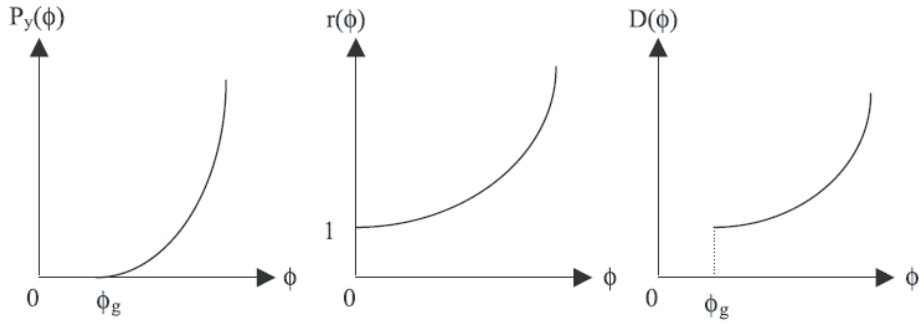

Figure 3.6: The theoretical development of the compressive yield stress, the hindered settling function, and the solid diffusivity as a function of the volume fraction [Glover *et al.*, 2004]

3.6 Filtration Theory

Landman and White (1997) proposed a linearised model for constant pressure filtration from which $P_y(\phi)$ and R(ϕ) can be determined. The model predicts that t varies linearly with V^2 in the cake formation step:

$$t = \left(\frac{V}{\beta} \right)^2 = \frac{T_c}{D(\phi_\infty)} \left(\frac{\phi_0}{\phi_\infty} \right) \frac{V}{(1 - H_c)})^2 : t \leq t_c \tag{3.8}$$

where T_c is the dimensionless time where the cake formation takes place, H_c is the scaled piston height at T_c, t is total filtration time, and t_c is cake formation time.

3.6.1 Traditional Filtration Behaviour

The cake formation curve is in traditional filtration theory employed to determine the filtration parameters R(ϕ) and D(ϕ). A traditional dewatering profile is dominated by cake formation which usually constitute up to 85% of the total filtration time (Figure 3.7).

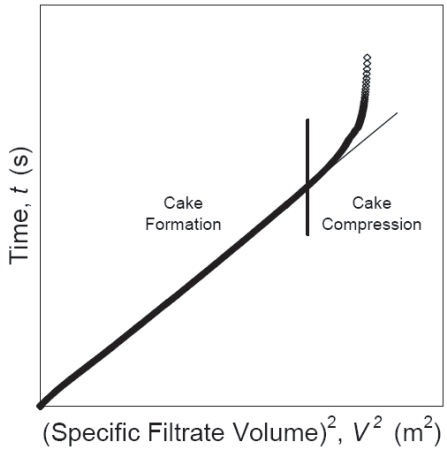

Figure 3.7: Traditional filtration behaviour [Stickland, 2005].

3.6.2 Non-Traditional Filtration Behaviour

Biological materials such as wastewater sludges exhibit a different filtration behaviour referred to as non-traditional filtration behaviour. In this filtration behaviour the cake formation only constitutes about 15% of the total filtration time and the filtration is dominated by a long cake compression (Figure 3.8). This behaviour is observed for sludges containing extra cellular polymers which are defined as cross linked high molecular weight polymers. Due to the fact that these materials are highly compressible and highly impermeable they are sometimes referred to as "super-compactable" [Tiller and Li, 2000].

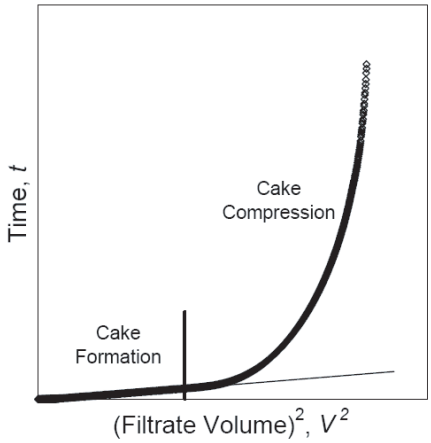

Figure 3.8: Non-traditional filtration behaviour [Stickland, 2005]

The issue with non-traditional filtration behaviour is that it is difficult to extract compressibility and permeability parameters from a single pressure filtration run with the traditional linearised method. As this method uses the slope during cake formation which is short, the results can be inaccurate. Furthermore, equilibrium is only reached after extremely long filtration times during which errors can occur such as aging of the sludge, as filtration often is performed at room temperature rather than fridge temperature. The filtration of such materials are thus not run to completion. As a consequence hereof a linearised cake compression theory from Landman and White (Landman and White) is employed to extrapolate the cake compression data to obtain the equilibrium volume fraction (ϕ_∞) and D(ϕ_∞) (cf. Enclosure III).

Chapter 4

Materials and Methods

4.1 Preparation of Alumina Suspensions

The alumina (APK-30) (Aluminum Oxide 99.99%, Al_2O_3, Sumitomo Shoji Chemicals Co., Tokyo, Japan) suspensions were prepared according to the method utilized by Zhou (2000). The powder was mixed with a 0.01M KNO_3 (Potassium nitrate 99.0%, BDH Laboratory Supplies Poole, England) solution, with a conductivity of about 1500 μS/cm, and the desired volume fraction prepared. The mixing was performed with a spatula and the suspensions were mixed until all particles were wetted. After mixing, the suspension was sonicated at 200 Watt (Branson Sonifier 450) for 2 minutes to break up any lumps. The pH was adjusted, to a value of 5 (PHM 92 pH meter, Radiometer Copenhagen, Denmark) where the suspension was fully dispersed, and it was then further sonicated for another minute. The suspension was then allowed to rest for 24 hours to achieve chemical and physical equilibrium. Before measurements, the pH was adjusted to 9.0$\pm$0.1 and allowed to rest for two hours. The acid and base used in the pH adjustment were 1M Nitric Acid (HNO_3, 69%, Merck Pty Limited, Kilsyth, Australia) and 1M Potassium Hydroxide (KOH, Chem supply, Gillman, South Australia). Different volume fractions were obtained by diluting a stock suspension with 0.01M KNO_3 solution and adjusting pH. The volume fraction was determined by weight loss on drying, where the samples were left to dry for 24 hour at 100°C (Lab-line Due-Vac oven, Melrose Park,ILL) (cf. Appendix D).

4.2 Preparation of Sewage Sludge Suspensions

The sewage sludge was a mesophilic anaerobically digested sewage sludge from the eastern treatment plant, Carrum, Victoria (Melbourne Water), collected 27. Aug 2007. It was stored at 4°C to avoid bacterial degredation. The sewage sludge had an initial volume fraction of 0.0097 v/v, pH=7.09, and a conductivity of 6.69 μS/cm. Higher volume fractions were attained by centrifugation (Jouan CT 422) at 4°C where the water was removed after centrifugation.

4.3 Preparation of Dual-Polymer Flocculated Alumina Suspensions

Alumina suspensions were flocculated with polyacrylic acid and a polyacrylamide polymer.

Alumina suspensions with an electrolyte concentration of 10^{-3}M KNO_3 were prepared according to Section 4.1. Diluted suspensions for flocculation were prepared by diluting the stock suspension to a 2.5 w/w% suspension with 10^{-3}M KNO_3 solution. The diluted dispersions were then sonicated for 1-2 min and left overnight to reach chemical equlibrium and the pH was adjusted to 7.29 $\pm$ 0.1. The conductivity was 183$\pm$12 μS/cm.

4.3.1 Preparation of Polymer Solutions

A 0.1% wt solution of polyacrylic acid (PAA 250,000 g/mol, Aldrich Chemical Company, USA) was prepared by dissolving PAA in demineralised water. The solution was stirred 1 hour, to ensure complete dissolution of the polymer, using a magnetic stirrer.

A 2 g/L stock polymer solution of non-ionic polyacrylamide (Magnafloc LT20, ca. 10-15 mill. g/mol) was produced by dissolving 0.2 g of Magnafloc LT20 (Allied Colloids, Australia) in 2 mL of ethanol (Merck Pty Limited, Kilsyth, Australia) and diluting with 98 mL of demineralised water. To ensure mixing, the solution was shaken vigorously for 1 minute and then left on an end-to-end rotating table, covered in aluminum foil to avoid UV degradation of the polymer, overnight. 1 hour before flocculation, a 0.01% wt diluted solution was produced by diluting the stock solution as follows: 25 mL of stock solution was transferred to a beaker and mixed with 250 mL of tap water whereupon 225 mL of demineralised water was added and the solution was stirred 1 hour using a magnetic stirrer.

4.3.2 Flocculation Procedure

The flocculation was preformed in a baffle reactor (Figure 4.1). The 2.5 w/w % suspension was decanted to the baffle reactor and the suspension was mixed for minimum five minutes at 500 rpm (Heidolph, RZR 2020 control) to achieve a homogeneous mixture. Prior to flocculation, the speed was reduced to 330 rpm. PAA was first added, through the inlet tube with a plastic syringe, and left to mix for 1 minute before the second polymer Magnafloc LT20 was added to the suspension and further 20 sec of mixing was performed. The suspension was left for flocs to settle and the settling rate was determined using a stop watch. After the flocs have settled, the stirrer and the baffles were removed from the suspension and the supernatant was gently removed using a syringe.

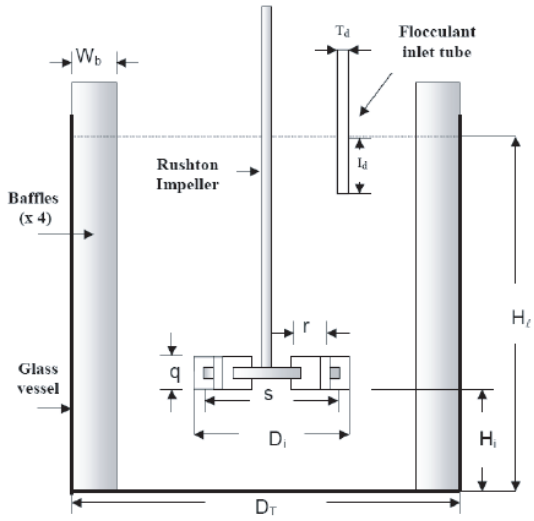

Description	Symbol	Dimensions (mm)
Tank diameter	D_T	87
Liquid height	H_l=D_T	87
Baffle width (4 baffles)	W_b=D_T/10	8.7
Impeller diameter (6 blades)	D_i=D_T/3	29
Impeller height from tank base	H_i=D_i/3	29
Impeller blade width	Q=D_i/5	5.8
Impeller blade length	R=D_i/4	7.25
Length of blade mounted onto disk	r_d=D_i/8	3.625
Diameter of disk	S=D_i-2(r-r_d)	21.75
Flocculant inlet tube diameter	T_d	4.37
Flocculant inlet tube diameter	I_d	15.6

Figure 4.1: Flocculation setup with baffle reactor and Rushton impeller [Hulston, 2005].

4.4 Density, Conductivity and Size Measurements

The density was measured using a 50 cm^3 density glass bottle where the lid contained a small hole in the middle to allow excess fluid to exit (Duran). The volume of the glass bottle was determined using water at a known temperature. The glass bottle was then filled with the sample. The mass of the sample together with a known mass fraction of the liquid sample enables calculation of the solid density of the particles (cf. Appendix D). Suspension conductivity was measured with (IONcheck65, Radiometer analytical). Particle size was measured with a Mastersizer (Mastersizer2000, Hydro 2000G, Malvern Instruments).

4.5 Scanning Electron and Optical Microscopy

Before Scanning electron microscopy (SEM, FEI Quanta 200 FEG) was utilised, the samples were gold coated with 10 nm of gold (1 minute of coating) using a Gold sputter mini coater (Dynavac, Australia) with associated vacuum pump (Edwards Model RV3, England). The optical microscopy used was Olympus (U-CMAD-2, Japan).

4.6 The Vane Technique

Shear yield stress and viscosity was measured with a vane on a Haake Viscometer (HAAKE VT550, Kahlsruhe, Germany) and an Advanced Rheological Expansion System rheometer (ARES, TA. Inc., New Castle, USA). The different vane dimensions employed are shown in Table 4.1.

Table 4.1: The different vane geometries employed to measure the shear yield stress of a suspension.

Vane	Height (H) $[\cdot 10^{-3}$ m]	Diameter (D_v) $[\cdot 10^{-3}$ m]
1	15.145	9.96
2	20.2025	20.2125
3	30.1725	25.02
4	50.0	25.0
5	75.0	25.0
6	100	50
7	200	100

The yield stress measurement was performed by loading the sample in a suitable container and shearing it well to avoid potential thixotropic effects that would influence the results. The vane is lowered into the suspension until the suspension covers the vane, plus a further distance corresponding to the vane radius. Then a shear rotation rate of 0.2 Ω $[\frac{1}{min}]$ was applied and the yield stress was calculated (cf. Appendix A) .

4.6.1 Procedure for Measuring High Shear Yield Stress

Due to the difficulty of preparing high volume fraction suspensions, filtration was utilised. Two instruments were used to measure the yield stress of the resulting volume fractions; namely the Haaake viscometer and the ARES rheometer. The ARES was used to measure the higher yield stresses as the Haake viscometer has a limiting torque of about 30,000 μNm corresponding to a stress of about 10,000 Pa when the smallest vane (vane 1) is employed. The ARES has a limiting torque of 100,000 μNm corresponding to a stress about 35,000 Pa (vane 1). The yield shear stress measured with the Haake viscometer could be measured directly in the filtration rig whereas the suspension had to be placed in a special cup when measured with the ARES rheometer as the vane is fixed in these measurements and the cup is rotating. To avoid disturbance of the sample caused by immersion of the vane, the vane was left in the sample 2 minutes prior to the measurement.

4.7 Equilibrium Pressure Filtration

A piston rig that uses a linear encoder to monitor piston height was used.

The piston was greased and set equal to the initially desired sample height. The rig was assembled using a membrane and the membrane wetted. The sample was then loaded in the filtration rig and the filtration rig closed and lowered to the correct position. The desired pressures were chosen and the airflow connected. The final volume fraction was determined by weight loss on drying.

4.8 Centrifugation

Clear, round bottomed, polycarbonate centrifuge tubes (height: 103 mm, inside diameter: 26.5 mm) (Naglene) were employed for the concentration profile technique. A constant radial stress distribution is required which was gained by flattening the bottom of the centrifuge tubes with epoxy resin. The measurement was then performed by measuring the initial height of the tubes. As the epoxy resin was not completely even, the height was determined with a steel ruler (precision 0.1 mm, Digital Caliper) from an average value of six measurements round the tube. The tubes were then loaded with sample at a desired volume fraction and initial sample heights between 7-50 mm. The alumina suspensions were tested at 20°C, whereas the sludge was run at 4°C to prevent bacterial growth. The samples were run until equilibrium was obtained, which was ensured by measure of the bed height until constant. As the height was not even an average of the height measured six places along the tube was calculated. When the centrifugation was complete the final sample was divided into about 10 slices. Each sub-sample was removed by scraping the sample from the tube using a flat spatula fixed at the desired sample height and the volume fraction for the sub-sample was found by weight loss on drying (Figure 4.2).

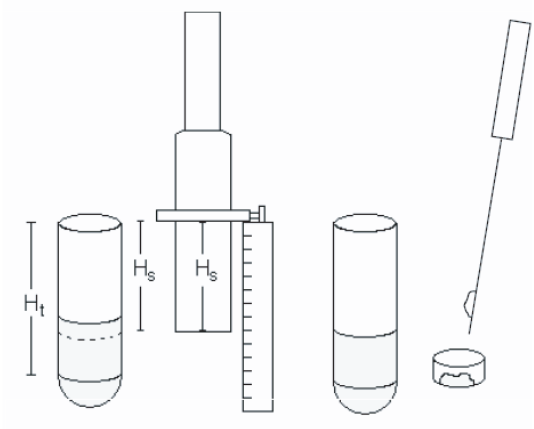

Figure 4.2: Schematic overview of the concentration profile technique after centrifugation. H_t is the total height of the tube and H_s is the height at which the scrape is taken.

4.9 Equilibrium Batch Settling

A concentration below the gel point was chosen. Cylinders with different initial suspension heights were left to settled and the sediment-liquid interface heights were measured until equilibrium was reached. The final height was then measured and the resulting volume fraction and the compressive yield stress calculated (cf. Enclosure II).

Chapter 5

Suspension Rheology of an Ideal Coagulated Particulate Suspension

In this chapter the rheology of a coagulated alumina suspension will be presented. The aim of this chapter is to compare the yield stress in compression and shear. The shear yield stress data have been obtained employing the vane technique. The limitations, using the vane technique on a Haake Viscometer, have been evaluated. Prediction of the shear yield stress will be compared with experimental data. Compressive yield stresses were determined by means of equilibrium pressure filtration, centrifugation, and batch settling. Additionally, the filtration behaviour of the coagulated alumina suspension will be presented.

5.1 Rheological Behaviour of the Alumina Suspension

Alumina is white spherical particles that when mixed with a potassium nitrate solution make up a gritty suspension. After the suspension was sonicated at pH 5 the particles were dispersed and the suspension appeared smooth with no signs of flocs. The particles had a density of 3990 kg/m^3. The zeta potential of the suspension decreases with increasing pH and the IEP was estimated to be approximately at pH 8.9-9 (cf. Figure 5.1).

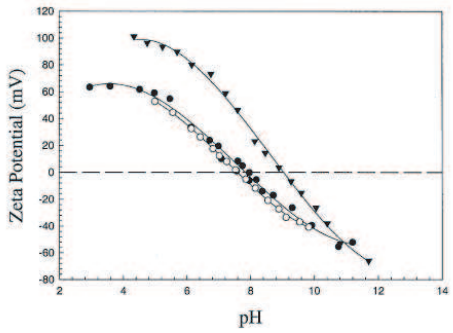

Figure 5.1: The zeta potential of alumina (▼), zirconia (●) and titania (○) as a function of pH [Zhou, 2000].

Figure 5.2 illustrates a scanning electron microscopy image that shows clusters of alumina particles in their coagulated form at the IEP.

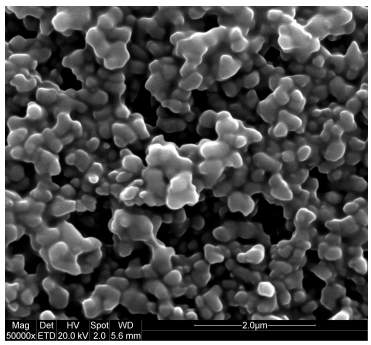

Figure 5.2: Scanning electron microscopy photo of an alumina suspension (pH 9.0±0.1, 10^{-2}M KNO_3).

From the supplier, the particle size is stated to vary from 0.23-0.43 μm with a mean of 0.31 μm. In Figure 5.3 the measured size distribution is shown. The particle size varied from 0.14-0.83 μm with a non-normalised distribution. The mean particle size was 0.30 μm and 74 % were in the range from 0.21-0.48 μm. This is in agreement with the values stated from the supplier.

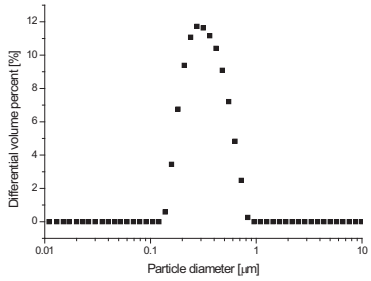

Figure 5.3: The particle size distribution of alumina particles.

5.1.1 Uncertainty Associated with Employing the Vane Technique on a Haake Viscometer

The flow properties of a suspension can be measured with the vane technique introduced by Nguyen and Boger (1983) from soil mechanics (cf. Appendix A). The validity of the technique will be considered. In earlier work, different authors have compared the shear yield stress values resulting from using different vane dimensions. The conclusion has been that the dimension, of the vane used, is insignificant [Liddell and Boger, 1995; Nguyen and Boger, 1983; James *et al.*, 1987]. However, these comparisons have only been made between the conventional employed vane dimensions, which are approximately up to 50 mm in height and 30 mm in diameter.

The accuracy of a measurement is determined by the vane dimension employed. Different vanes were used at different volume fractions. To obtain high accuracy at low volume fraction two large vanes were additionally produced. They had diameters and heights of 50 and 100 mm and 100 and 200 mm, respectively. By use of Equation (A.2) (Appendix A) the stress range of the different vane dimensions can be calculated, when the measurable torque range for the viscometer is known.

The results suggest that all the vanes except vane 1 can be used to measure low shear stresses down to approximately 6 Pa (cf. Table I.1 Enclosure I). It is assumed that the highest measurable torque is the most precise. In order to verify whether the shear yield stress calculated from the lower torque is in agreement with the shear yield stress calculated from the higher torque, comparisons between the shear yield stress, obtained by using different vane geometries on the Haake viscometer, were performed. The shear yield stress of the alumina suspension as a function of volume fraction is illustrated in Figure 5.4.

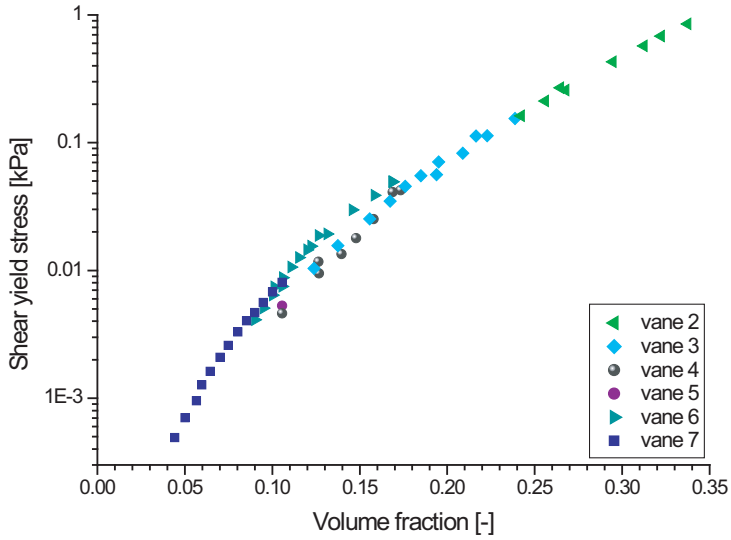

Figure 5.4: Shear yield stress of alumina suspension (pH 9.0±0.1, 10^{-2}M KNO_3) as a function of volume fraction obtained using different vane geometries on a Haake Viscometer.

The standard deviation calculated from three repeat measurements of the shear yield stress was insignificant (error $\leq 4\%$) and therefore not shown on the graph. In the shear yield stress range from about 4-50 Pa overlap is observed. Disagreement arises between shear yield stresses calculated from a lower torque using vane 3,4, and 5, and shear yield stresses calculated from a high torque obtained by using vane 6 and 7. The error, on the repeated shear yield stress measurement, was insignificant and does not make up for the difference in the shear yield stresses. The error on the measured torque values was determined. This was done by utilising least square linear regression on the apparent linear part of the stress vs. time the curve, where the suspension yields. A line was fitted through the points and the difference between the points and the fitted line was determined (cf. Figure I.1 Enclosure I). From this method it was estimated that a minimum torque of 3,400 μNm is valid for measuring on the Haake Viscometer. A torque $\leq$ 3,400 μNm leads to a $\geq 6\%$ lower shear yield stress value. The new minimum stress limit for the different vanes can be seen in Enclosure I (cf. Table I.3).

5.1.2 Shear Yield Stress of the Alumina Suspension

The shear yield stress of a suspension is determined by the surface chemistry of the suspension. At low volume fractions, at and above the gel point, aggregate overlap results in a reasonable weak three dimensional network structure. As the number of aggregates per unit volume of the suspension increases, aggregate interactions are increased. The number of attractive forces

per unit volume of the suspension is increased and thus the force required to break down this network. An ideal suspension, is expected to form a crystal-like close packing structure near the maximum packing fraction. Based on these expectations, the strength of the three dimensional network structure formed in a suspension is expected to increase with an increasing rate as the volume fraction increases.

Based on knowledge of the surface chemistry of a suspension Kapur *et al.* (1997) proposed a theoretical model which was further modified by Scales *et al.* (1998). At the IEP, where the repulsive electrostatic forces are non-existent, the model can be reduced to Equation (5.1) and can be used to predict the shear yield stress of the alumina suspension.

$$\tau_y = 0.011 \cdot \frac{A\phi K(\phi)}{\pi D^2 d} \tag{5.1}$$

where A is the Hamaker constant, D is the particle separation distance, d is the diameter of the particles, and $K(\phi)$ is the mean coordination number which can be expressed by the Gotoh's equation cited by Suzuki *et al.* (1981):

$$K(\phi) = \frac{36}{\pi}\phi, \qquad \phi \leq 0.47 \tag{5.2}$$

In prediction of the shear yield stress of the alumina suspension the Hamaker constant of the suspension was assumed to be $5.3{\cdot}10^{-20}$ J [Hough and White, 1980], d was 0.30 μm, and K(ϕ) is expressed by Equation (5.2). D is by Zhou (2000) calculated to be 2.3 nm from experimental data (Scaled shear yield stress values (τ_y/τ_{ymax}) as a function of the zeta potential were fitted to an equation proposed by Scales *et al.* (1998)).

In Figure 5.5 both the predicted shear yield stress from Equation (5.1) and experimental shear yield stress data are shown on both a linear and a log scale.

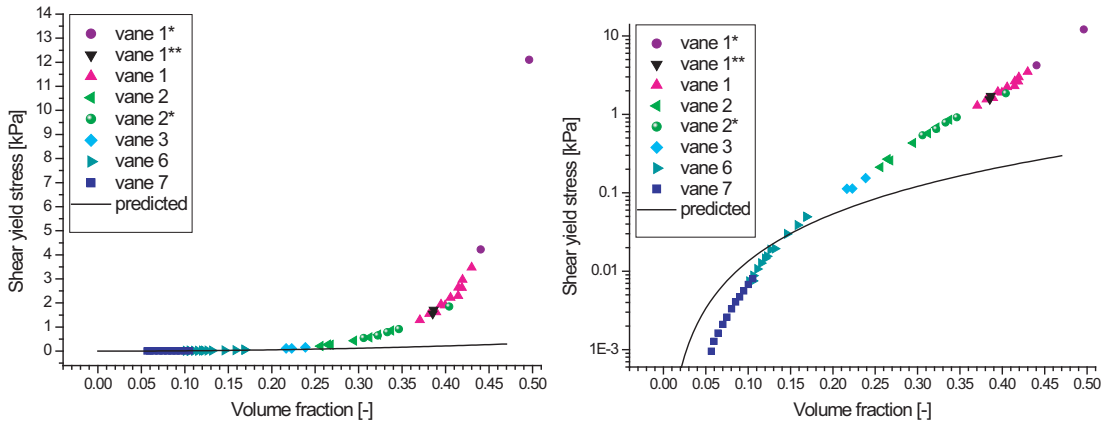

Figure 5.5: Shear yield stress of the alumina suspension (pH 9.0±0.1, 10^{-2}M KNO_3). Symbols marked with * and ** indicate that the samples are concentrated by means of pressure filtration, * indicates that the samples are measured on the ARES rheometer with a vane, and ** on the Haake Viscometer.

The shear yield stress of the alumina suspension increases with an increasing rate with volume fraction, as expected. Agreement between the measured values are observed, as they increase monotonically. Experimental shear yield stress data from 0.9-12,000 Pa have been determined in the volume fraction range from about 0.05-0.43 v/v using five different vanes. High volume

fractions were obtained by filtration and the corresponding shear yield stresses were measured on either Haake Viscometer or the ARES rheometer. The different vane dimensions, measure equipments, and methods for concentrating the suspensions do not seem to affect the shear yield stress measurements, as overlaps of the measured shear yield stress values are observed.

The predicted shear yield stress is not in agreement with the experimental shear yield stress values. At low volume fractions < 0.10 v/v, the predicted shear yield stress is too high. Above a volume fraction of 0.10 v/v the predicted shear yield stress is too low. It appears that the predicted shear yield stress does not account for the rapid increase in particle interactions with volume fraction. Choose of coordination number will have an influence on the predicted shear yield stress, as this predicts the increase of aggregate interactions, as the volume fraction increases.

The shear yield stress data as a function of volume fraction are illustrated on a log plot in Figure 5.6.

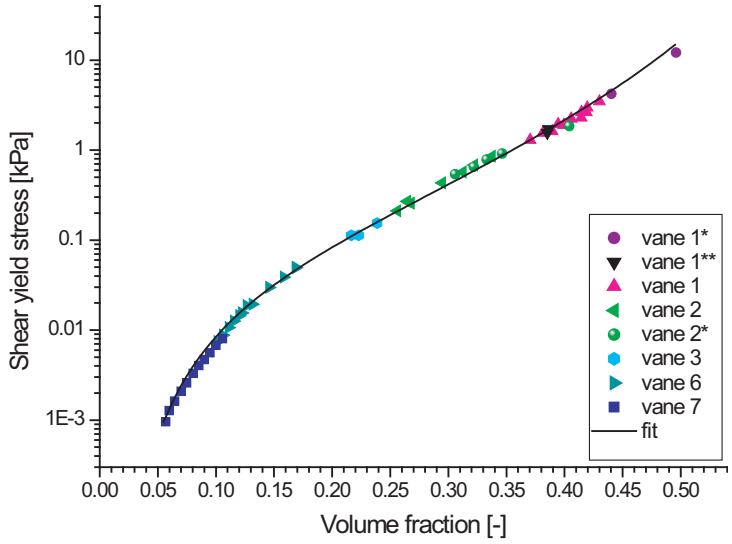

Figure 5.6: Shear yield stress of the alumina suspension (pH 9.0±0.1, 10^{-2}M KNO_3). *, ** indicate that the samples are concentrated by means of pressure filtration. * indicates that the samples are measured on the ARES rheometer with a vane and ** on the Haake Viscometer. The fit is given by Equation (5.3) where a=0.55, b=0.085, k=5, ϕ_g=0.006, and ϕ_{cp}=0.72.

Shear yield stress data have been obtained over four orders of magnitude. The shear yield stresses at low and high volume fractions were the most difficult to determine. At low volume fractions a sample volume of 20 L was required. At high volume fractions, samples were difficult to prepare. These were obtained by filtration. The high shear yield stresses were measured on the ARES rheometer as this has a higher torque limit than the Haake Viscometer. Different shear yield stress values could be obtained from the same sample. Two different measurements of a sample are shown in Figure 5.7.

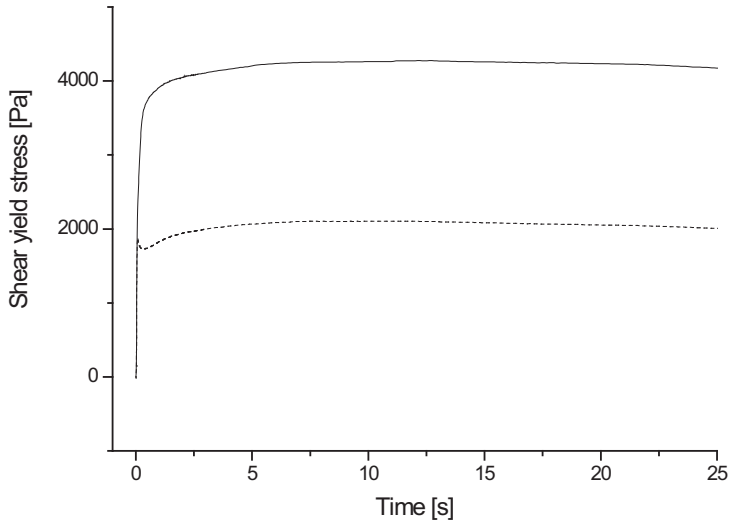

Figure 5.7: The stress of a filtration concentrated alumina suspension (ϕ=0.44, pH 9.0±0.1, 10^{-2}M KNO_3) measured with a vane connected to an ARES rheometer. The solid line is the correct measurement while the dotted line is a result of e.g. air bubbles present in the solution during measurement.

The difference in the development of stress in the two curves is believed to be caused by trapped air bubbles in the suspension, which are difficult to avoid in high volume fraction suspensions. Air bubbles would cause a drop in stress as no resistance would be measured, as the vane reaches an air bubble.

The shear yield stress values in Figure 5.6 can be modelled by Equation (5.3). This functional form is able describe the shear yield stress data with high precision.

$$\text{Yield stress} = \left(\frac{a(\phi_{cp} - \phi)(b + \phi - \phi_g)}{(\phi - \phi_g)} \right)^{-k} \tag{5.3}$$

where ϕ_g and ϕ_{cp} are the theoretical gel point and the close packing volume fraction, respectively, and a, b, and k are fitting parameters. The fitting parameters of the shear yield stress of the alumina suspension are a=0.55, b=0.085, k=5, ϕ_g=0.006, and ϕ_{cp}=0.72. The theoretical gel point and maximum packing fraction are just fitting parameters as well as a,b, and k. If they are compared with the expected volume fractions the suggested theoretical gel point of the suspension is low. The lowest shear yield stress measured at 0.057 v/v is 0.9 Pa, which indicates that the gel point, properly, is close to this value. The maximum packing fraction of mono-dispersed spherical particles is often 0.63 for particles at rest or at low shear rates. A maximum packing fraction of 0.71 v/v is observed at high shear rates [Barnes, 2000] which is in agreement with the theoretical maximum packing fraction of 0.72 v/v.

5.1.3 Viscosity of the Alumina Suspension

The viscosity of the alumina suspension was measured with the vane technique. An increase in shear rate followed by a decrease in shear rate will show if the suspension is thixotropic. A thixotropic behaviour is a decrease in viscosity with shearing time. If the resulting viscosity from the increase and the decrease is alike, the suspension does not show time dependent behaviour. The result for this test is shown in Figure 5.8.

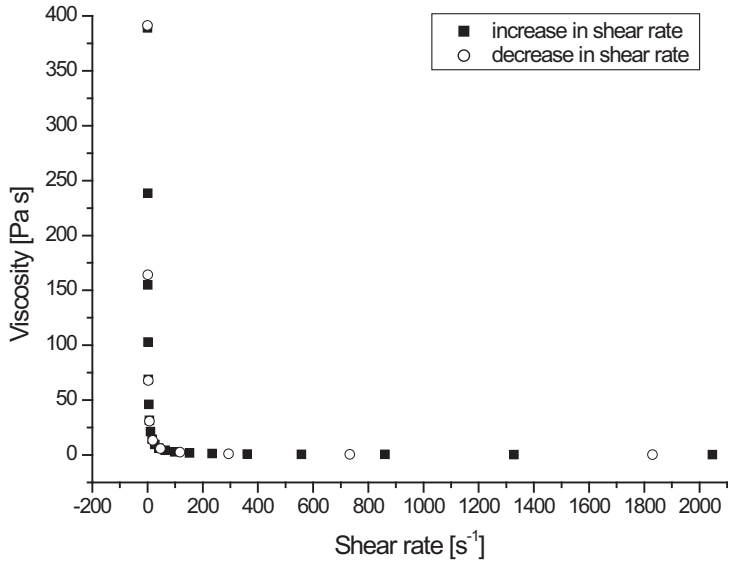

Figure 5.8: The viscosity of a ϕ=0.26 alumina suspension (pH 9±0.1, 10^{-2}M KNO_3) measured with an increase in shear rate followed by a decrease in shear rate.

The viscosity of the alumina suspension decreases with shear rate, which indicates that the suspension is shear thinning. A steep decrease in the viscosity from about 400-1 Pa s is observed with an increase in shear rate from 0-200 s^{-1}. The alumina suspension shows complete recovery of the viscosity, which indicates that the alumina suspension is not thixotropic.

A decrease in viscosity can often be described by the power law model (Ostwald de Waal model): $\tau = m\ \dot{\gamma}^{\,n}$. On a log-log scale this functional form is linear. The viscosity of alumina suspensions a log-log scale is shown in Figure 5.9.

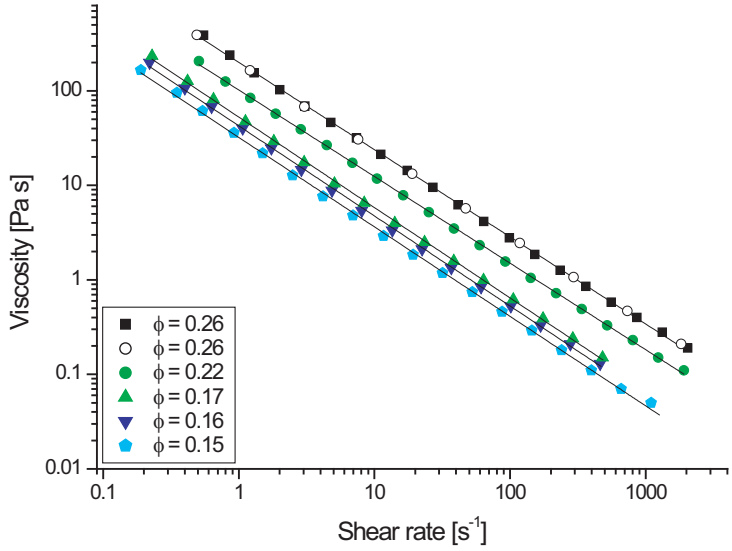

Figure 5.9: Viscosity as a function of shear rate for alumina suspensions (pH 9.0±0.1, 10^{-2}M KNO_3) measured on the Haake Viscometer. ○ indicate the viscosity measure with a decrease in shear rate directly after an increase. η=200.02· $\dot{\gamma}^{-0.9228}$, R^2=0.9997 (ϕ=0.26), η=102.28· $\dot{\gamma}^{-0.9164}$, R^2=0.9998 (ϕ=0.22), η=52.82· $\dot{\gamma}^{-0.9569}$, R^2=0.9997 (ϕ=0.17), η=42.64· $\dot{\gamma}^{-0.9533}$, R^2=0.9996 (ϕ=0.16) and η=32.219· $\dot{\gamma}^{-0.9471}$, R^2=0.9994 (ϕ=0.15).

The viscosity of alumina suspensions, ϕ=0.15-0.26, decreases linearly with shear rate. The viscosity increases with volume fraction. A decrease from about 100-0.1 Pa s is observed in the shear rate range from 0.2-2000 s^{-1}. The power law model has been fitted to the data: η=200.02$\cdot$ $\dot{\gamma}^{-0.9228}$, R^2=0.9997 (ϕ=0.26), η=102.28$\cdot$ $\dot{\gamma}^{-0.9164}$, R^2=0.9998 (ϕ=0.22), η=52.82$\cdot$ $\dot{\gamma}^{-0.9569}$, R^2=0.9997 (ϕ=0.17), η=42.64$\cdot$ $\dot{\gamma}^{-0.9533}$, R^2=0.9996 (ϕ=0.16) and η=32.219$\cdot$ $\dot{\gamma}^{-0.9471}$, R^2=0.9994 (ϕ=0.15). The squared R values indicate that all fits have a high precision and are able to describe the viscosity.

The reason for the decrease in viscosity with shear rate can be explained by the relative importance of convection (shear) vs. Brownian motion. At low shear rates, the suspension has a high Pe number and the Brownian motion is able to maintain or rebuild the structure of the suspension. As the shear rate increases, the particles will rearrange into string like structures (cf. Section 3.2) which eases flow, and hence, a decrease in viscosity is observed. When only the hydronamic forces are in play at high shear rates the suspension will act purely Newtonian.

Instead of considering the viscosity as a function of shear rate, the increase in stress can be viewed (Figure 5.10).

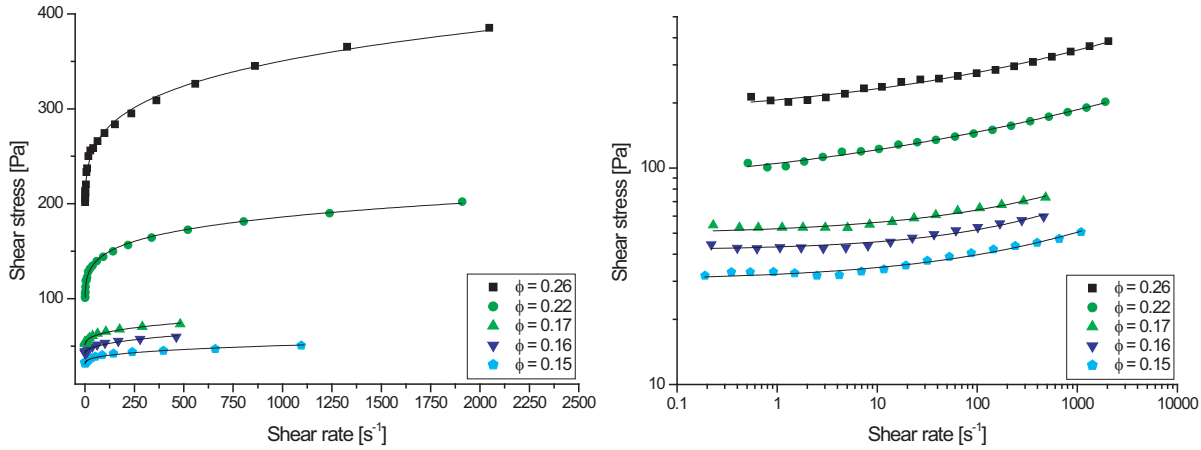

Figure 5.10: Shear stress as a function of shear rate of alumina suspensions (pH 9.0±0.1, 10^{-2}M KNO_3) with Herschel and Bulkley fit (cf. Table 5.1).

The increase in shear stress as a function of shear rate of the alumina suspensions, ϕ=0.15-0.26, is illustrated both on a linear and a log-log scale. The shear stress increases rapidly at the low shear rates and approaches an asymptotic value at higher shear rates. Shear stress in the range from 30-400 Pa is observed in the shear rate range from 0.2-2000 s^{-1}. On a log-log scale the increase appears linear. The shear stress increases with volume fraction and asymptote at about 400 Pa for ϕ=0.26 and about 40 Pa for ϕ=0.15.

Shear stress vs. shear rates data can be extrapolated to a zero shear rate which will give an indication of the shear yield stress value of the suspension. This has been done by fitting the data in Figure 5.10 to the Herschel and Bulkley Equation (3.3) and Casson's Equation (3.4) (cf. Section 3.2). The fitting parameters are listed in Table 5.1 together with the measured shear yield stress values, at the respective volume fraction (cf. Section 5.1.2).

Table 5.1: Fitting parameters to shear rate vs. shear stress data for alumina suspensions and the measured shear yield stress.

ϕ	τ	Herschel and Bulkley				Casson		
[-]	[Pa]	τ_{HB}	k	m	R^2	τ_C	η_∞	R^2
0.26	212	169	37.50	0.2281	0.9948	221	0.013624	0.9878
0.22	113	75	29.75	0.1902	0.9983	114	0.0084	0.9798
0.17	49	49	3.11	0.3363	0.9950	53	0.0040	0.9891
0.16	39	42	1.5093	0.4150	0.9899	43	0.003648	0.9902
0.15	30	30	2.097	0.3289	0.9950	33	0.00205	0.9849

From the results in Table 5.1 it can be observed, that the extrapolated shear yield stress from the Herschel and Bulkley fit, at ϕ=0.26, is 169 Pa and 221 Pa from the Casson fit. Compared to the measured value of 212 Pa the Herschel and Bulkley fit predicts a lower shear yield stress and the Casson fit predicts a higher and more correct shear yield stress. The same case is observed at ϕ=0.22, where the Herschel and Bulkley fit predicts a value of 75 Pa and the Casson fit predicts a value of 114 Pa compared to the measured value 113 Pa. At the volume fractions from ϕ=0.15-0.17 the extrapolated values are in agreement with the measured shear yield stress values. The validity of the extrapolated shear yield stress values can be ascribed to the presence of low shear rate data. In Figure 5.10 the lowest shear rate measured, at the volume fractions ϕ=0.26 and ϕ=0.22, was 0.5 s^{-1} and the first number of points are associated with error. At the lower volume fractions (0.15-0.17 v/v), shear rate data down to 0.2 s^{-1} could be measured. It can thus be concluded, that extrapolation of shear rate vs. shear stress data to a zero shear rate to determine the shear yields stress, can be misleading if low shear rate data are not present or associated with error. The R^2 value of the fits indicates that the Herschel and Bulkley fit has the highest precision as these values are closest to 1. From this it can be concluded that the R^2 value does not give an indication of the validity of the estimated shear yield stress as the Herschel and Bulkley fit estimated the most erroneous shear yield stress values for the suspensions with the volume fractions ϕ=0.26 and ϕ=0.22.

Measurements of viscosity using parallel plates on a stress controlled rheometer (AR-G2) were also attempted, but without success as the rheometer showed overshoot.

5.1.4 Compressive Yield Stress of the Alumina Suspension

Equilibrium pressure filtration was used to achieve the highest compressive yield stresses. The compressive yield stress determined from both stepped and single pressure filtration is illustrated, on both a log and linear scale, in Figure 5.11 as a function of volume fraction.

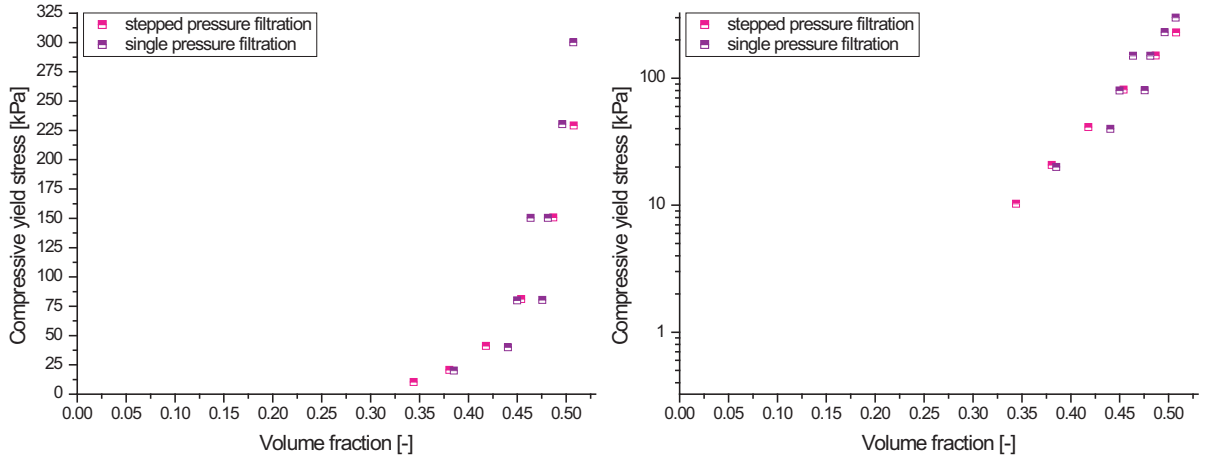

Figure 5.11: Stepped and single equilibrium pressure filtration of the alumina suspension (pH 9.0±0.1, 10^{-2}M KNO_3).

The compressive yield stress increases in an exponential manner on a linear scale with volume fraction. On the log scale an almost linear increase is observed. Compressive yield stresses in the range from 0.34-0.51 v/v were obtained by applying pressures in the range from 10-300 kPa. Scattering of the points are observed, but the results from single and stepped pressure filtration are in agreement with each other as expected.

The broadest range of compressive yield stresses has been obtained by means of centrifugation. The compressive yield stress determined from this technique is in Figure 5.12 shown on both a log and a linear scale.

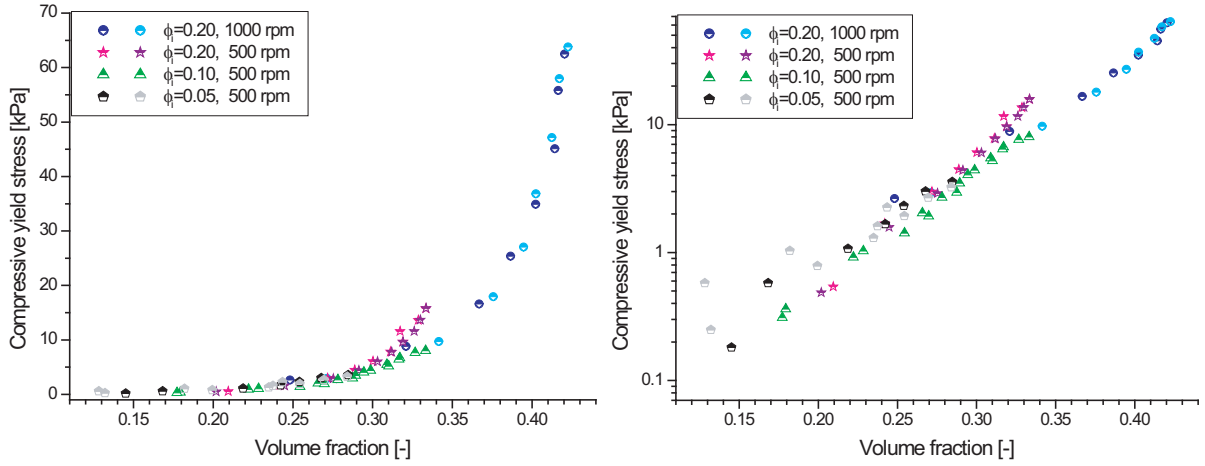

Figure 5.12: The compressive yield stress of the alumina suspension (pH 9.0±0.1, 10^{-2}M KNO_3) is determined by centrifugation. Two samples are run for a given speed and initial volume fraction (ϕ_i).

The compressive yield stress increases as a function of volume fraction. As was the case for the filtration results, the compressive yield stresses from centrifugation increases in an exponential manner and on a log scale the increase appears linear. From applying pressures, in the range from 0.2-64 kPa, volume fractions from 0.12-0.42 v/v resulted. Compressive yield stress data from eight different samples were obtained. The determined compressive yield stress data are overall in agreement with each other. Deviating points are observed at the lowest pressures (0.2-1

kPa) and at pressures around 10-20 kPa from the samples centrifuged at 500 rpm with an initial volume fraction, ϕ_i, at 0.20 v/v.

Centrifugation equilibrium was reached after approximately 24 hours. Errors associated with using centrifugation and the concentration profile technique are sampling errors and that equilibrium may not have been reached. The samples, centrifuged at 500 rpm with ϕ_i=0.20 with deviating points around 10-20 kPa, are expected not to have reached equilibrium as lower volume fractions than expected is observed at the highest pressures. It can be difficult to scrape out the layers in the bed. Furthermore, an uneven bed height at the top is often observed. The results, of samples run at the same conditions, are in agreement except for the samples run at 500 rpm with ϕ_i=0.05, where scattering is observed. Sampling errors are assumed to be the main reason for this disagreement which is expected when a low initial volume fraction and a low centrifuge speed are employed. A technique to minimise sampling errors could be employing centrifugation tubes with a mobile bottom. Division of the bed, by pushing up the bed and scraping off the desired layer, could then be done. This technique would be more precise compared to measuring out the depth and scraping out the layers which have been done.

Batch settling tests were performed in order to obtain compressive yield stress data near the gel point. The compressive yield stresses obtained from batch settling can be seen in Figure 5.13 together with the compressive yield stresses determined from centrifugation and filtration.

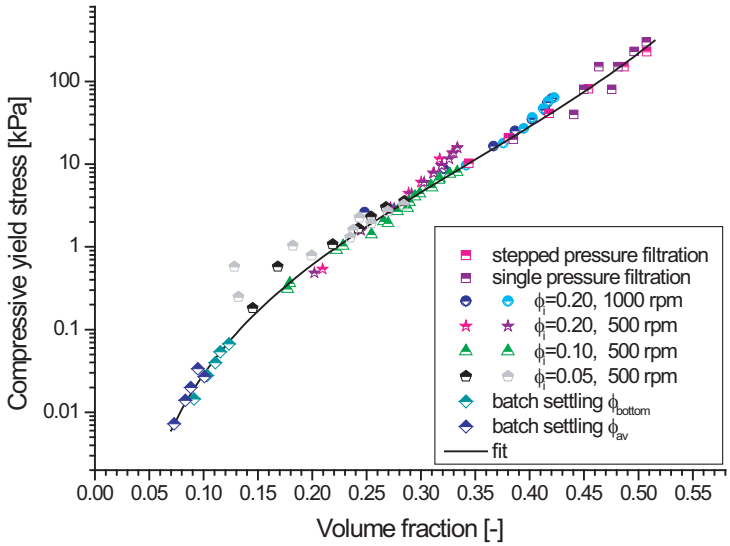

Figure 5.13: The compressive yield stress of the alumina suspension (pH 9.0±0.1, 10^{-2}M KNO_3) from equilibrium pressure filtration, centrifugation, and batch settling tests. The data are fitted to Equation (5.3) with a=0.13, b=0.43, k=4.2, ϕ_g=0.006, and ϕ_{cp}=0.72.

Compressive yield stress data increases from 0.007-300 kPa in the volume fraction range from 0.07-51 v/v. Complete overlap is observed between data from the samples centrifuged at 1000 rpm and the equilibrium pressure filtration data. Comparing the centrifugation data obtained at 500 rpm with ϕ_i=0.20 and ϕ_i=0.10, the data with ϕ_i=0.10 appear to confirm the trend suggested by equilibrium pressure filtration data and the data from the samples centrifuged at 1000 rpm. The data with ϕ_i=0.20 centrifuged at 1000 rpm appear not to have reached equilibrium as the high volume fraction data deviate from the trend in a similar way as were the case for the samples

with ϕ_i=0.20 centrifuged at 500 rpm. At around 0.25-0.30 v/v overlap and agreement is observed between the compressive yield stress data determined from seven different samples.

Two data points are calculated for each batch settling test. The first is the average pressure and the average volume fraction in the bed. The second is the pressure and the volume fraction at the bottom of bed (cf. Enclosure II). The data, calculated from the two different methods, are in agreement with each other. The data estimated at the bottom of the bed are expected to be associated with less error compared to the average values. The bed in the batch settling tests appeared to have a steady final height after about 24 hours. In order to be able to compare the different compressive yield stresses they have to be obtained in the same time frame, as time effects can change the results. The batch settling tests were further left to settle for 85 days. After this time period it could be observed that the samples had undergone creep, which means that the bed has been densified by bonds breaking up and reforming. This further consolidation of the suspension increased the final volume fraction up to 0.02 v/v.

The compressive yield stresses from the batch settling tests determine the compressive yield stress fit in the volume fraction range from 0.15-0.22 v/v where that data are associated with uncertainty. Lack of batch settling results could lead to the conclusion that the compressive yield stress data can be fitted to a linear fit on a log scale. In Figure 5.13 the fit of Equation (5.3) to the compressive yield stress data can been seen. The fitting parameters of the fit is given by: a=0.13, b=0.43, k=4.2, ϕ_g=0.006, and ϕ_{cp}=0.72. The fit describes the compressive yield stresses, in the investigated pressure range, well.

5.1.5 Comparison between Shear and Compressive Yield Stress for an Alumina Suspension

All the compressive and shear yield stress data, can be seen in Figure 5.14, as a function of volume fraction with their respective fit.

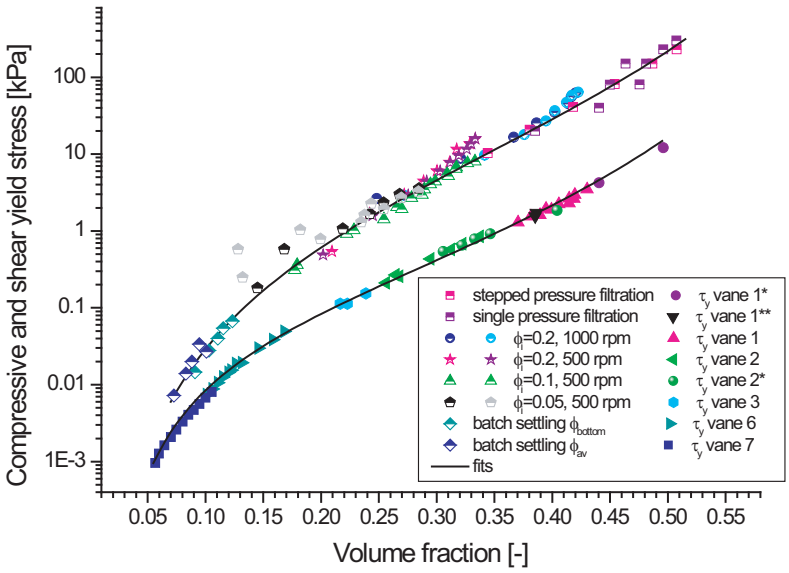

Figure 5.14: The compressive and shear yield stress of an alumina suspension (pH 9.0±0.1, 10^{-2}M KNO_3) as a function of volume fraction.

Yield stress data have been obtained over five orders of magnitude, $9{\cdot}10^{-4}$-300 kPa, in the volume fraction range from 0.05-0.51 v/v. The compressive and shear yield stresses approach each other as the volume fraction decreases, as expected, with the smallest ratio observed closest to the gel point. Yield stresses at higher volume fractions than 0.51 v/v could not be obtained. Shear yield stress data would be difficult to determine above this volume fraction. At the highest concentrations measured, the suspension was almost behaving as a solid material, which "crumbled", and inserting the vane without disturbing the sample would be difficult.

The ratio between shear and compression has been determined by employing the two fits describing the shear and compressive yield stress data (Figure 5.15).

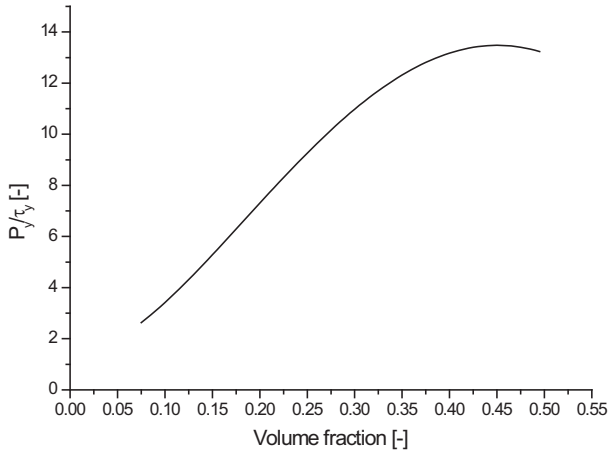

Figure 5.15: Ratio between compressive (P_y) and shear (τ_y) yield stress of the alumina suspension (pH 9.0±0.1, 10^{-2}M KNO_3) as a function of volume fraction.

The P_y/τ_y ratio observed for the coagulated alumina suspension is not independent of volume fraction and increases from about 2-14 with volume fraction, until a volume fraction of about 0.40 v/v is reached. At this concentration a plateau appears to be reached. From the expected behaviour of $P_y(\phi)$ and $\tau_y(\phi)$, the ratio is expected to start decreasing again as the volume fraction approaches the maximum packing fraction.

The ratio of the coagulated alumina suspension estimated by Zhou (2000) was 14. Compared to the fact that only volume fractions above 0.20 v/v were investigated, the two estimated ratios are in agreement. The rapid increase Zhou (2000) observed in the ratio above 0.40 v/v is though not observed. Compared to the results observed by Channel and Zukoski (1997) the ratio is lower. A different suspension preparation method, and method to measure the shear yield stress, can have an influence on this. Dispersion of the suspension was by Channel and Zukoski (1997) obtained by high shear mixing. Sonicating the suspensions was performed in this work and by Zhou (2000). The use of sonication is expected to produce a more uniform suspension consisting of primary particles. If high shear mixing fails to break up lumps of particles, this would lead to a suspension with a higher average particle size and a lower particle interaction number per suspension volume. The consequence of this would be a lower shear yield stress value. Leong *et al.* (1995) has compared the effect of these two preparation methods on the shear yield stress value of a zirconia suspension. An almost halving of the shear yield stress was observed, at the IEP, by use of high shear mixing instead of sonication. τ_y was by Channel and Zukoski (1997) determined indirectly by extrapolation of low shear rate vs. shear stress data, measured on a

rate controlled oscillatory rheometer, to a zero shear rate. This technique requires that low shear rate data are present and wall slip in the measurements is avoided. These errors can lead to lower misleading shear yield stress values, which was observed for some of the extrapolated values determined in Section 5.1.3 (Table 5.1).

5.1.6 Equilibrium Pressure Filtration

In order to measure the high shear yield stresses at high volume fractions, which were difficult to prepare, equilibrium pressure filtration was employed to concentrate the suspensions. Eight different filtrations at six different pressures can be seen in Figure 5.16.

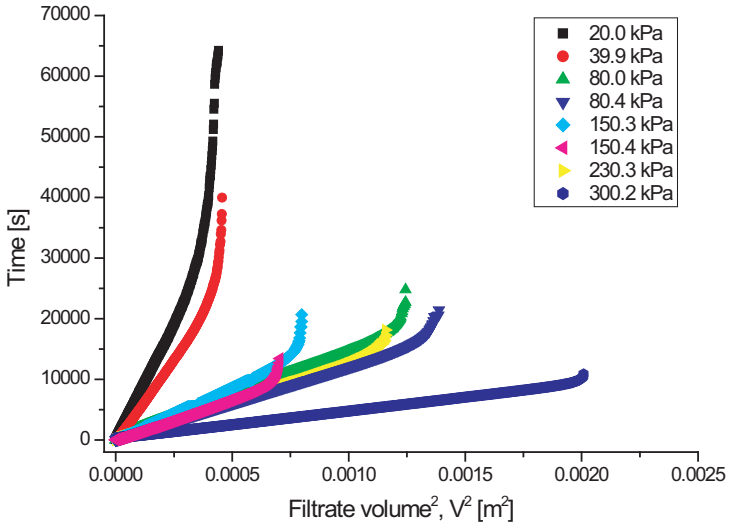

Figure 5.16: The filtration behaviour of the alumina suspension (pH 9±0.1, 10^{-2}M KNO_3). Time as a function of the squared specific filtration volume.

Filtrations ar pressures from 20-300 kPa is illustrated with time as a function of specific filtrate volume. A filtration time up to around 65,000 seconds is observed at the lowest pressure, 20 kPa. Shorter filtration times, as a function of increasing pressure, are observed. The typical traditional filtration behaviour, with a long cake formation times and a short cake compression times, is observed for the alumina suspension. At the low pressures, 20-40 kPa, reasonable long cake compression is observed whereas almost no cake compression occurs at 300 kPa. All the filtrations have different starting conditions. The different initial volume fractions and initial heights are listed in Table 5.2.

Table 5.2: Initial (ϕ_0) and equilibrium (ϕ_∞) volume fraction and initial sample height (h_i) for single equilibrium pressure filtration of the alumina suspension (pH=9.0±0.1, 10^{-2}M KNO_3).

P_y [kPa]	ϕ_0 [-]	ϕ_∞ [-]	h_i [mm]
20.0	0.27	0.39	61
39.9	0.31	0.44	67
80.0	0.23	0.45	73
80.4	0.22	0.48	70
150.3	0.31	0.48	77
150.4	0.27	0.46	65
230.3	0.29	0.50	81
300.2	0.22	0.51	65

In order to produce a large filter cake volume for the shear yield stress measurements, reasonable high initial heights and volume fractions have been used. Initial volume fractions from 0.22-0.31 v/v were employed together with initial heights from 61-81 mm. An increase in initial volume fraction and height increases the filtration time. This can be observed by comparing the two filtrations at 80 kPa and 150 kPa where a ϕ_0=0.22 and h_i=70 mm results in faster dewatering than a ϕ_0=0.23 and h_i=73 mm at 80 kPa and a ϕ_0=0.22 and h_i=65 mm results in a faster dewatering than ϕ_0=0.31 and h_i=77 mm at 150 kPa. At the low pressures, 20-40 kPa, relatively long cake compression times are observed. This is a consequence of a high initial solid (ϕ_0=0.27) concentration compared to the resulting volume fraction (ϕ=0.39) and a high initial piston height (h_i=61 mm).

The inverse dewatering rate as a function time is shown in Figure 5.17.

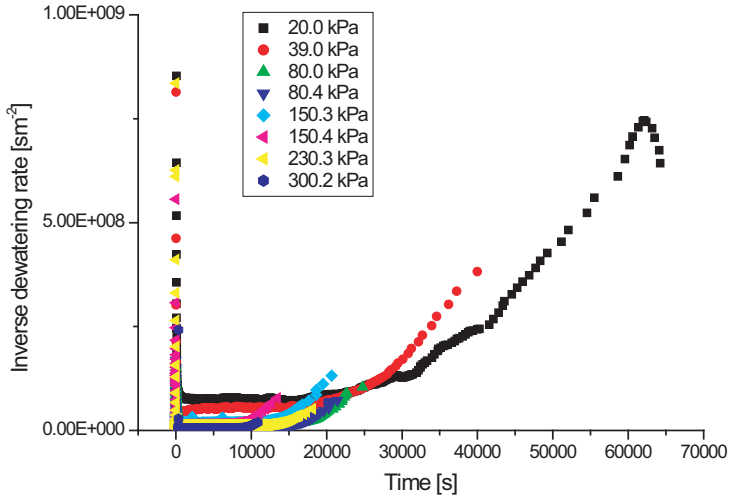

Figure 5.17: Inverse dewatering rate of the alumina suspension (pH 9±0.1, 10^{-2}M KNO_3) as a function of time.

In the cake formation region a constant dewatering rate is observed. The rate increases, with the pressure applied, from $1.4{\cdot}10^{-8}$ m^2/s at 20 kPa to $2.5{\cdot}10^{-7}$ m^2/s at 300 kPa. In the cake compression state decreasing dewatering rate is observed.

From the equilibrium pressure filtrations and batch settling, the hindered settling function of the

coagulated alumina suspension, has been determined. Figure 5.18 shows the hindered settling function as a function of volume fraction

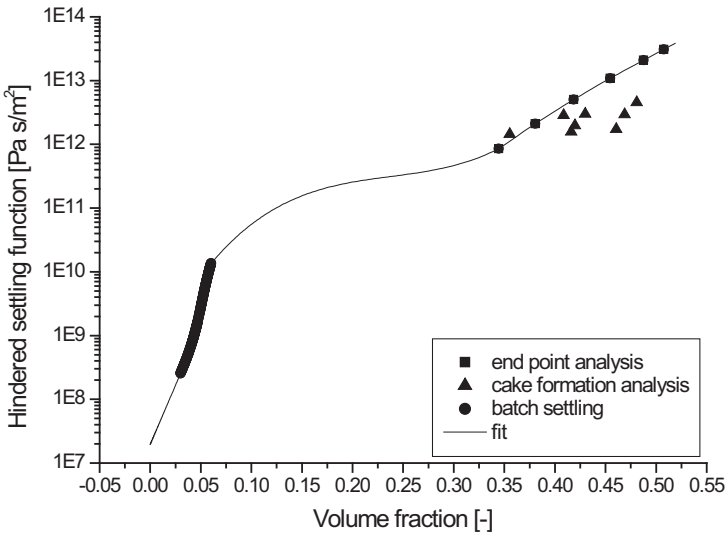

Figure 5.18: The hindered settling function of the alumina suspension (pH 9±0.1, 10^{-2}M KNO_3) as a function of the volume fraction.

The hindered settling function increases with volume fraction from about $1{\cdot}10^{8}$-$3{\cdot}10^{13}$ Pa $\cdot$ s/m^2 in the volume fraction range from 0.03-0.51 v/v. This is an increase of about 5 orders of magnitude. From batch settling test the hindered settling function below the gel point can be calculated (cf. Enclosure III). The two methods to calculated the hindered settling function from the filtration data show overall agreement, considered that scattering in the compressive yield stress values was observed. A curve was fitted through the data points by first estimating the gradient of each point and then fitting a suitable functional form between each of the points.

The hindered settling function from the stepped pressure filtration data has been calculated by an end point analysis by employing Equation (3.6) (cf. Section 3.5). This method requires a similar initial volume fraction in all the different filtrations. This is not the case for single pressure filtrations. Another method, to calculate the hindered settling function from these data, has been used. The method employed, calculates the average hindered settling function, R(ϕ_c), from the cake formation curve, with ϕ_c being the average volume fraction in the cake (Enclosure III). The average volume fraction of the cake is close to the final volume fraction, as the filtrations are dominated by cake formation. In the volume fraction range from 0.07-0.35 v/v no hindered settling function data was determined. In order to determine values in this range lumifuge tests, which measures the sedimentation height as a function of time, could be an option.

The solids diffusivity function includes both the compressive yield stress behaviour and the hindered settling function behaviour. The variation in solids diffusivity with volume fraction of the alumina suspensions is shown in Figure 5.19.

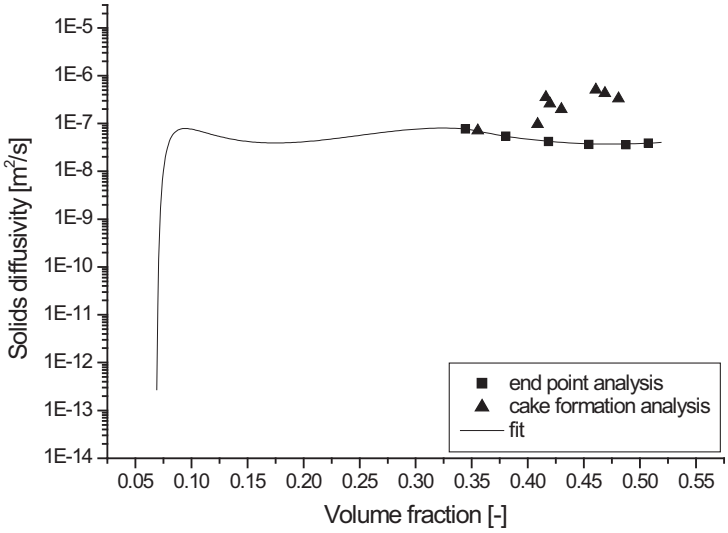

Figure 5.19: The diffusivity of the alumina suspension (pH 9±0.1, 10^{-2}M KNO_3) as a function of the volume fraction.

The diffusivity of the alumina suspension is determined by use of Equation 3.7 (cf. Section 3.5). Above a volume fraction of 0.07 v/v, a constant solids diffusivity at $1{\cdot}10^{-7}$ m^2/s is observed with volume fraction. From the definition of $D(\phi)$, this indicates that $R(\phi)$ increases, with a similar rate as $dP_y(\phi)/d\phi$, with volume fractions. The diffusivity determined from the average volume fraction of the cake is higher than the diffusivity determined from end point analysis, but overall agreement between the two methods is observed.

5.2 Summary of the Rheological Behaviour of the Alumina Suspension

The coagulated alumina suspension exhibited shear thinning behaviour, but did not exhibit thixotropic behaviour. The shear yield stress of the suspension could be predicted from extrapolation of shear rate vs. shear stress data to a zero shear rate, if low shear rate data were present. Lack of low shear rate data resulted in misleading values, and the R^2 value of the fits could not indicate the uncertainty.

The shear yield stress increased in an exponential manner with volume fraction. Shear yield stress values from $9{\cdot}10^{-4}$-12 kPa were obtained in the volume fraction range from 0.05-0.5 v/v. Compressive yield stress was obtained in the range from 0.07-300 kPa in the volume fraction range from 0.07-51 v/v. The ratio between compression and shear increased with volume fraction from 2-14, until a volume fraction of about 0.40 v/v was reached. A plateau was reached between 0.40-0.51 v/v.

The coagulated alumina suspensions exhibited a traditional filtration behaviour with short cake compression times. The hindered settling function increased from $1{\cdot}\ 10^8$-$3{\cdot}\ 10^{13}$ $Pa \cdot s/m^2$ in the volume fraction range 0.03-0.51 v/v. The solids diffusivity was independent of volume fraction above a volume fraction of 0.07 v/v with the value of $1{\cdot}10^{-7}$ m^2/s.

Chapter 6

Suspension Rheology of Non-Ideal Particulate Suspensions

The scope of this chapter is to investigate the behaviour of sewage sludge and a flocculated alumina suspension in compression and shear as a function of volume fraction. In order to do this, a dual-polymer flocculated alumina suspension is produced. The shear properties are characterised with the vane technique and the compressive properties are characterised by equilibrium pressure filtration, centrifugation, and batch settling. The filtration behaviour of the two suspensions is presented to determine whether the suspensions exhibit non-traditional filtration behaviour as expected. The dual-polymer flocculated alumina suspension is expected to exhibit short filtration times compared to the sewage sludge. This would make this system ideal for further characterisation in the attempt to understand non-traditional filtration behaviour.

6.1 Rheological Behaviour of Sewage Sludge

In this section the rheology of sewage sludge and compression will be presented. Furthermore, characterisation of filtration behaviour and determination of filtration parameters R(ϕ) and D(ϕ) of sewage sludge will be presented.

The sewage sludge had a low initial solids concentration (ϕ=0.0097 v/v) and the density of the liquid and the solid was 1.0036 and 1.4715 g/cm^3, respectively. The heterogeneous structure of sewage sludge was visible by eye and a 100 times magnification is shown in Figure 6.1.

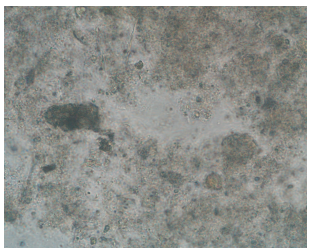

Figure 6.1: Optical microscope picture of sewage sludge, 100 times magnification.

The sewage sludge was concentration by centrifugation to obtain the desired volume fractions. Due to the complex structure of the sewage sludge dilution from higher to lower volume fractions was not possible as the structure of the sewage sludge undergoes irreversible change during centrifugation. After centrifugation and removal of the supernatant the sewage sludge looked jelly-like and the suspension was sheared well before all measurements to ensure reproducible and comparable measurements.

6.1.1 Shear Yield Stress of Sewage Sludge

The shear yield stress, on a log-scale, of sewage sludge as a function of volume fraction is illustrated in Figure 6.2.

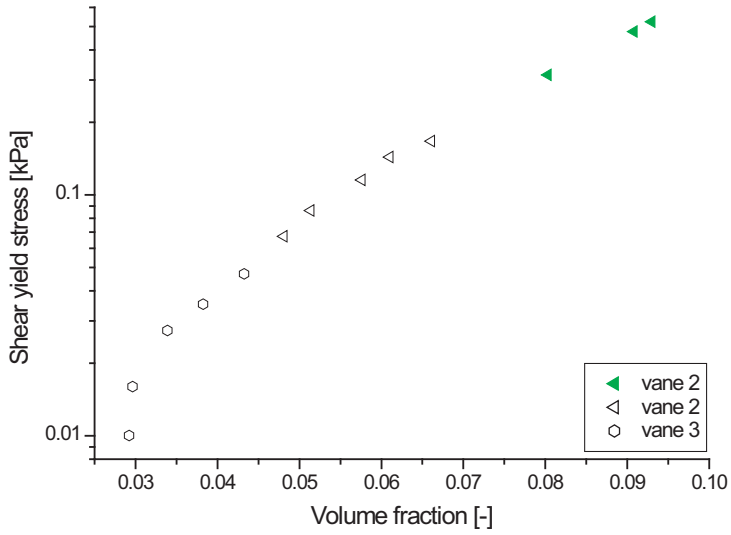

Figure 6.2: Shear yield stress of sewage sludge as a function of volume fraction measured on the Haake rheometer. The empty symbols indicate that the shear yield stress has an error $\geq$ 6%.

Shear yield stresses from 10-500 Pa have been measured in the volume fraction range from 0.03-0.09 v/v. The shear yield stress increases continuously with volume fraction. The reason no shear yield stresses above a volume fraction of 0.09 v/v has been determined is due to the high impermeability of sewage sludge. The highest volume fraction, that could obtained by centrifugation, was 0.09 v/v. In order to obtain higher shear yield stress data filtration could be employed. This issue is that a high final bed is required in order to measure the shear yield stress. The filtration times would be long and the temperature should be kept around 4°C to avoid bioactivity. The lowest measured volume fraction is 0.03 v/v. A small increase in volume fraction around this concentration results in a rapid increase in the shear yield stress. This indicates that the gel point is just below a concentration of 0.03 v/v.

Due to the minimum valid torque estimated in Enclosure I the empty symbols on Figure 6.2 indicate that the shear yield stress values have an error $\geq$ 6%. Ideally, the values would be disregarded but even though they are associated with errors they give an indication of the magnitude of the shear yield stress. The amount of sample is the determining factor in choise of which vane to employ. A reasonable large amount of concentrated sewage sludge is required to measure the shear yield stresses below 190 Pa without large errors.

6.1.2 Viscosity of Sewage Sludge

The viscosity of sewage sludge as a function of shear rate is shown on a log-log scale in Figure 6.3.

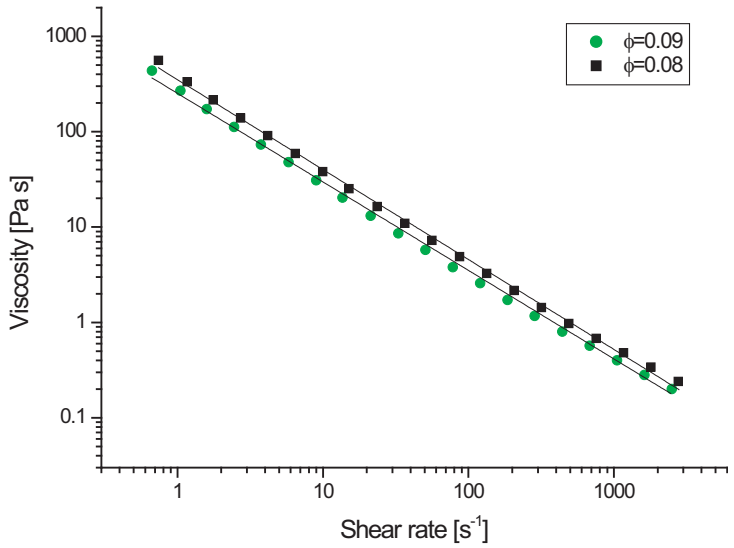

Figure 6.3: Viscosity as a function of shear rate of sewage sludge measured on the Haake Viscometer. η=252.64$\cdot\ \dot{\gamma}^{-0.9385}$, R^2=0.9984 (ϕ=0.08) and η=351.65$\cdot\ \dot{\gamma}^{-0.9432}$, R^2=0.9987 (ϕ=0.09).

A decrease in viscosity from about 700-0.2 Pa s as the shear rate increases from 0.7-2600 s^{-1} is observed. The viscosities of the two different concentrations appear to be parallel. The sample with the lowest volume fraction has the lowest viscosity. The viscosity decreases linearly on a log-log-scale which indicates that the viscosity can be fitted to a power law function. The fits can be seen in Figure 6.3 and are given by: η=252.64$\cdot\ \dot{\gamma}^{-0.9385}$, R^2=0.9984 (ϕ=0.08) and η=351.65$\cdot\ \dot{\gamma}^{-0.9432}$, R^2=0.9987 (ϕ=0.09). The squared R values close to 1 indicates that the fits have a high precision.

The viscosity of the sewage sludge is higher than the viscosity of alumina suspensions as expected which can be concluded from comparing Figure 5.9 with Figure 6.4. The EPC and non-spherical particles in sewage sludge are assumed to be responsible for this. The viscosity is a result of the hydrodynamic forces in the sewage sludge and is determined by the energy dissipated as heat resulting from diverging the liquid around these non-spherical particles.

The viscosity has been measured by an increase in shear rate subsequently followed by a decrease in shear rate and the result is shown in Figure 6.4.

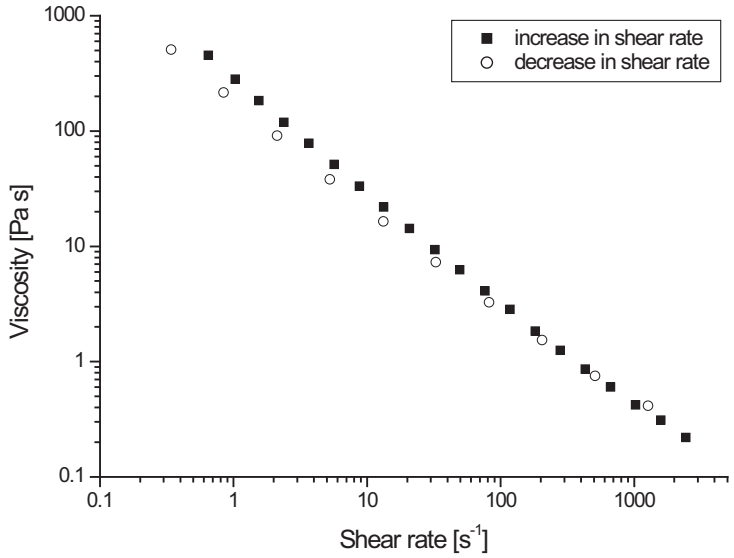

Figure 6.4: The viscosity of sewage sludge (ϕ=0.08) measured by an increase in shear rate followed by a decrease in shear rate measured on the Haake Viscometer.

The viscosity measured by the increase in shear rate is higher than the viscosity measured by the followed decrease in shear rate. The difference is largest at the highest viscosities which are the first and the last measured in the test. The result from Figure 6.4 show that the viscosity of sewage sludge is changing/decreasing during shear and not recovering immediately after shear. This time dependent behaviour is classified as an thixotropic behaviour.

Shear stress as a function of shear rate has been measured and is shown on a log-log scale in Figure 6.5.

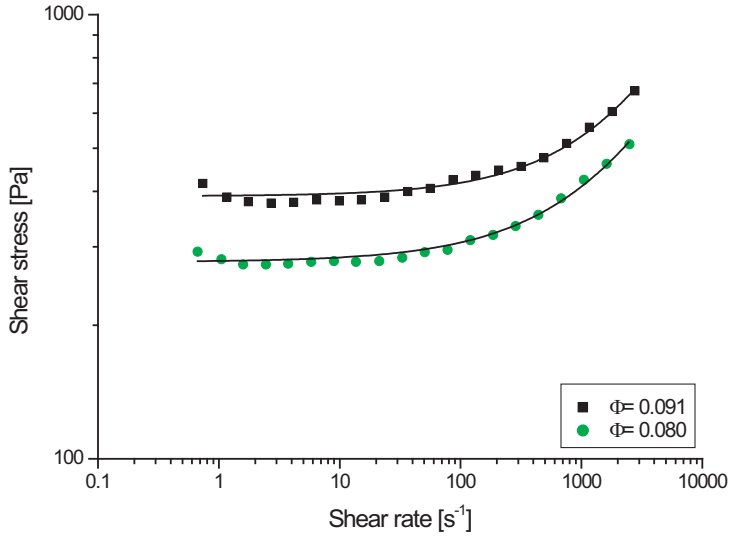

Figure 6.5: Shear stress as a function of shear rate for sewage sludge measured on the Haake Viscometer.

Shear yield stresses from 300-700 Pa have been measured in the shear rate interval from 0.7-2600 s^{-1}. The shear stress increases with shear rate on a log-log scale. An almost linear part is observed followed by an increasing part. The lowest volume fraction has the lowest shear stress value. The data indicate that shear thinning is observed. The Herschel and Bulkley Equation

(3.3) and the Casson Equation (3.4) can model the data. The resulting fits are shown in Table 6.1.

Table 6.1: The measured shear yield stress of sewage sludge and fitting parameters of shear rate-shear stress data of sewage sludge to Herschel & Bulkley and Casson's equations (cf. Section 3.2).

ϕ	τ	Herschel and Bulkley				Casson		
[-]	[Pa]	τ_{HB}	k	m	R^2	τ_C	η_∞	R^2
0.08	314	278	1.458	0.6529	0.9976	271	0.0145	0.9967
0.091	476	390	1.0949	0.7042	0.9927	401	0.108	0.9907

Comparison between the direct measured shear yield stress and the shear yield stress estimated by extrapolation has been done. The extrapolated shear yield stress is about 15% lower than the measured. The difference is properly related to the fact that sewage sludge exhibit time-dependent behaviour. A decrease in viscosity with shearing time is expected. The shear stress measurements are an average of three repeating measurements in the respective sample. The viscosity is expected to decrease further with each repeating measurement. Viscosity measurements are thus not considered useful for shear yield stress determination of materials exhibiting time-dependent behaviour.

From Table 6.1 is can be concluded that both the Herschel and Bulkley and the Casson equation can be employed to describe the viscosity of sewage sludge. Both fits have a high degree of precision according to the squared R value.

6.1.3 Compressive Yield Stress of Sewage Sludge

The compressive yield stress of sewage sludge is determined by single equilibrium pressure filtration and centrifugation. The compressive yield stresses are shown on a log scale as a function of volume fraction in Figure 6.6.

Compressive yield stress in the range from 5-300 kPa results in volume fraction ranging from 0.1-0.3 v/v. These values have been obtained by use of equilibrium single pressure filtration. Compressive yield stresses from 0.03-2 kPa result in volume fractions from 0.03-0.10 v/v. These values have been determined by centrifugation. The three repeats run at 2000 rpm show agreement and overlap to the sample run at 1000 rpm. The highest compressive yield stresses determined from centrifugation deviate toward higher volume fraction. This phenomenon is due the segregation in the samples. The compressive yield stress obtained from centrifugation and pressure filtration show no directly overlap but the data show agreement.

The equilibrium single pressure filtration data are adapted from Studer (2008). The sewage sludge was highly impermeable and a filtration test could run up to five days. Stepped pressure filtration cannot be performed on sludge. The characterisation time would be too long and errors associated with degradation of the sludge and evaporation from the filter cake are likely to occur. To ensure the equilibrium pressure filtration results were reproducibility, a single pressure filtration test at 230 kPa was run. Due to the low permeability of the sewage sludge, the single pressure filtration runs have not reached equilibrium (Section 3.6.2). The final cake concentration

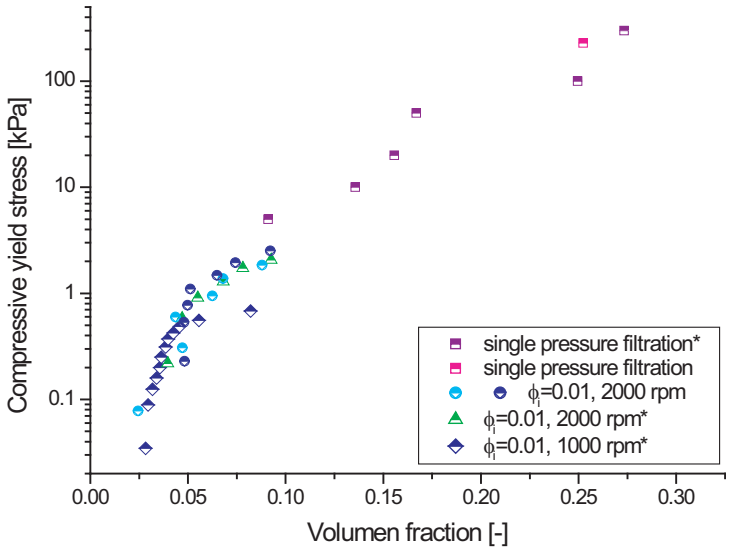

Figure 6.6: The compressive yield stress of sewage sludge determined by equilibrium pressure filtration and centrifugation. The symbols marked with * indicate that data are obtained by ([Studer, 2008]). ϕ_i is the initial volume fraction for centrifugation.

is thus not the equilibrium cake concentration (ϕ_∞). An estimation of ϕ_∞ has been done by extrapolating the cake compression curve to predict the equilibrium conditions (Enclosure III).

The compressive yield stress data obtained from centrifugation at 1000 rpm and 2000 rpm by Studer (2008) were determined after 2.5 days of centrifugation. In order to confirm the data two repeats at 2000 rpm were run. The samples were centrifuged for approximately 10 days before equilibrium was reached. The bed height is shown as a function of time on a log scale in Figure 6.7.

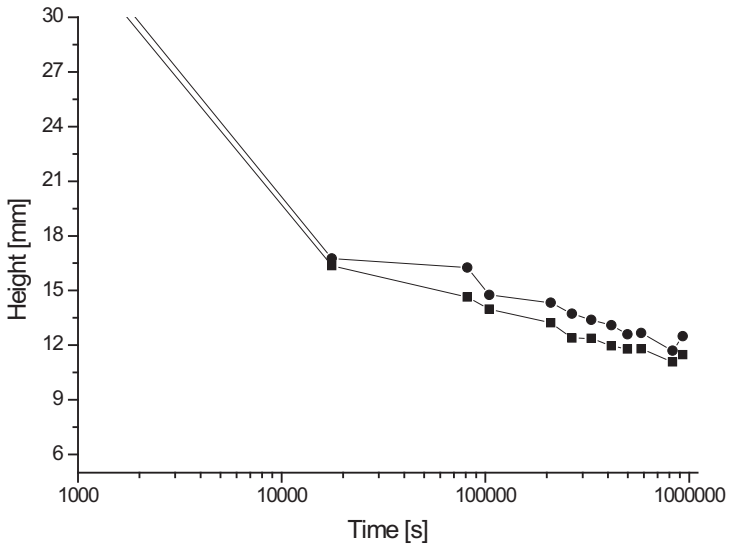

Figure 6.7: Bed height for two centrifugated sewage sludge samples at 2000 rpm.

The bed height of the centrifuged sewage sludge samples decreases from around 17-12 mm in the time period from ca. 2000-7,000,000 seconds. During the centrifugation time, the centrifuge was stopped for a short time and other samples run. This can be seen in the Figure 6.7 as the sample

height raises after the centrifuge was stopped. This is especially obvious when considering the two last points in the graph. The sewage sludge exhibited some elasticity and was able to restore some of it structure with time. The scrape test analysis should thus be performed directly after the centrifuged is stopped. From the data in Figure 6.7 it is assumed that the samples are close to equilibrium as a true equilibrium is time consuming to reach. Compared to the test run at 2000 rpm by Studer (2008) the difference in the centrifugation time does not appear to affect the results.

6.1.4 Comparison between Shear and Compressive Yield Stress for Sewage Sludge

The compressive and shear yield stress of sewage sludge on a log scale as a function of the volume fraction is shown in Figure 6.8.

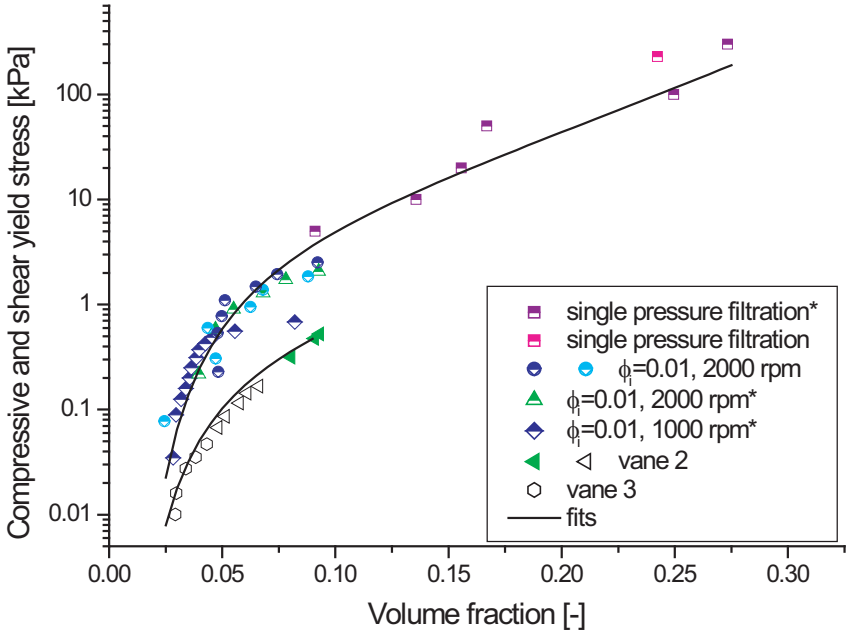

Figure 6.8: The compressive and shear yield stress of sewage sludge determined by equilibrium pressure filtration, centrifugation and the vane technique (Haake viscometer). The symbols marked with * indicate that data are obtained by [Studer, 2008]. ϕ_i is the initial volume fraction for centrifugation. The empty symbols indicates that the shear yield stress has an error $\geq$ 6%. Fits are given by Equation (5.3). P_y: a=0.48, b=0.018, k=8.6 ϕ_g=0.007, and ϕ_{cp}=0.75. τ_y: a=0.59, b=0.0161, k=8 ϕ_g=0.007, and ϕ_{cp}=0.75.

The compressive yield stress value, at a volume fraction, is higher than the corresponding shear yield stress value. As the volume fraction decreases the compressive and shear yield stresses approaches each other as expected. In order to determine the difference between the two yield stress Equation (5.3) is fitted to the data. The parameters for the two fits, shown in Figure 6.8, are a=0.425, b=0.021, k=8.7 ϕ_g=0.007, and ϕ_{cp}=0.79 for the compressive yield stresses and a=0.59, b=0.161, k=8, ϕ_g=0.007, and ϕ_{cp}=0.75 for the shear yield stresses. The two fits estimate the gel point to be at the volume fraction 0.007 v/v and the maximum packing fraction to be at 0.79 v/v. From the experimental data the gel point is expected to be about 0.03 v/v and from theoretical knowledges the maximum packing fraction is expected to be lower than 0.79 v/v.

The ratio between the compressive and shear yield stress behaviour of sewage sludge, as a function of volume fraction, is calculated from the above fits and is illustrated in Figure 6.9.

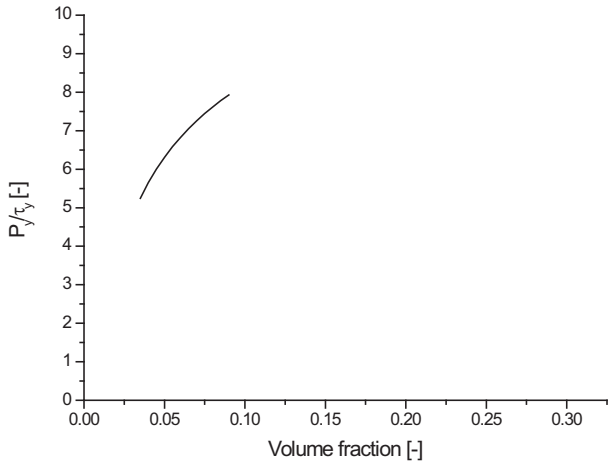

Figure 6.9: Ratio between compressive and shear yield stress of sewage sludge.

The P_y/τ_y ratio increases with volume fraction as expected. The ratio increases from around 5-8 in the volume fraction range from 0.03-0.9 v/v. This ratio is low compared to previous estimated P_y/τ_y ratios. This indicates that the micro structure of sewage sludge is difficult to break down both with shear and compression. The presence of ECP could be responsible for this behaviour. It is impossible to predict the shear yield stress behaviour above a volume fraction of 0.09 v/v and thus the behaviour of the P_y/τ_y at higher volume fractions.

6.1.5 Filtration Behaviour of Sewage Sludge

Equilibrium pressure filtration analyses from 5-300 kPa are shown in Figure 6.10 with time as a function of the squared specific filtrate volume.

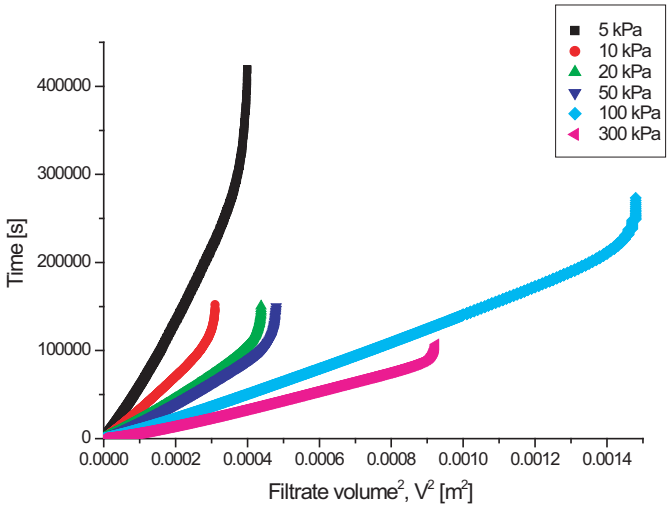

Figure 6.10: Filtration behaviour of sewage sludge from 5-300 kPa. The time as a function of the squared specific filtration volume [Studer, 2008].

Six filtration analyses are shown. The cake formation curve of the six filtrations is long compared

the cake compression curve. The filtration behaviour of the sewage sludge appears to be more traditional than non-traditional. It is difficult to determine whether the cake formation curve is linear and traditional filtration behaviour is observed.

In order to determine whether the cake formation region is linear the inverse dewatering rate as a function of time is shown in Figure 6.11.

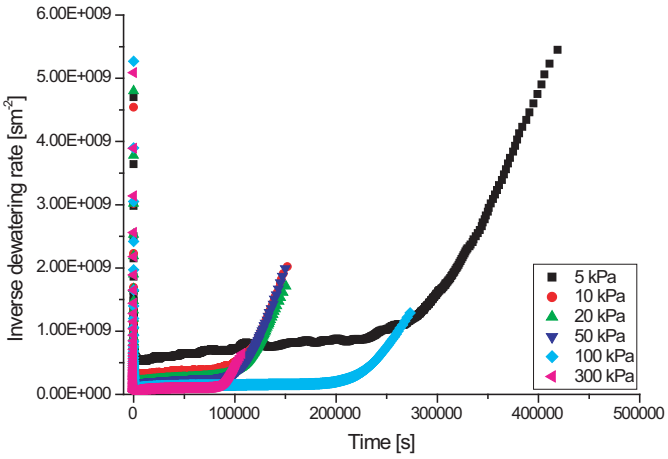

Figure 6.11: The inverse dewatering rate of sewage sludge as a function of time [Studer, 2008].

The inverse dewatering rate indicates that 2/3 of the filtration time, at all pressures, is constituted by cake formation. The dewatering rate of the cake formation region appears to decrease slightly with time. This is more evident at low pressures. Due to a non-constant cake formation rate the filtration do not exhibit traditional filtration behaviour. On the other hand, the filtration of the sludge does not exhibiting non-traditional filtration behaviour either. An issue with suspensions exhibiting a non-classified filtration behaviour is that extraction of filtration parameters is based on traditional filtration theory.

The hindered settling function of sewage sludge on a log scale as a function of the volume fraction is shown in Figure 6.12.

The hindered settling function increases with volume fraction from $1{\cdot}10^{8}$-$4{\cdot}10^{16}$ Pa s/m^2 in the volume fraction range from 0-0.3 v/v. This is an increase of 8 orders of magnitude. Lumifuge data have been employed to determine the hindered settling function at volume fractions close to the gel point. At a volume fraction from 0.03-0.04 v/v the hindered settling function increases from $3{\cdot}10^{9}$-$5{\cdot}10^{12}$ Pa s/m^2. The hindered settling function at the higher volume fractions has been obtained from pressure filtration. Volume fractions in the interval from 0.10-0.30 v/v yield hindered settling function values from $1{\cdot}10^{15}$-$1{\cdot}10^{17}$ Pa s/m^2. Together, the two methods yield a broad range of hindered settling function values. The curve fit to the data points has been performed by estimating the gradient of each point and then fitting a functional form trough the points. An almost smooth curve was the result.

The permeability of the sewage sludge has been calculated according Equation (3.6). The diffusivity has been determined from the cake compression region by extrapolating the data to determine ϕ_∞ (Enclosure III). Batch settling is often performed to obtain the low R(ϕ) data. For this particular sewage sludge this was proven difficult and time vs. height data from a lumifuge test was used by Studer (2008).

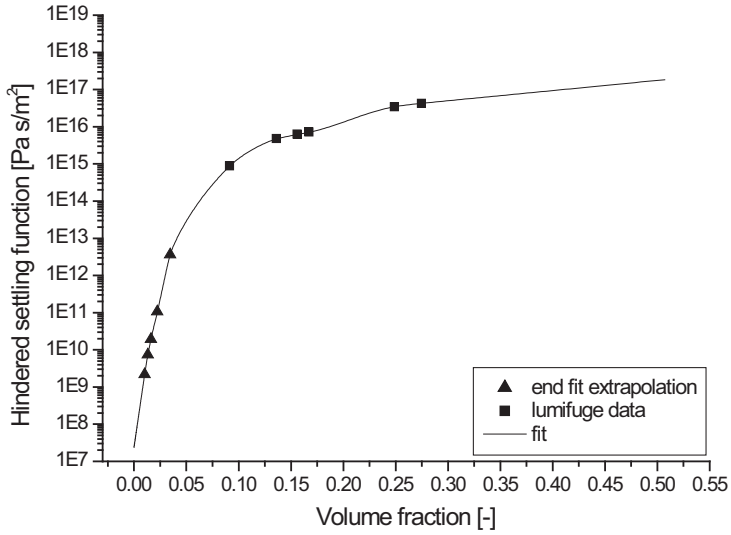

Figure 6.12: The hindered settling function of sewage sludge as a function of volume fraction determined from filtration and lumifuge data [Studer, 2008].

The solids diffusivity of sewage sludge is shown as a function of volume fraction in Figure 6.13.

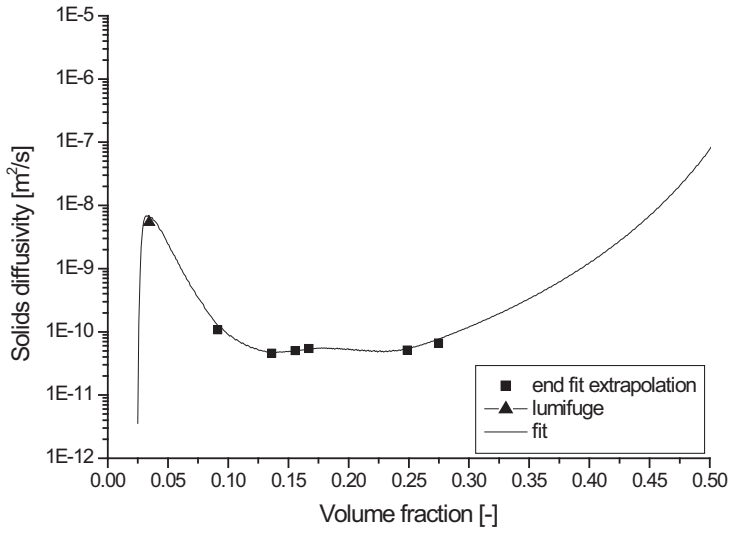

Figure 6.13: The solids diffusivity of sewage sludge as a function of volume fraction determined from lumifuge and filtration data [Studer, 2008].

The solids diffusivity increases rapidly near the gel point from $6{\cdot}10^{-11}$-$5{\cdot}10^{-9}$ m^2/s. Just above the gel point a peak is observed. The solids diffusivity decreases until a volume fraction of 0.15 v/v is reached. Above this volume fraction the diffusivity is constant at a value of $8{\cdot}10^{-11}$ m^2/s until a volume fraction of 0.25 v/v is reached. Above this volume fraction the diffusivity starts to increase again. The diffusivity is calculated from the knowledge of the compressive yield stress and the hindered settling function. The peak observed at low volume fractions indicate that $P_y(\phi)$ is more significant than $R(\phi)$ at low volume fractions.

6.2 Summary of the Rheological Behaviour of Sewage Sludge

The characterised sewage sludge exhibited shear thinning behaviour and was thixotropic. Extrapolation of shear rate vs. shear rate data to a zero shear rate could not be employed to determine the shear yield stress due to the time dependency of the material.

The sewage sludge was concentrated by centrifugation. Shear yield stress data above a volume fraction of 0.09 v/v could not be obtained due to the high impermeability of the sewage sludge. Uncertain shear yield stress values, at low volume fractions, were determined due to a limited amount of sample. Compressive yield stresses could be obtained in the volume fraction range from 0.03-0.30 v/v. The ratio between compression and shear was determined to increase from 5.5-8 in the volume fraction range from 0.03-0.9 v/v.

The sewage sludge exhibited a non-classified filtration behaviour. The cake formation time constituted 2/3 of the filtration time and a weak decrease in dewatering rate during cake formation was observed. The hindered settling function increased rapidly with volume fraction about 9 orders of magnitude. The solids diffusivity of the sewage sludge was low at a value about $1{\cdot}10^{-10}$ m^2/s. A maximum, at low volume fractions, was observed in the solids diffusivity curve fit.

6.3 Rheological Behaviour of the Dual-Polymer-Flocculated Alumina Suspension

In this section a dual-polymer flocculated alumina suspension is produced on basic of knowledge from previous investigations. The dual-polymer flocculated alumina suspension behaviour in shear and compression is characterised. The filtration behaviour is presented in order to verify if the suspension exhibit non-traditional filtration behaviour as expected. Prediction of filtration behaviour of the suspension is performed on basis of the determined the hindered settling function and compressive yield stresses.

6.3.1 Test of Polymer Dose for Dual-Polymer Flocculation of an Alumina Suspension

In the work done by Sutanto and Ho (2007), it was attempted to recreate a dual-flocculated-system developed by Glover (2003). This proved difficult as no flocculation occurred by addition of the prescribed polymer doses which are 10 ppm of PAA and 4 ppm of Zetag. The chosen polymer doses which were 280 ppm of PAA and 140 ppm of Magnafloc LT20 did not result in non-traditional filtration behaviour. Different polymer doses were thus tried with the assumption that creation of larger flocs possibly would result in non-traditional filtration behaviour.

The different PAA doses tested are shown in Table 6.2.

Table 6.2: Polymer doses tried for flocculation of alumina suspensions. A concentration of 652 ppm PAA is chosen before the second polymer (Magnafloc LT20) is added.

PAA [ppm]	Supernatant	Magnafloc LT20 [ppm]	Supernatant
300	non-clear	50	non-clear
500	non-clear	200	non-clear
697	non-clear	445	non-clear
652	clear	392	clear
699	clear	597	clear
1177	clear	699	clear
		1177	clear

Dilute alumina suspensions were prepared and the pH was adjusted to 5.5 before they were left overnight. The criteria for an optimum polymer dose was in this work defined as a reasonably clear supernatant after flocculation which together with the settling rate can help indicate whether reproducible flocculation can be obtained (Figure 6.14). As only weak flocculation occurred after addition of 280 ppm of PAA doses from 300 ppm and above were tried.

The final chosen polymer doses were 652 ppm of PAA and 392 ppm of Magnafloc LT20 and the pH was raised to 7.29 as the flocculation appeared to be more reproducible at this pH. The chosen doses are remarkably higher than the one used by Glover (2003). The electrolyte concentration in this work is increased from 10^{-4}M KNO_3 to 10^{-3}M KNO_3 compared to Glover (2003) and the pH is increased from 5-7.5. A pH closer to the isoelectric point and a higher salt concentration

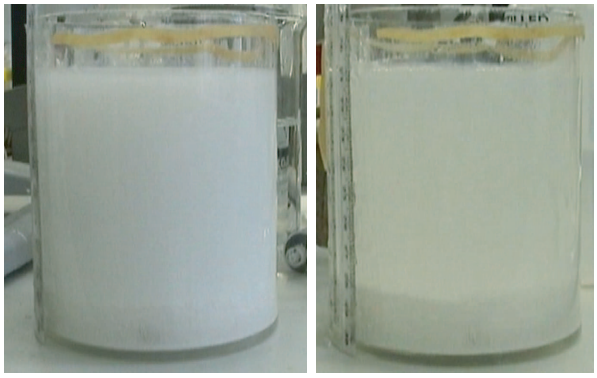

Figure 6.14: Suspensions after settling of the flocs. Left picture shows a non-clear supernatant and the right picture shows a more clear supernatant.

leads theoretically to a lower surface potential which is expected to require a lower dosage of polymer to flocculate the suspension but this was not observed here.

The settling rate for flocculation is $8{\cdot}10^{-4}$ ms^{-1} if only PAA is added and $1.8{\cdot}10^{-3}{\pm}1.7{\cdot}10^{-4}$ ms^{-1} when both PAA and Magnafloc LT20 are added. The volume fraction after settling and removal of the supernatant was about 0.03 v/v. The suspension was concentration by means of centrifugation to obtain different volume fractions. The aggregate size after addition of PAA was 86±3.5 μm and after addition of the Magnafloc LT20 the aggregate size increases to 189±2.6 μm. In Figure 6.15 the size distribution is illustrated.

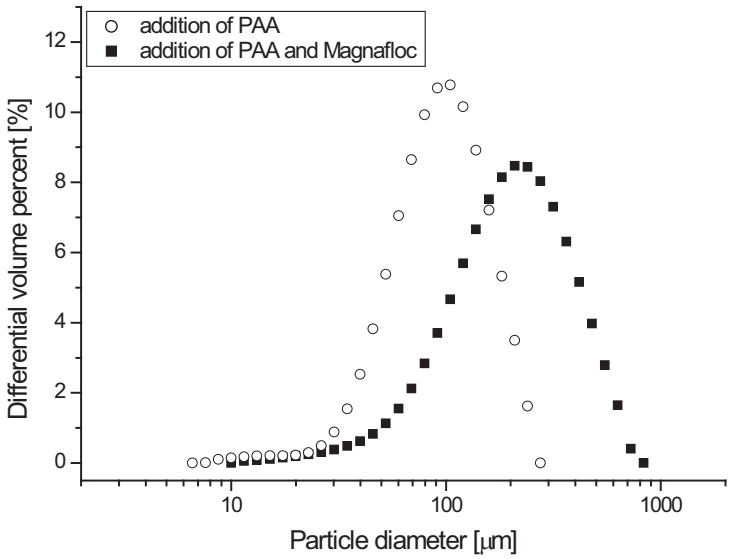

Figure 6.15: Particle diameter of flocculated alumina suspensions (pH=7.3, 10^{-3}M KNO_3) with Polyacrylic Acid (PAA) and then a polyacrylamide polymer (Magnafloc).

A more narrow size distribution of the aggregates is observed after flocculation with only PAA compared to the dual-polymer flocculation.

6.3.2 Shear Yield Stress of the Dual-Polymer Flocculated Alumina Suspension

The shear yield stress of the flocculated alumina suspension on a log scale as a function of shear rate is shown in Figure 6.16.

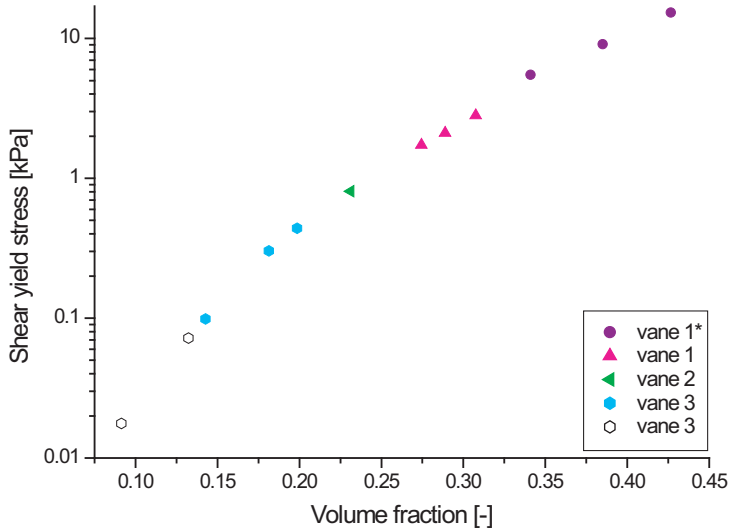

Figure 6.16: Shear yield stress of flocculated alumina suspension. * indicate data points obtained from measurements on the ARES rheometer and the remaining points are measured on the Haake Viscometer. The empty symbols indicates that the shear yield stress has an error $\geq$ 6%.

The shear yield stress increases with volume fraction. Shear yield stresses from 0.2-15 kPa were measured in the volume fraction range from 0.09-0.42 v/v. The flocculated alumina suspension was easily concentrated by centrifugation to high volume fractions contrary to the sewage sludge. Due to the limited amount of sample, the measurements at the lowest volume fractions are associated with error. At high shear yield stresses (>3 kPa) the ARES rheometer was used to measure the shear yield stress for the following reasons. A higher precision is obtained, the maximum torque limit is not exceeded, and the cup is fixed which will prevent the cup from turning during the measurement. The last mentioned problem is an issue when high concentrations are measured on the Haake Viscometer.

6.3.3 Compressive Yield Stress of the Dual-Polymer Flocculated Alumina Suspension

The compressive yield stress is measured by both single and stepped pressure equilibrium filtration, centrifugation, and batch settling. The compressive yield stress as a function of volume fraction is shown in Figure 6.17.

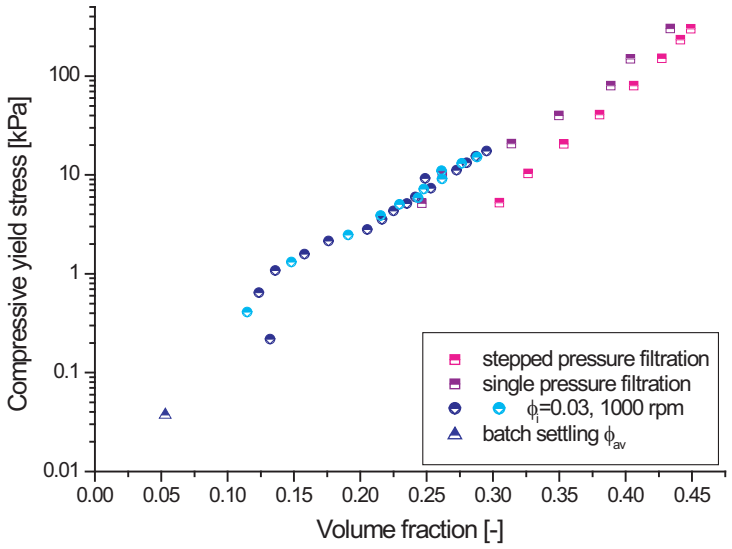

Figure 6.17: Compressive yield stresses as a function of volume fraction of a dual-polymer flocculated alumina suspension.

Compressive yield stress increases with volume fraction. The compressive yield stress has been determined in the stress interval from 0.04-300 kPa resulting i volume fractions from 0.05-0.45 v/v. The lowest compressive yield stress data have been determined with batch settling. In the volume fraction range from 0.05-0.10 no data was obtained. From 0.10-0.30 v/v, compressive yield stress was determined by centrifugation. Agreement between the samples in duplicate is observed. At volume fraction from 0.25-0.45 v/v compressive yield stress data from filtration were obtained. The compressive yield stress from single pressure filtration and centrifugation overlaps.

The results obtained by single and stepped pressure equilibrium filtration deviate from each other. It appears that the single pressure filtration results are in agreement and the stepped pressure filtrations results are erroneous. The results of the single pressure filtrations arise from flocculation of seven different sample and the stepped pressure filtration only from one sample. No difference can be observed in the flocculation rate, pH or conductivity between the samples that could indicate a change in the surface chemistry. A possible explanation could be that the sample used for the stepped pressure filtration run was left to settle in a tube (diameter=40 mm) for 5 days before the filtration. Aggregates in the bottom of the bed could to some extent be broken up by the weight of the solid above. This would lead to formation of a denser cake. All the single pressure filtration tests were run immediately after the flocculation process.

6.3.4 Comparison between Shear and Compressive Yield Stress for the Dual-Flocculated Alumina Suspension

The compressive and shear yield stresses as a function of shear rate on a log scale is shown in Figure 6.18.

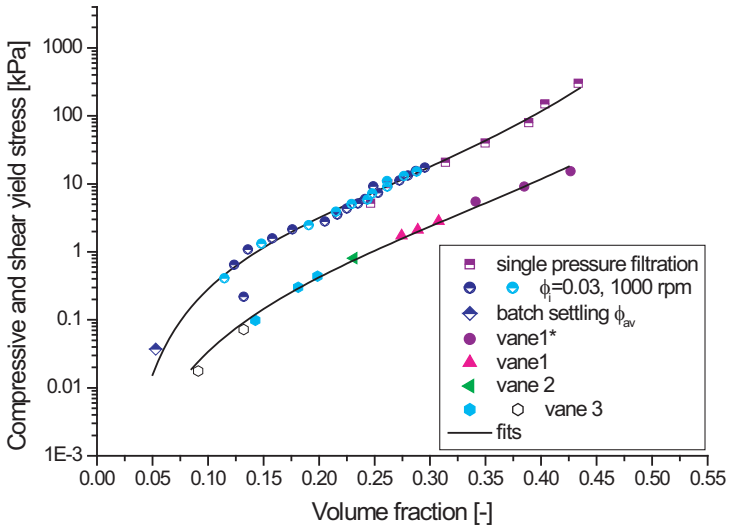

Figure 6.18: Compressive and shear yield stress as a function of volume fraction of a dual-polymer flocculated alumina suspension. The empty symbols indicates that the shear yield stress has an error $\geq$ 6%. * indicate data points obtained from measurements on the ARES. Fits is given by Equation (5.3). P_y: a=0.26, b=0.09, k=4.55 ϕ_g=0.015, and ϕ_{cp}=0.64. τ_y: a=0.015, b=2.5, k=2.6 ϕ_g=0.019, and ϕ_{cp}=0.64.

The compressive yield stress of the flocculated alumina suspension is higher than the corresponding shear yield stress. The yield stresses are determined over four orders of magnitude from 0.02-300 kPa. It appears that the difference between the compressive and shear yield stress decreases with decreasing volume fraction. In order to determine the ratio the yield stress data are fitted to Equation (5.3). The two fits are illustrated in Figure 6.18 and the parameters are a=0.54, b=0.024, k=5.75 ϕ_g=0.024, and ϕ_{cp}=0.62 for the compressive yield stresses and a=0.10, b=0.33, k=3.65, ϕ_g=0.0024, and ϕ_{cp}=0.81 for the shear yield stresses. Equation (5.3) is able to describe the change is yield stress with volume fraction. The estimated gel point and maximum packing fraction of the flocculated alumina suspension are ϕ_g=0.024 and ϕ_{cp}=0.62/81. The estimated gel point is in agreement with an expected gel point value which from the experimental data is below ϕ=0.05 v/v. The suggested maximum packing fraction of 62 is a reasonable estimate.

The ratio between compressive and shear yield stress on a log scale as a function of volume fraction is shown in Figure 6.19.

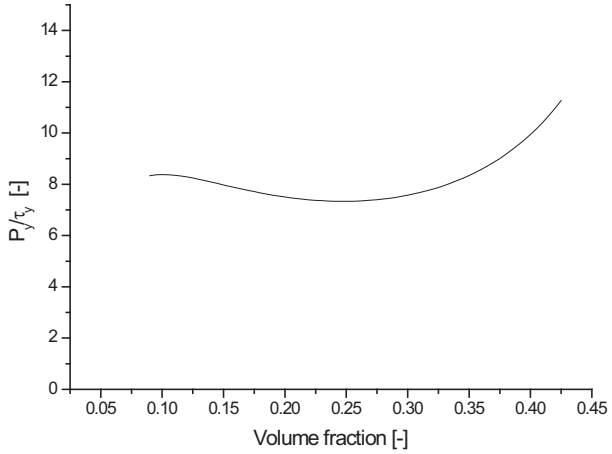

Figure 6.19: The ratio of compressive and shear yield stress as a function of volume fraction for a dual-polymer flocculated alumina suspension.

The ratio between the compressive and shear yield stress has an overall increasing tendency from 8-11 in the volume fraction range from 0.1-0.43 v/v. In the volume fraction range from 0.10-0.25 a constant ratio is observed. The validity of this tendency is unknown. If Figure 6.18 is considered the P_y/τ_y ratio is expected to decrease at low volume fraction. The number of data points determines the uncertainty on the estimated curve fit. At higher volume fractions more yield stresses have been determined and the validity of the fit is larger.

6.3.5 Filtration Behaviour of the Dual-Polymer Flocculated Alumina Suspension

The filtration behaviour of the dual-polymer flocculated alumina suspension is shown in Figure 6.20.

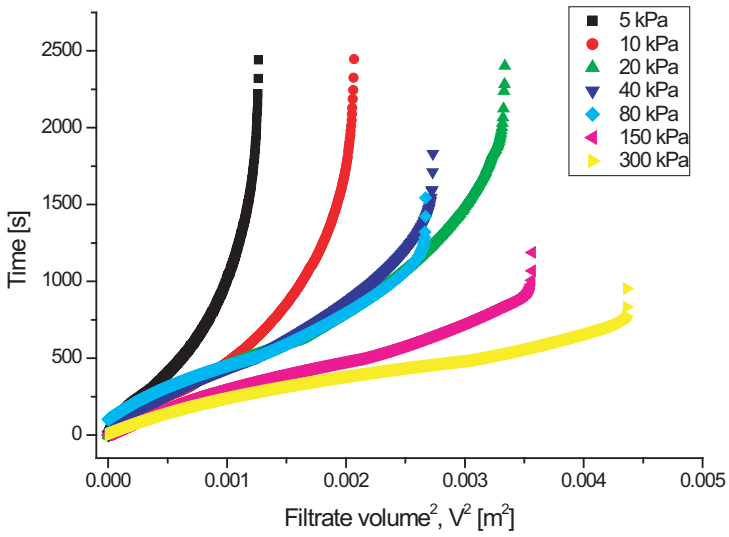

Figure 6.20: Filtration behaviour of the dual-polymer flocculated alumina suspension. Time as a function of the squared specific filtrate volume.

The filtration behaviour is shown as time as a function of the squared specific filtrate volume. At low pressures, 5-20 kPa, the expected non-traditional filtration behaviour with longer cake

compression times than cake formation times is observed. The filtration behaviour approaches a more traditional behaviour with longer cake formation times as the pressure is increased. Contrary to the constant dewatering rate during cake formation in traditional filtration behaviour an increase in the rate is observed here. The filtration behaviour of the dual-polymer flocculated alumina suspension is reasonable short, up to 2500 seconds, and is not traditional.

The inverse dewatering rate of the dual-polymer flocculated alumina suspension as a function of time is illustrated in Figure 6.21.

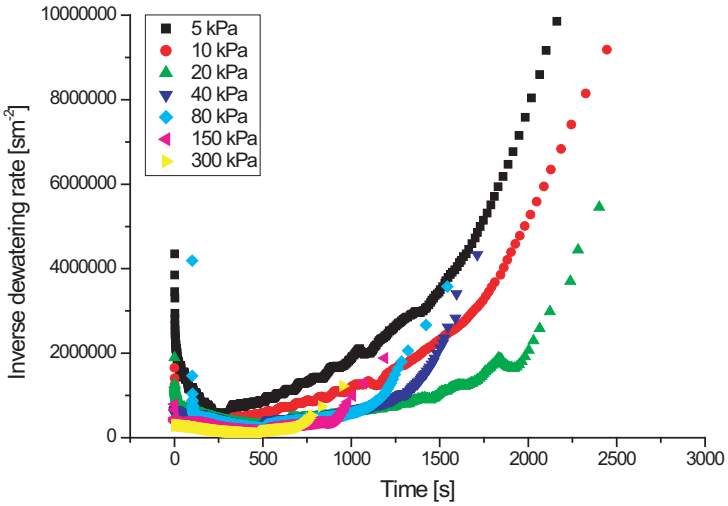

Figure 6.21: Inverse dewatering rate of the dual-polymer flocculated alumina suspension as a function of time.

At the low pressures, 5-20 kPa, the filtration time is dominated by long cake compression times with an almost non-existing cake formation state. At the higher pressures, the increase in dewatering rate during cake formation can be observed. The reason for this increase is unknown. A possible explanation can be that the suspension settles in the filtration rig before filtration the is started. As the filtration is started the water on the top of the bed has to move through the bed.

The hindered settling function is shown as a function of time in Figure 6.22.

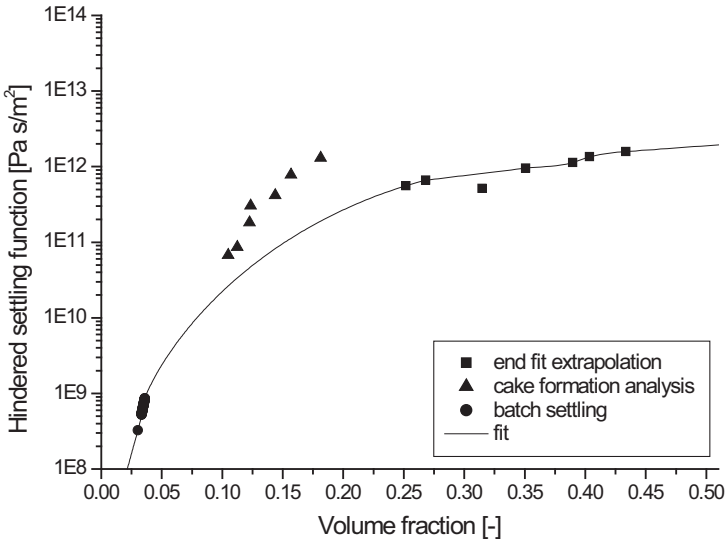

Figure 6.22: The hindered settling function of the dual-polymer flocculated alumina suspension as a function of volume fraction.

The hindered settling function increases from about $1{\cdot}10^{8}$-$2{\cdot}10^{12}$ Pa s/m^2 in the volume fraction range from 0.025-0.50 v/v. Near the gel point, batch settling has been employed to determine the hindered settling function. In the volume fraction range from 0.05-0.10 v/v no hindered settling function data are obtained. Above 0.10 v/v the hindered settling function has been determined from filtration data. The hindered settling function from filtration data is determined by two methods. One is the log end fit method where the cake compression curve is extrapolated to equilibrium conditions. The other uses the cake formation curve to extract the hindered settling function data (Enclosure III). As the filtration behaviour was dominated by cake compression the calculated values from the former method were employed to create the curve fit together with the batch settling data. The fit has been done by estimating the gradient between all the point whereupon a functional form has been fitted between all the points. The R(ϕ) determined from the cake formation curve are higher than the predicted values from the remaining results. The values from the low pressures were expected to be associated with most error due to the short cake formation times. Despite this expectation these values appear to be most in agreement with the predicted values. The method assumes a constant slope during cake formation and this slope is the determining factor in the determination of R(ϕ_c). The non-constant slope at the higher pressures could therefore be an important factor in the determination of R(ϕ_c).

The solids diffusivity is shown as a function of volume fraction in Figure 6.23. The solids diffusivity curve fit is calculated from the hindered settling function curve and the compressive yield stress curve fit.

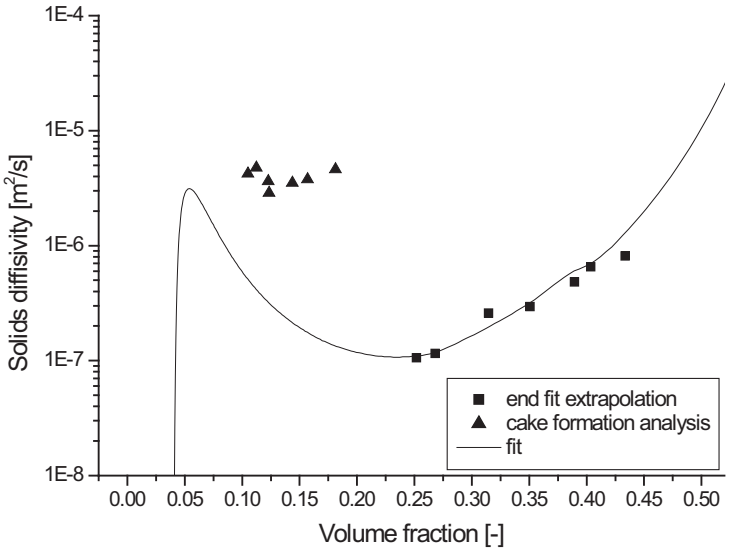

Figure 6.23: Solids diffusivity of flocculated alumina suspension as a function a volume fraction D is calculated from an exponential fit of β vs ϕ.

The solids diffusivity varies in the range from $1{\cdot}10^{-7}$-$6{\cdot}10^{-5}$ m^2/s in the volume fraction range from 0.02-0.43 v/v. A maximum at low volume fractions, near the gel point, is observed. Above the gel point a decrease followed by an increase is observed with volume fraction. This indicates that $P_y\phi$ is more significant than $R(\phi)$ at low and at high volume fractions. The values calculated from the cake formation curve confirm the presence of the peak at low volume fractions. The values are higher than the curve fit predicts but indicate that cake formation is easily achieved.

In order to verify the validity of the estimated filtration parameters, prediction of filtration behaviour has been performed on basis of these parameters. The solids diffusivity determined from the cake compression curve has been employed to predict the filtration behaviour at 5 and 300 kPa (Figure 6.24).

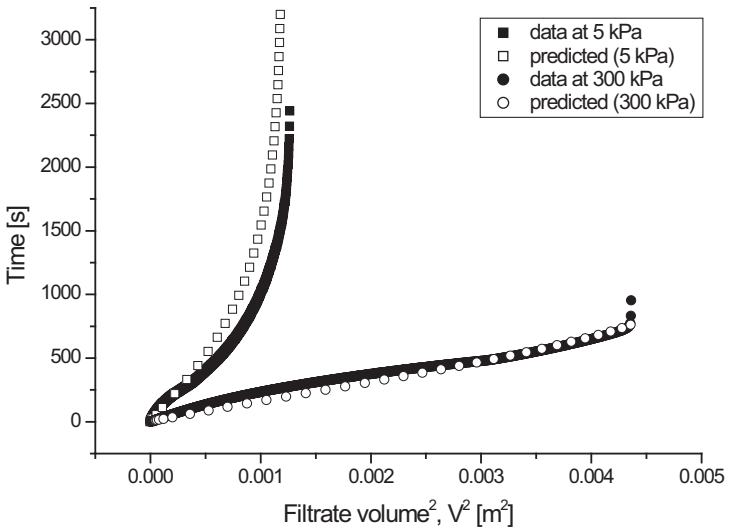

Figure 6.24: The predicted filtration behaviour of the dual-polymer flocculated alumina suspension. Time as a function of the specific filtrate volume.

There is agreement between the predicted and experimental filtration behaviour which shows that the estimated filtration parameters are associated with low error. The predicted filtration behaviour at 5 kPa is slower than the experimental. Due to the strongly dominated cake compression filtration, an incomplete filtration resulted at this pressure and it appears that the predicted filtration behaviour is unable to account for this. At 300 kPa, the predicted filtration behaviour is unable to describe the unexpected increase in the dewatering rate at cake formation but predicts the cake compression. A more correct prediction of the filtration behaviour at higher pressures is expected as the estimated diffusivities at lower pressures are included in these predictions.

A membrane resistance of $1.68{\cdot}10^{7}$ m^{-1} for 5 kPa and $1.66{\cdot}10^{8}$ m^{-1} for 300 kPa were estimated from extrapolating experimental filtration data to the intercept of a t/V vs. V plot and calculating the membrane resistance, R_m:

$$\text{intercept} = \frac{\eta R_m}{\Delta P} \tag{6.1}$$

where η is the filtrate viscosity and Δ P is the pressure difference. The estimated membrane resistances were employed in the prediction together with the initial volume fraction and initial sample height.

6.4 Summary of the Rheological Behaviour of the Dual-Polymer Flocculated Alumina Suspension

A dual-polymer flocculated alumina suspension was produced. The suspension was concentration by means of centrifugation and volume fractions from 0.09-0.42 v/v were obtained. Corresponding shear yields stresses were determined to be in the order of 0.2-15 kPa. Compressive yield stresses was determined from 0.04-300 kPa in the volume fraction range from 0.05-0.45 v/v. The ratio estimated between compression and shear increased from 8-11 in the volume fraction range from 0.09-0.42 v/v.

The filtration behaviour of the flocculated suspension changed with increasing pressure. At low pressures, 5-20 kPa, the expected non-traditional filtration behaviour was observed. At higher pressures, the filtration behaviour appeared to be more traditional. Contrary to traditional filtration behaviour, an increase in dewatering rate during cake formation was observed.

The solids diffusivity was determined to be of the order $1{\cdot}10^{-7}$-$2{\cdot}10^{-6}$ m^2/s in the volume fraction from 0.5-0.43 v/v. The filtration behaviour at 5 kPa and 300 kPa was predicted from the solids diffusivity data and agreement between predicted and experimental filtration behaviour was observed.

Chapter 7

Comparison of the Rheological Behaviour of Sewage Sludge and the Inorganic Suspensions

The purpose of this chapter is to compare and discuss the difference observed in the rheological behaviour of the sewage sludge and the two inorganic particulate suspensions. Comparision of the compressive and shear yield stress behaviour of the three suspensions will be performed followed by a comparison of the filtration parameters.

7.1 Shear and Compressive Behaviour of Sewage Sludge and the two Inorganic Suspensions

The shear yield stress of the sewage sludge, the flocculated and the coagulated alumina suspension is shown in Figure 7.1 as a function of volume fraction.

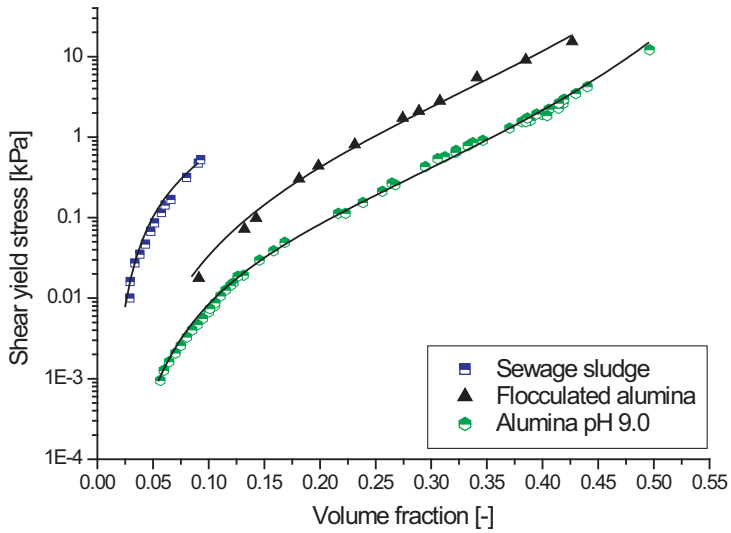

Figure 7.1: Shear yield stress of sewage sludge, the flocculated (pH 7.29±0.1, 10^{-3}M KNO_3) and the coagulated (pH 9.0±0.1, 10^{-2}M KNO_3) alumina suspension as a function of volume fraction.

Shear yield stress data have been obtained in the range from 0.9-15,000 Pa where the broadest range of stresses was obtained for the coagulated alumina suspension. The shear yield stress of the three suspensions increases with a similar functional form but at different slopes with volume fraction. The network strength of sewage sludge increases most rapidly with volume fraction compared to the two inorganic suspensions.

Sewage sludge creates a strong network structure as the volume fraction increases. The shear yield stress increases about 1 1/2 orders of magnitude (10-520 Pa) when the volume fraction is raised from 0.03-0.09 v/v. Just above the gel point, a small increase in volume fraction will increase the network strength rapidly. The strength of the network formed by the coagulated spherical Al_2O_3 particles increases more gradually. To reach a network strength of 10 Pa the volume fraction has to be raised from the gel point, which is can be estimated to be around 0.03 v/v, to 0.11 v/v. Sewage sludge consists of particles and polymers of different size and shape. A decrease in particle size increases the shear yield stress value due to a stronger attraction and reduced repulsion between the particles. The high molecular polymers (ECP) expected present in sewage sludge will most likely form bridges between the particles and further stabilize and strengthen the network formed. The particles in the flocculated alumina suspension are expected in a similar way to be stabilized by the added polymers through bridge formation and other stabilizing forces such as depletion forces. An increase in the network strength of the flocculated alumina suspension can be observed by comparing it to the coagulated alumina suspension. The network strength, of the flocculated alumina suspension, in shear is about a factor of 5 higher at a volume fraction of 0.9 v/v. The difference in network strength between the sewage sludge and the coagulated alumina particles at this concentration is about a factor of 100.

The compressive yield stress of the sewage sludge, the flocculated and the coagulated alumina suspension is shown in Figure 7.2 as a function of volume fraction.

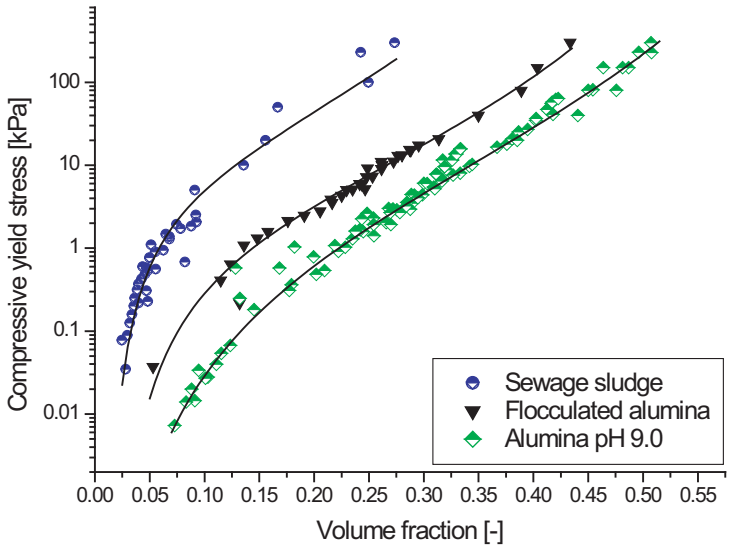

Figure 7.2: Compressive yield stress of sewage sludge, the flocculated (pH 7.29±0.1, 10^{-3}M KNO_3) and the coagulated (pH 9.0±0.1, 10^{-2}M KNO_2) alumina suspension as a function of volume fraction.

Compressive yield stress values are determined over four orders of magnitude of the three sus-

pensions with the broadest range observed for the coagulated suspension, 0.007-300 kPa. The compressive yield stress required to break down the network formed in sewage sludge increases rapidly with volume fraction. The highly impermeable network only allows the suspension to be concentrated to a volume fraction about 0.27 v/v by compression at 300 kPa. Compared to the coagulated and flocculated alumina suspensions which reaches concentrations around 0.50 v/v and 0.43 v/v, respectively, at this pressure. The strength, of the flocculated network, against compression appears to decrease with volume fraction compared to the strength of the coagulated network. The small change could be related to the expectation that the created flocs are easier destroyed at higher loads which would allow the bed to compact further during compression. Whether this is the case, or the difference in compression behaviour observed between the two suspensions is just related to uncertainties in the measurement or the flocculation of the suspensions, cannot be determined. Another possibility could be that the results from centrifugation are erroneous. For sewage sludge segregation, of the samples during centrifugation, occurred. It would be reasonable to assume that this problem also would occur in the flocculated samples. If this is the case, the volume fractions at the lowest compressive yield stresses would be too low. The volume fractions, at the highest pressure, would be too high.

The P_y/τ_y ratio of the sewage sludge, the flocculated and the coagulated alumina suspension is shown in Figure 7.3.

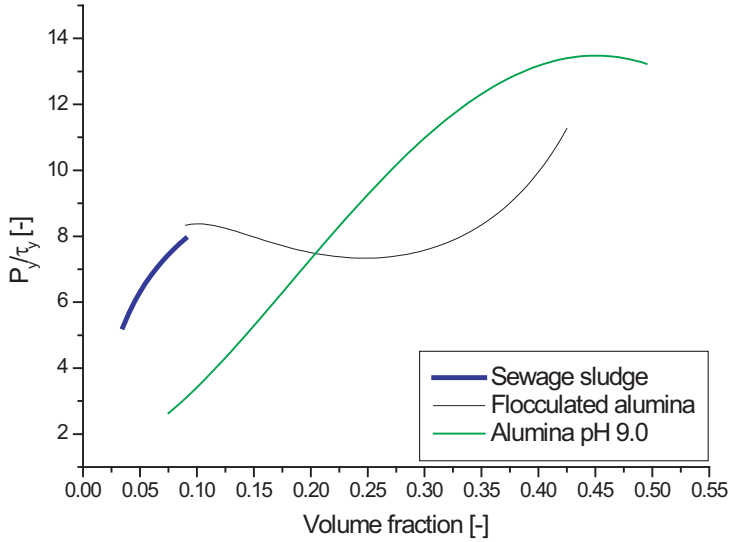

Figure 7.3: Ratio between compressive (P_y) and shear (τ_y) yield stress of sewage sludge, the flocculated (pH 7.29±0.1, 10^{-3}M KNO_3) and the coagulated (pH 9.0±0.1, 10^{-2}M KNO_3) alumina suspension as a function of volume fraction.

Ratios from 2-14 have been determined in the volume fraction range from 0.025-0.50 v/v. The three ratios show overall an increasing tendency with volume fraction.

Due to the difficulties related to concentrate the sewage sludge for shear yield stress measurements, the ratio of sewage sludge can only be estimated for a small volume fraction range. In this range, the the P_y/τ_y ratio appears to be parallel to the ratio estimated of coagulated alumina. The majority of the estimated shear yield stress values of sewage sludge are expected to be lower than the "true" shear yield stress value in which case the ratio would decrease.

The ratio estimated of the flocculated alumina suspension shows to some point a similar behaviour as the ratio of sewage sludge and coagulated alumina suspension. Based on the knowledge of these, the ratio of the flocculated alumina suspension would be expected to lie somewhere in the interval between these. The reliability of the estimated P_y/τ_y ratios should be based on the measured data points, and the fit made to those, as the reliability of ratio is based on these. The chosen fit can have a large influence on the resulting ratio. All the measured data points and the three fits are shown in Figure 7.4.

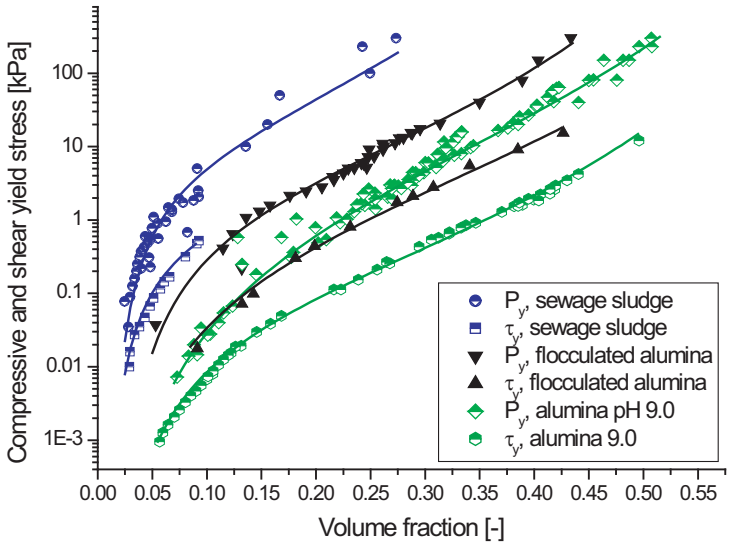

Figure 7.4: Compressive (P_y) and shear (τ_y) yield stress of sewage sludge, the flocculated (pH 7.29±0.1, 10^{-3}M KNO_3) and the coagulated (pH 9.0±0.1, 10^{-2}M KNO_3) alumina suspension as a function of volume fraction.

The trend of the compressive and shear yield stresses, as a function of volume fraction, is similar for the three particulate suspensions. At low volume fraction, the two yield stresses do not deviate significantly from each other, at higher volume fractions, a greater different is observed but the two values are still relatively close related for all the systems. A reasonable large ratio, at the lowest volume fractions, are observed for the flocculated alumina suspension. If the flocculated alumina system is considered it can be observed that fewer data point are obtained for this suspension compared to the sewage sludge and the coagulated alumina suspension. In Section 6.3.3, it was observed that overlap only occurred at a narrow volume fraction range about 0.25 v/v. The reliability of the data points below and above this concentration is thus questionable and the trend of the ratio is thus difficult to predict. A lower ratio, at volume fractions near the gel point, would be in agreement with the expected behaviour.

7.2 Filtration Properties of Sewage Sludge and the two Inorganic Suspensions

The hindered settling function of the sewage sludge, the flocculated and the coagulated alumina suspension is shown in Figure 7.5 as a function of the volume fraction.

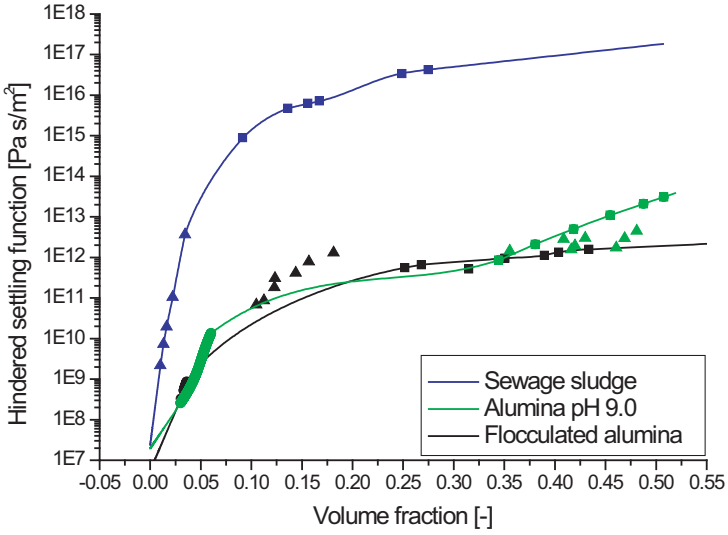

Figure 7.5: The hindered settling function of sewage sludge, the flocculated (pH 7.29±0.1, 10^{-3} M KNO_3) and the coagulated (pH 9.0±0.1, 10^{-2} M KNO_3) alumina suspension as a function of volume fraction.

The hindered settling function increases 4-5 orders of magnitude for both the alumina suspensions, $1{\cdot}10^{8}$-$3{\cdot}10^{13}$ Pa s/m^2, and 8 orders of magnitude for sewage sludge, $1{\cdot}10^{8}$-$4{\cdot}10^{16}$ Pa s/m^2. Resemblance between the hindered settling function behaviour of the two alumina suspensions are observed together with overlapping data points.

Solids diffusivity of the sewage sludge, the flocculated and the coagulated alumina suspension is shown in Figure 7.5 as a function of the volume fraction.

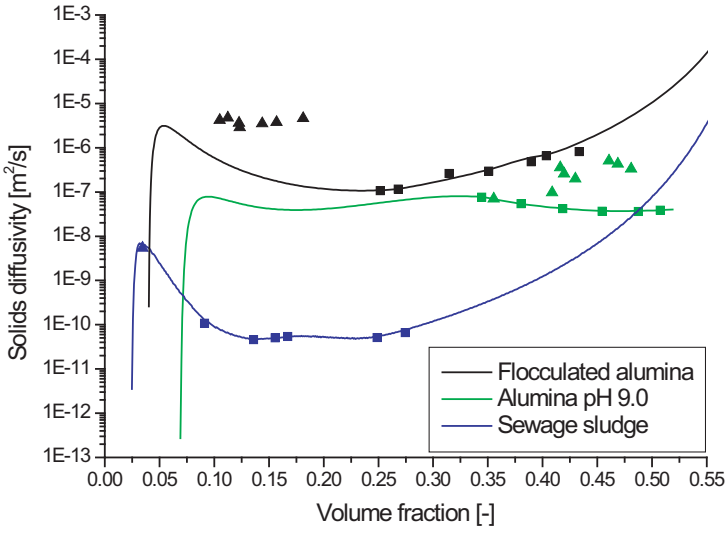

Figure 7.6: Solids diffusivity of sewage sludge, the flocculated (pH 7.29±0.1, 10^{-3} M KNO_3) and the coagulated (pH 9.0±0.1, 10^{-2} M KNO_3) alumina suspension as a function of volume fraction.

The solids diffusivity varies from $1{\cdot}10^{-11}$-$1{\cdot}10^{-5}$ m^2/s for the three suspensions. Contrary to the hindered settling function data, resemblance between the fit for sewage sludge and the fit for the flocculated alumina suspension is observed. Both fits exhibit a maximum near the gel point. The decrease in the diffusivity, with volume fraction, is followed by an increase. A difference of

about 3 orders of magnitude is observed in the solids diffusivity. From the knowledge about the filtration behaviour of the two suspensions, the flocculated alumina suspension cannot directly act as a substitute to sewage sludge. On the other hand, the flocculated alumina suspension could be an ideal suspension for understanding non-traditional filtration behaviour at low pressures and then the transition to more traditional filtration behaviour at higher pressures.

Chapter 8

Conclusion

The compressive and shear yield stress of sewage sludge, a coagulated alumina suspension, and a dual-polymer flocculated alumina suspension increased as a function of volume fraction. The three suspensions were more easily deformed by shear than by compression. The P_y/τ_y ratio of three suspensions increased with volume fraction in the investigated volume fraction ranges. The ratios appeared to have a similar shape. The ratio of the sewage sludge increased from 5-8 in the volume fraction range from 0.035-0.09 v/v, the coagulated alumina suspension from 2-14 in the volume fraction range from 0.075-0.50 v/v, and the flocculated alumina suspension from 8-11 in the volume fraction range from 0.09-0.43 v/v. The ratio determined for the coagulated alumina suspension is in agreement with previous investigations done by Zhou (2000).

The compressive and shear yield stress of sewage sludge increased more rapidly with volume fraction than was the case for the alumina suspensions. Small particles and the ECP in sewage sludge are believed to be responsible for sewage sludge's stronger three dimensional network structure. The flocculated alumina suspension exhibited a stronger network structure as a function of volume fraction than the coagulated alumina suspension did, which can be ascribed to polymer effects as bridging and depletion forces.

The coagulated alumina suspension exhibited traditional filtration behaviour with a linear dominating cake formation state and short cake compression times. The hindered settling function of the suspensions increased over 5 orders of magnitude, from $1{\cdot}10^{8}$-$3{\cdot}10^{13}$ Pa s/m^2, with volume fraction. The solids diffusivity of the suspension was almost independent of volume fraction at $1{\cdot}10^{-7}$ m^2/s. Sewage sludge did not exhibit non-traditional filtration behaviour as expected. A more traditional filtration behaviour, with long formation times with a weak decreasing dewatering rate, was observed. The hindered settling function of sewage sludge increased over 8 orders of magnitude, $1{\cdot}10^{8}$-$4{\cdot}10^{16}$ Pa s/m^2, with volume fraction. The solids diffusivity of sewage sludge varied from $6{\cdot}10^{-11}$-$5{\cdot}10^{-9}$ m^2/s and showed a maximum near the gel point and the decrease with volume fraction was followed by an increase. Non-tradional filtration behaviour was observed at low pressures, 5-40 kPa, for the flocculated alumina suspension. A short almost non-existing cake formation was followed by long cake compression times. At the higher pressures, a weak increasing dewatering rate in cake formation was followed by shorter cake compression times. The hindered settling function of the suspensions was determined to increase from $1{\cdot}10^{8}$-$1{\cdot}10^{12}$ Pa

s/m^2. The flocculated alumina suspension exhibited a similar solids diffusivity behaviour with volume fraction as the sewage sludge thus three orders of magnitude larger, $1{\cdot}10^{-7}$-$2{\cdot}10^{-6}$ m^2/s. Determination of filtration parameters, from linarisation of the cake compression region, resulted in reasonable prediction of the filtration behaviour of the flocculated alumina suspension.

Bibliography

[Ackerson, 1990] B. J. Ackerson. Shear Induced Order and Shear Processing of Model Hard Sphere Suspensions. *J. Rheol*, 34(4):553–590, May 1990.

[Aziz, 2004] A.A.A. Aziz. Characterisation of Shear Upon Dewaterability of Colloidal Suspensions. *PhD thesis, University of Melbourne, Parkville, Victoria, Australia*, 2004.

[Barnes and Walters, 1985] H. A. Barnes and K. Walters. The Yield Stress Myth? *Rheologica Acta*, 24:323–326, 1985.

[Barnes *et al.*, 1989] H.A. Barnes , J.F. Hutton, and K. Walters. *An Introduction to Rheology.* Elsevier Science Publishers B.V, Amsterdam, The Nederlands, 1989.

[Barnes, 1997] H.A. Barnes. Thixtropy- a review. *J. Non-Newtonian Fluid Mechanics*, 70:1–33, Jan 1997.

[Barnes, 2000] H.A. Barnes. *A Handbook of Elementary Rheology.* Institute of Non-Newtonian Fluid Mechanics, University of Wales, 2000.

[Bingham and Green, 1920] E.C. Bingham and H. Green. Paint a Plastic Material and not a Viscous Liquid; the Measurements of its Mobility and Yiled Value. *Proc. Am. Soc. Test. Matl.*, 20:640–675, 1920.

[Buscall and White, 1987] R. Buscall and L.R. White. The Consolidation of Concentrated Suspensions. *Journal of Chemical Society Faraday Transactions*, 83:873–891, 1987.

[Buscall *et al.*, 1987] R. Buscall , I.J. McGowan , P.D.A Mills , R.F. Stewart , D. Sutton , L.R. white, and G.E. Yates. The Rheology of Strongly-Flocculated Suspensions. *Journal of Non-Newtonian Fluid Mechanics*, 24:183–202, 1987.

[Channel and Zukoski, 1997] G.M. Channel and C.F. Zukoski. Shear and Compressive Rheology of Aggregated Alumina Suspensions? *AIChE Journal*, 43(7):1700–1708, July 1997.

[Chhabra, 2007] R. P Chhabra. *Bubbles, Drops, and Particles in Non-Newtonian Fluids.* CRC Press, 2007.

[de Kretser *et al.*, 2005] R.G. de Kretser , S.P.Usher, and P.J. Scales. Comprehensive Dewatering Behaviour Analysis for Fine and Flocculated Materials. *Proceedings of American Filtration and Seperation Society*, April 10-13 2005.

[Dignac *et al.*, 2007] M.F. Dignac , V. Urbain , D. Rybacki , A. Bruchet , D. Snidaro, and P. Scribe. Chemical Description of Extracellular Polymers: Implication on Wastewater Sludge. *Water Research*, 41:206–216, 2007.

[Glover *et al.*, 2004] S.M. Glover , Y. Yan , G.J. Jameson, and S. Biggs. Dewatering Properties of Dual-Polymer-Flocculated Systems. *Int. J. Miner. Process.*, 73:145–160, 2004.

[Glover, 2003] S.M. Glover. Novel Routes for Polymer-Assisted Solid-Liquid Separation. *Ph.D thesis, The University of Newcastle*, 2003.

[Goodwin and Hughes, 2000] J.W. Goodwin and R.W Hughes. *Rheology for Chemists An Introduction.* The Royal Society of Chemistry, 2000.

[Green, 1997] M.D. Green. Characterisation of Suspensions in Settling and Compression. *PhD thesis, University of Melbourne, Parkville, Victoria, Australia*, 1997.

[Hartnett and Hu, 1989] J.P. Hartnett and R.Y.Z. Hu. Technical Note: The Yield Stress- An Engeneering Relity. *Journal of Rheology*, 33(4):671–679, 1989.

[Herschel and Bulkley, 1926] V. W. H. Herschel and R. Bulkley. Konsistenzmessungen von Gummi-Benzollosungen. *Kolloid Zeit*, 39:291–300, 1926.

[Hiemenz and Rajagopalan, 1997] P. C. Hiemenz and R. Rajagopalan. *Principles of Colloid and Surface Chemistry.* Marcel Dekker, Inc., thrid edition, 1997.

[Hough and White, 1980] D.B. Hough and L.R. White. The Calculation of Hamaker Constants from Lifshitz Theory with Applications to Wetting Phenomena. *Adv. Colloid Interface Sci.*, 14:3–41, 1980.

[Hulston, 2005] J. Hulston. Effect of Flocculation Conditions on the Dewaterability of Hematite and Red Mud Suspensions. *PhD thesis, University of Melbourne, Parkville, Victoria, Australia*, 2005.

[Israelachvili, 1992] J. Israelachvili. *Intermolecular and Surface forces.* Academic Press, Elsevier Science, California USA, 1992.

[James *et al.*, 1987] A.E. James , D.J.A. Williams, and P.R. Williams. Direct Measurement of Static Yield Properties of Cohesive Suspensions. *Rheologica Acta*, 26:437–446, 1987.

[Johnson *et al.*, 2000] S. B. Johnson , G. V. Franks , P.J. Scales , D.V. Boger, and T.W. Healy. Surface Chemistry- Rheology Relationships in Concentrated Mineral Suspensions. *International Journal of Mineral Processing*, 58:267–304, 2000.

[Kapur *et al.*, 1997] P.C. Kapur , P.J. Scales , D.V. Boger, and T.W. Healy. Yield Stress of Suspensions Loaded with Size Distributed Particles. *AIChE Journal*, 43(5):1171–1179, May 1997.

[Landman and White, 1994] K.A. Landman and L.R. White. Solid/Liquid Separation of Flocculated Suspensions. *Advances in Colloid and Interface Science*, 51:175–246, 1994.

[Landman and White, 1997] K.A. Landman and L.R. White. Predicting Filtration Time and Maximizing Throughput in a Pressure Filter. *AIChE Journal*, 43(12):3147–3160, Dec 1997.

[Landman *et al.*, 1995] K.A. Landman , L.R. White, and M. Eberl. Pressure Filtration of Flocculated Suspensions. *AIChE Journal*, 41(7):1687–1700, July 1995.

[Landman *et al.*, 1999] K.A. Landman , J.M. Stankovich, and L.R. White. Measurement of the Filtration Diffusivity D(ϕ) of a Flocculated Suspension. *AIChE Journal*, 45(9):1875–1882, Sep 1999.

[Leong *et al.*, 1995] Y.K Leong , P.J Scales , T.W. Healy, and D.V. Boger. Effect of Particle Size on Colloidal Zirconia Rheology at the Isoelectric Point. *Journal of American Ceramic Society*, 78:2209–2212, 1995.

[Lester *et al.*, 2005] D.R. Lester , S.P. Usher, and P.J. Scales. Estimation of the Hindered Settling Function R(ϕ) from Batch-Settling Tests. *American Institute of Chemical Engineers*, 51(4), April 2005.

[Liddell and Boger, 1995] P.V. Liddell and D.V. Boger. Yield Stress Measurement with the Vane. *Journal of non-Newtonian Fluid Mechanics*, 63:235–261, 1995.

[Mascosko, 1994] C.W. Mascosko. *Rheology: Principles, Measurements, and Application.* VCH Publishers, New York, 1994.

[Meeten, 1994] G.H. Meeten. Shear and Compressive Yield in the Filtration of a Bentonite Suspension. *Colloid and Surfaces*, 82:77–83, 1994.

[Miller *et al.*, 1996] K.T. Miller , R.M. Melant, and C.F. Zukoski. Comparison of the Compressive Yield Response of Aggregated Suspensions: Pressure Filtration, Centrifugation, and Osmotic Consolidation. *Journal of Ceramic Society*, 79(10):2545–56, 1996.

[Nguyen and Boger, 1983] Q.D. Nguyen and D.V. Boger. Yield Stress Measurement for Concentrated Suspensions. *Journal of Rheology*, 27(4):321–349, 1983.

[Nguyen and Boger, 1985] Q.D. Nguyen and D.V. Boger. Direct Yield Stress Measurement with the Vane Method. *Journal of Rheology*, 29(3):335–347, 1985.

[Nguyen and Boger, 1992] Q.D. Nguyen and D.V. Boger. Measuring the Flow Properties of Yiels Stress Fluids. *Annual Reviews Fluid Mechanics*, 24:47–88, 1992.

[Ohshima, 2006] H. Ohshima. *Theory of Colloid and Interfacial Electric Phenomena.* Academic Press, Elsevier Science, Amsterdam, The Netherlands, 2006.

[Rheology Solutions Pty Ltd, 2008] Rheology Solutions Pty Ltd. http://www.rheologysolutions.com/viscotester550_techs.html, march 2008.

[Ruth *et al.*, 1933] B.F. Ruth , G.H. Montillon, and R.E. Montonna. Studies in Filtration: I Critical Analysis of Filtration Theory. *Industrial and Engineering Chemistry*, 25:76–82, 1933.

[Scales *et al.*, 1998] P.J. Scales , S.B. Johnson , T.W. Healy, and P.C. Kapur. Shear Yield Stress of Partially Flocculated Colloidal Suspensions. *AIChE Journal*, 44(3):538–544, March 1998.

[Scales *et al.*, 2004] P.J. Scales , D.R. Dixon , P.J. Harbour, and A.D. Stickland. The Fundamentals of Wastewater Sludge Characterization and Filtration. *Water Science and Technology*, 49(10):67–72, 2004.

[Stickland and Buscall, 2008] A.S. Stickland and R. Buscall. Whither Compressional Rheology? 2008.

[Stickland *et al.*, 2007] A.D. Stickland , P.J. Harbour, and D.R. Dixon P.J. Scales. Scaling Filtration Time Initial Dependencies of Wastewater Sludge. *Water Research*, 41:206–216, 2007.

[Stickland, 2005] A.D. Stickland. Solid-Liquid Separation in the Water and Wastewater Industries. *PhD thesis, University of Melbourne, Parkville, Victoria, Australia*, June 2005.

[Studer, 2008] L. Studer. New Approaches to the Optimisation of Wastewater Dewatering and Processing. *PhD thesis in progress, University of Melbourne, Parkville, Victoria, Australia*, 2008.

[Sutanto and Ho, 2007] C. Sutanto and E.C.S. Ho. Developing a well Behaved Model System to mimic the Mechanics of Wastewater Sludge Filtration. *Research Project, University of Melbourne, Parkville, Victoria, Australia*, 2007.

[Suzuki *et al.*, 1981] M. Suzuki , K. Makina , M. Yamada, and K. Iinoya. A Study on the Coordination Number in a System of Randomly Packed Uniform-Sized Spherical Particles. *Int Chem. Eng.*, 21:482, 1981.

[Tiller and Li, 2000] F.M. Tiller and W.P. Li. Strange Behaviour of Super-Compactible Filter Cakes. *Chem. Process.*, 63(9), 2000.

[Usher *et al.*, 2001] S.P. Usher , R.G. De Kretser, and P.J. Scales. Validation of a New Filtration Technique for Dewaterability Characterization. *AIChE Journal*, 47(7):1561–1570, July 2001.

[Zhou, 2000] Z. Zhou. *Rheology of Metal Oxide Suspensions*. Advanced Minerals Products Special Research Centre, Department of Chemical Engineering, University of Melbourne, Victoria 3010, Australia, 2000.

Appendix A

The Vane Technique

The advantage of using the vane technique is that slip effects are avoided (Section 3.4). The vane consists of a cylindrical shaft equipped with 4-8 thin blades arranged with equal angles between them and compared with a cylinder, immersion of the vane geometry causes a minimum of disturbance of the sample (Figure A.1a). The vane apparatus is a simple setup consisting of a vane attached to a torsion head which is attached to a motor (Figure A.1b) [Nguyen and Boger, 1985].

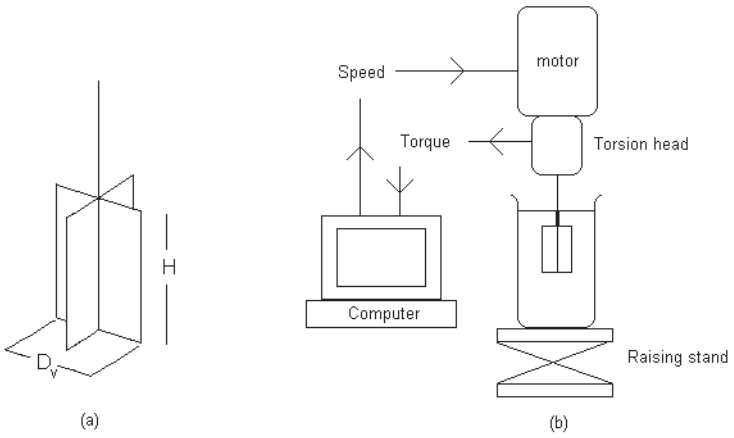

Figure A.1: (a) a vane (b) The vane apparatus consisting of a motor, a torsion head, the vane, and a computer.

Nguyen and Boger (1983) proposed that to avoid the containers side walls and base to affect the yield stress measurement, the length and diameter of the container should be twice as large as the dimensions of the vane. The vane technique is often used in a rate controlled mode. In this mode, a low rotational shear rate is applied to the vane and the resultant torque is measured. Nguyen and Boger (1985) calculated the shear stress from the torque by making the assumption that the material is sheared along a cylinder with the same dimensions as the vane. In this case the torque (T) can be measured as the sum of all the shearing components acting on the top,

bottom, and the side of this localized cylinder (Equation (A.1)).

$$T = T_s + 2T_e = (2\pi R_v H)\tau_s R_v + 2(2\pi \int_0^{R_v} \tau_e(r) r \; dr \; r) \tag{A.1}$$

Where T_s and T_e are the torque resulting from shearing on the side and on the end surfaces, respectively, R_v is the vane radius, τ_s the shear stress along the side of the cylinder, and τ_e the shear stress at the end surfaces. If the stress applied to the cylinder is distributed uniformly on the cylinders sides and end surfaces then the magnitude of τ_s and τ_e must be equal and Equation (A.1) can be simplified to Equation (A.2).

$$\tau = \frac{T}{K} \tag{A.2}$$

Where τ is the shear stress and K becomes the vane parameter constant defined as:

$$K = \frac{\pi \cdot D_v^3}{2}(\frac{H}{D_v} + \frac{1}{3}) \tag{A.3}$$

The yield stress can then be calculated from the maximum torque. Different authors have showed that these assumptions are not completely correct. The sheared surface is slightly larger than the vane dimensions (up to 5%) and the stress acting on the end surfaces is not uniformly distributed but peaks sharply (the latter error is shown to be negligible) [Liddell and Boger, 1995] . Various authors have investigated the effect of the vane dimensions on the measured yield stress value and have observed no effect within the experimental errors. These include dimensions from 0.95-27 mm in diameter and 3.2-50 mm in height [Liddell and Boger, 1995; Nguyen and Boger, 1983; James *et al.*, 1987].

Appendix B

Equilibrium Pressure Filtration

The filtration equipment consists of a cylinder filled with sample. A piston with an incorporated pressure transducer is located at the top of cylinder and presses downward. At the bottom of the cylinder a membrane is placed allowing filtrate to leave the cylinder when the pressure is applied (Figure B.1).

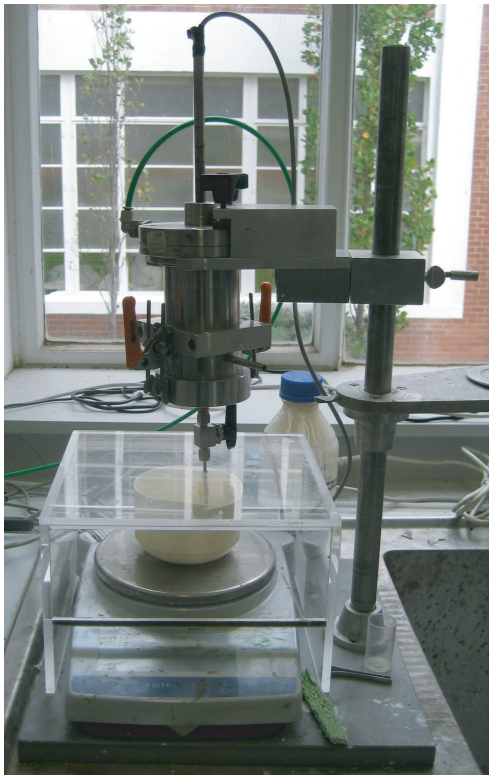

Figure B.1: Filtration rig.

Single Pressure filtration The compressive yield stress and the volume fraction are easily obtained from single pressure filtration. At equilibrium the applied pressure is equal to the compressive yield stress and the solid volume fraction can be determined directly by the weight

lost and drying method or indirectly by use of Equation (B.1.) [de Kretser *et al.*, 2005].

$$\phi_f = \phi_0 \frac{h_0}{h_f} \tag{B.1}$$

Stepped Pressure filtration The smallest pressure is applied until the filter cake stops compressing. The pressure is then raised and the procedure repeated until all chosen pressures have been applied to the filter cake [Usher *et al.*, 2001].

Appendix C

Centrifugation

In the centrifugation technique, the sample is centrifuged until equilibrium is achieved i.e. until a steady sediment height is reached. Then the pressure at any point in the particle network can be determined by the weight of the particles above that point (Equation (C.1)) [Miller *et al.*, 1996].

$$P(z) = \int_{z}^{H_{eq}} \Delta\rho \; g(z) \; \phi(z) \; dz \tag{C.1}$$

where P is the pressure acting on the particle network, z denotes the height of the given point measured from the bottom of the column, H_{eq} is the sediment height at equilibrium, $\Delta\rho$ is the difference between the density of the solid and liquid, $g(z)$ the centrifugal acceleration, and the solid volume fraction is given by $\phi(z)$. The centrifugal acceleration is given:

$$g(z) = g_0(1 - z/R) \tag{C.2}$$

and is determined by the acceleration at the base of the column (g_0) and the distance from the centre of the rotor to the bottom of the column (R) [Miller *et al.*, 1996]. The consolidation equilibrium is reached when the particle network is able to sustain the applied pressure elastically ($P_y\phi(z)=P(z)$). Equation (C.1) can therefore be used to determine the compressive yield stress. To two most common techniques used to determine the compressive yield stress are either a concentration profile technique where the volume fraction is measured directly or a multiple speed sediment height technique where the volume fraction is determined indirectly [Miller *et al.*, 1996; Buscall and White, 1987].

Appendix D

Solid Concentration Calculations

The solid mass fraction (x) of a suspension can be calculated as follows:

$$x = \frac{m_{wet} - m_{empty}}{m_{dry} - m_{empty}} \tag{D.1}$$

where m_{wet} is the mass of the tray and the suspension before drying, m_{empty} is the mass of the empty tray, and m_{dry} is the mass of the tray and the suspension after drying.

The solid mass fraction (x) of the solution can be converted to solid volume fraction (ϕ) if the particle density (ρ_p) and the liquid density (ρ_l) is known D.2.

$$\phi = \frac{1}{1 + \frac{\rho_p}{\rho_l}\left(\frac{1}{x} - 1\right)} \tag{D.2}$$

Conversion from solid volume fraction (ϕ) to solid mass fraction (x) is as follows:

$$x = \frac{1}{1 + \frac{\rho_l}{\rho_p}\left(\frac{1}{\phi} - 1\right)} \tag{D.3}$$

and the suspension density ρ_s can be calculated as follows:

$$\rho_s = \frac{1}{\frac{x}{\rho_p} + \frac{(1-x)}{\rho_l}} \tag{D.4}$$

Enclosure I

Calculation of the Error in using Low Torque Data from the Haake Viscometer

On the Haake viscometer the torque range is from 100-30,000 μNm $\pm$ 5% (fsd) [Rheology Solutions Pty Ltd, 2008] and the calculated min. and max. stesses for the different vanes are given in Table I.1.

Table I.1: The stress ranges that can be measured at the Haake Viscometer with the different vane geometries calculated on basis of the sensibility of torque in the instrument.

Vane	min. measurable stress [Pa]	max. measurable stress [Pa]
1	34.8	10,426
2	5.8	1,735
3	2.6	792.2
4	1.7	523.8
5	1.2	366.7
6	0.2	65.5
7	0.03	8.2

The error on the measured torque values is determined using least square linear regression on the apparent linear part of the torque vs stress curve where the suspension yields (Figure I.1). A line is fitted through the points and the difference between the points and the fitted line is determined.

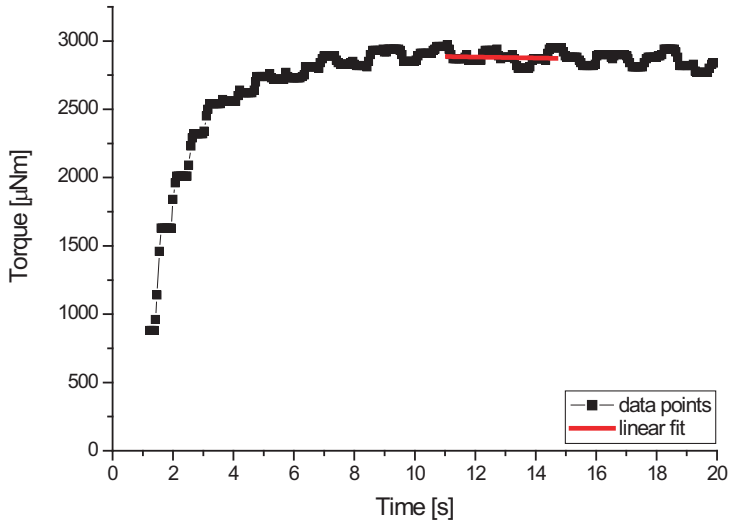

Figure I.1: Calculation of the error on the torque for a measurement with vane 1 on a 0.36 v/v alumina suspension.

The error is then determined by:

$$Error\% = \sum_{n=1}^{n} \left(\frac{M - \overline{M}}{M} \cdot 100\% \right) /n \tag{I.1}$$

where M is the torque and $\overline{M}$ is the torque calculated from the linear fit. The results are given in Table I.2.

Table I.2: The different vane geometries and the stress ranges that can be measured at the Haake Viscometer with each of them calculated on basis of the sensibility of the transducer/sensor? in the instrument.

ϕ	Vane 7			Vane 6			Vane 4		
[-]	τ_y [Pa]	M [μNm]	error [%]	τ_y [Pa]	M [μNm]	error [%]	τ_y [Pa]	M [μNm]	error [%]
0.169				49.3	22,600	0.44	41.0	2,300	1.29
0.126				18.8	8,600	0.64	11.6	670	3.18
0.106	8.0	29,400	0.43	7.5	3,400	1.17	4.6	260	3.52
0.100	6.8	24,800	0.37	6.4	2,900	1.19			
0.095	5.6	20,500	0.48	5.1	2,300	1.22			
0.090	4.7	17,100	0.37	4.1	1,900	1.64			

From Table I.2 the difference in shear yield stress, the measured torque, and the error on the torque can be viewed for three different vanes. According to the Haake instrument manual the error on the torque is $\pm$ 0.5% which means that the vaules measured with Vane 7 are within the accepted error range. On basis of the data, it can then be concluded that an error$\geq$ 1.17% on the measured torque/stress and a torque $\leq$ 3,400 μNm leads to a $\geq$ 6% lower shear yield stress value. It is therefore determined that 3,400 μNm is the minimum torque valid for measuring on the Haake. This leads to the following limits for the different vanes (Table I.3).

Table I.3: The stresses for the different vane geometries corresponding to the torque of 3,400 μNm which is the minimum torque considered to yield a reliable shear yield stress value on the Haake Viscometer.

Vane	min. measurable stress [Pa]
1	1182
2	196.7
3	89.8
4	59.4
5	41.6
6	7.4
7	0.9

Enclosure II

Calculation of Compressive Yield Stress from Equilibrium Batch Settling

The principle of batch settling is that a suspension is settled under gravity until equilibrium is reached. The pressure gradient ($\frac{dp}{dz}$) is determined by the density difference between the solid and the liquid ($\Delta\rho$), the gravitational force (g), and the volume fraction of the bed (ϕ):

$$\frac{dp}{dz} = -\Delta\rho g\phi \tag{II.1}$$

At equilibrium the network pressure (P) acting on the bed is equal to the compressive yield stress (P_y) at all heights. At initial solids concentrations below the gel point ($\phi_0 < \phi_g$) the network pressure at the top of the bed is zero while that at the base, due to the overlying suspension is determined according to:

$$P_{z=0} = \Delta\rho g\phi_0 h_0 \tag{II.2}$$

where $\Delta\rho$ is the difference in density between the solid and liquid, g is the gravitational force, and h_0 is the initial sample height. Employing the end conditions, Equation (II.1) can be integrated to yield:

$$\int_0^{h_f} dz = \frac{1}{\Delta\rho g}\int_{\Delta\rho g\phi_0 h_0}^{0} \frac{-1}{\phi} dp \quad \Rightarrow \quad h_f = \frac{h_0\phi_0}{\phi} \tag{II.3}$$

As Equation (II.3) is employed to calculate the average solid volume concentration, the average P_y can be calculated as $P_{z=0}/2$.

Five batch settling tests were performed by employing a fixed initial volume fraction and different initial heights. The samples were left to settle for 86 days. By viewing the final height as a function of log time it can be determined whether equilibrium has been reached (Figure II.1).

After 24 hours the five batch settling test appear to have settled to equilibrium as the subsequent points are steady at that height. After 86 days the suspensions appear to have undergone further settling, which properly can be ascribed to creep in the samples, which occur as bond breaks and reform between the particles.

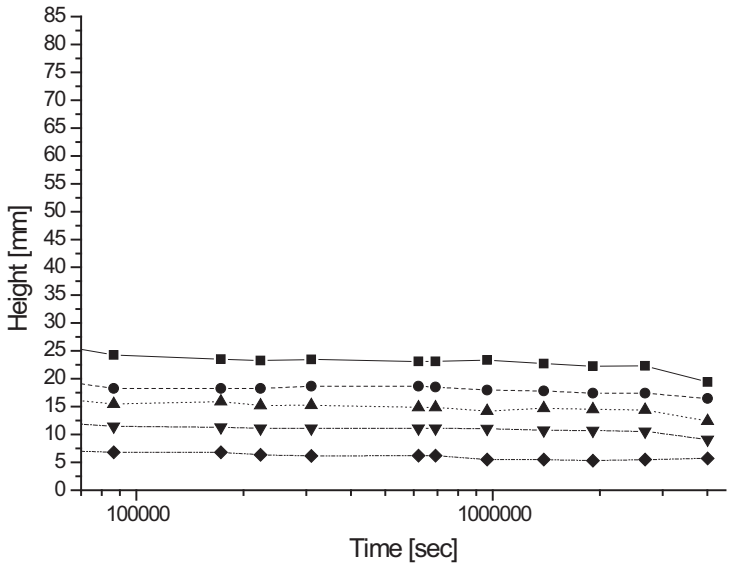

Figure II.1: Bed height as a function of settling time for alumina suspensions (pH 9±0.1, 10^{-2}M KNO_3) with an initial volume fraction of 0.03 v/v.

The final volume fraction at the bottom of the suspension after 24 hours and 86 days is estimated by viewing $\phi_0 h_0$ as a function of the final height. By fitting a line through the points with origin being zero the final height can be determined as: $\phi(h) = \frac{\phi_0 h_0}{dh}$. The points are shown in Figure II.2 where an exponential fit have been done for the two sets of points.

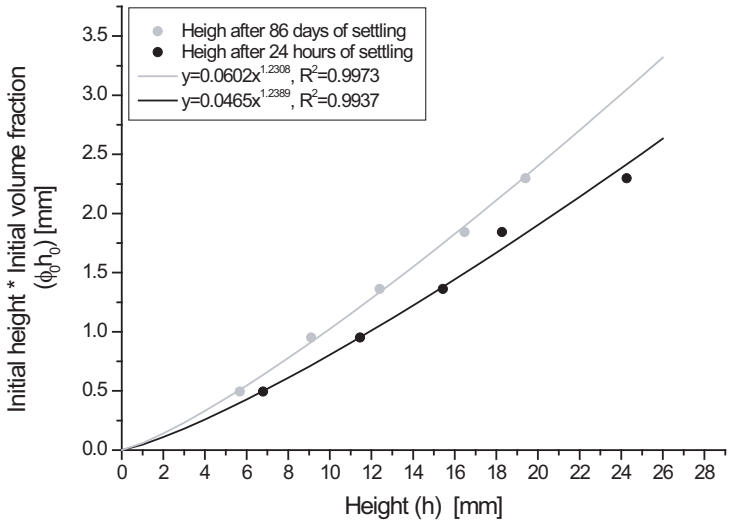

Figure II.2: Initial batch settling height of ($\phi = 0.03$) alumina suspensions (pH=9.0±0.1, 10^{-2}M KNO_3) timed the initial volume fraction as a function of the equilibrium bed height.

Enclosure III

Determination of Filtration Parameters

Two methods to determine either R(ϕ) or D(ϕ) from filtration and a method to determine R(ϕ) from settling data are presented in the following. The first method include extrapolation of the cake compression curve to equilibrium conditions and the second method is a calculation of R(ϕ) from the cake formation curve.

III.1 Extrapolation of the Cake Compression Curve from Filtration to Equilibrium Conditions

The linearised theory from Landman and White (1997) of the cake compression curve resulting from equilibrium filtration has been used to create an expression were time varies logarithmical with the filtration volume, which is done by truncation of Fourier series [Stickland, 2005]:

ϕ_∞ and D(ϕ_∞) is determined from:

$$t = E_1 - E_2 ln(E_3 - V) \tag{III.1}$$

where

$$t = E_1 - E_2 ln(V_{\infty - V}) \tag{III.2}$$

$$E_1 = \frac{h_0^2 \phi_0^2}{D(\phi_\infty)\phi_\infty^2} \left[T_c + \frac{4}{\pi^2} ln\left(\frac{2A_0 A_0 \phi_0 h_0}{A_0 \pi} \right) \right] \tag{III.3}$$

$$E_2 = \frac{4h_0^2 \phi_0^2}{\phi^2 D(\phi_\infty)\phi_\infty^2} \tag{III.4}$$

$$E_3 = h_0 \left(1 - \frac{\phi_0}{\phi_\infty} \right) \tag{III.5}$$

where h_0 is the initial sample height, ϕ_0 is the initial volume fraction, ϕ_∞ is the solids concentration at equilibrium, $D(\phi_\infty)$ is the solids diffusivity at equilibrium, T_c is the scaled filtration time, and A_0 is a constant [Stickland, 2005]. An example of the end point fit is shown in Figure III.1.

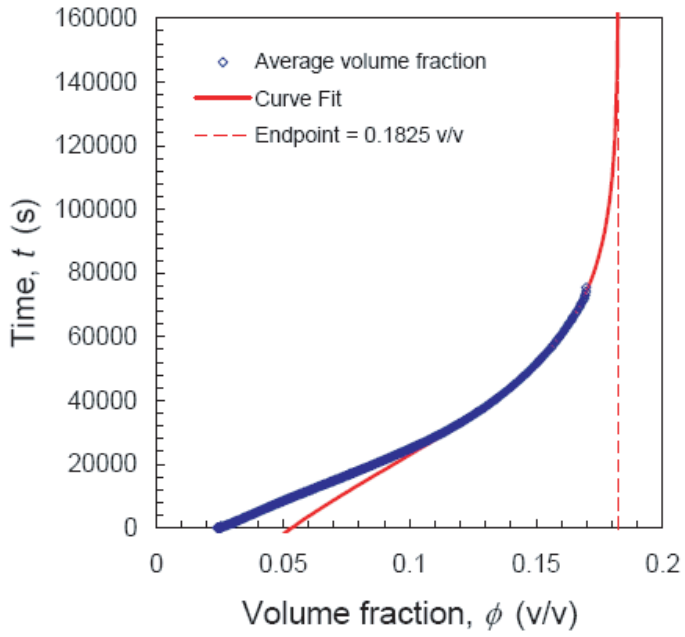

Figure III.1: Example of end point fit from extrapolation of the cake formation region to yield ϕ_∞ and D(ϕ_∞) [Stickland, 2005].

III.2 Hindered Settling Function From the Cake Formation Filtration Curve

The hindered settling function, R(ϕ), is related to the specific cake resistance, α:

$$\alpha = \frac{R(\phi)}{(1-\phi)^2 \rho_s \eta} \tag{III.6}$$

where ρ_s is the solids density and η is the filtrate viscosity.

From the traditional Ruth/Darcian filtration equation, which assumes a linear cake formation region, the specific cake resistance can be determined;

$$\alpha_{av} = \frac{2\Delta P}{\eta \rho_s} \left(\frac{1}{\phi_0} - \frac{1}{\phi_c} \right) \cdot \frac{\delta(t/V)}{\delta V} \tag{III.7}$$

where $\Delta\ P$ is the pressure difference, ρ_s is the solids density, η is the filtrate viscosity, ϕ_0 is the initial volume fraction, and ϕ_c is the average solids concentration in the cake. Combining Equation (III.6) and (III.7):

$$R(\phi_c) = 2\Delta P (1-\phi_c)^2 \left(\frac{1}{\phi_0} - \frac{1}{\phi_c} \right) \cdot \frac{\delta(t/V)}{\delta V} \tag{III.8}$$

III.3 Hindered Settling Function From the Batch Settling

The hindered settling function below the gel point can be determined from batch settling experiments. Lester *et al.* (2005) developed a method for determining hindered settling function data

in the volume fraction range from ϕ_0-ϕ_g from one test. This method divide the time vs. height plot of a batch settling test in four regions a-d:

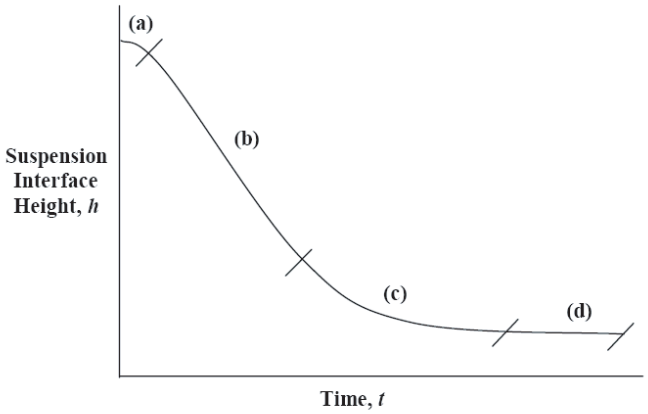

Figure III.2: Time vs. height profile of a batch settling test [Aziz, 2004].

Region a is defined as the initiation periods where the particles start to settle. In the following region the particles settles at a constant rate ($\mu_0(\phi)$) and as no network is formed ($\phi<\phi_g$) the hindered settling function can be determined from the inverse settling rate:

$$\mu_0(\phi) = \frac{\delta\rho g(1-\phi)^2}{R(\phi)} \tag{III.9}$$

where $\delta\rho$ is the difference in density, g is the gravitational force. In region c the hindered settling function cannot be calculated analytically and the expression for calculation the hindered settling function is solved by simplifying the problem and employing both analytical and numerical methods to solve it [Lester *et al.*, 2005].